EASTLAND PORT MAINTENANCE DREDGING AND DISPOSAL PROJECT

Morphological model validation

Report prepared for Eastland Port

January 2018

MetOcean
SOLUTIONS

MetOcean Solutions Ltd: Report P0331-03

December 2017

Report status

Version	Date	Status	Approved by
RevA	15/01/2018	Draft for internal review	Monetti
RevB	18/01/2018	Draft for internal review	Beamsley
RevC	31/01/2018	Draft for internal review	Weppe
RevD	31/01/2018	Draft for client review	Beamsley

It is the responsibility of the reader to verify the currency of the version number of this report.

TABLE OF CONTENTS

LIST OF FIGURES

LIST OF TABLES

1. INTRODUCTION

Eastland Port Ltd are seeking to renew their maintenance dredging and disposal consents at the Port of Gisborne.

Currently, dredged sediment is disposed at an offshore disposal site situated in approximately 18 – 20 m water depth (**Error! Reference source not found.**), with an average annual rate of approximately 73,000 m^3 based on estimates obtained between 2002 and 2019 by Eastland Port.

Maintenance dredging is expected to occur using the Trailing Suction Hopper Dredge (TSHD) “Pukunui” although, if there are significant inflows of sediment due to large storm events, a higher productivity Trailing Suction Hopper Dredge (TSHD) may be required to ensure the required port and channel depths can be maintained. It is likely that some maintenance dredging may also be undertaken using a Backhoe Dredger (BHD) or Cutter Suction Dredger (CSD).

MetOcean Solutions (MOS) has been contracted to provide coastal oceanographic expertise to investigate both physical and morphological effects and associated sediment transport patterns resulting from the dredging and disposal of maintenance dredging material at the current disposal site.

For this purpose the process-based model Delft3D was used to hindcast the sediment dynamics over northern Poverty Bay and Eastland Port. The present report presents a methodology to replicate the annual sediment transport controlled by a relative large range of physical processes. This includes the use of combined reduction techniques and morphological acceleration factors (MORFACs) as well as storm-induced morphological simulations.

The calibration and validation of the morphological models were performed using measured sediment infilling rates within the channel and in the port provided by single- and multi-beam surveys. Seaward and river open-boundary conditions were derived from high-resolution hydrodynamic and wave hindcast (Figure 1.2) described in MetOcean Solutions (2017a, 2017b). The present report is a technical reference document that details:

- The establishment of numerical models for replicating the existing and proposed morphodynamics at Eastland Port.
- The methodology applied to assess the numerical model performance.
- The degree of confidence in the models results for future applications in the case of deepened channel and inner basin.

The complete methodology is presented in Section 2, including a description of the model domains, model settings, forcing and boundary conditions and validation methods. Results of the validation process are given and discussed in Section 3. A brief summary is presented in Section 4 while the references cited in this document are listed in Section 5.

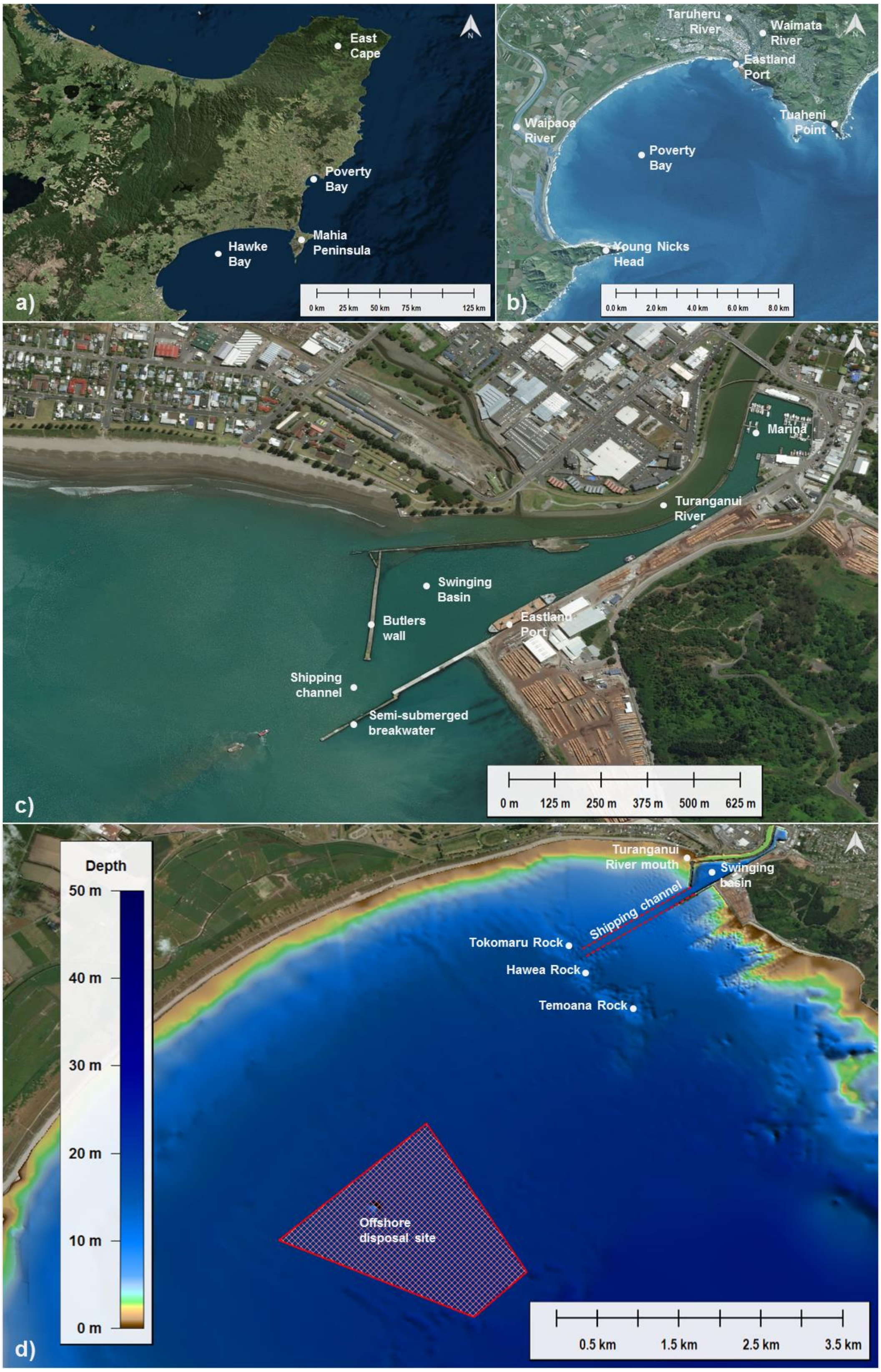

Figure 1.1 Maps showing the location of Poverty Bay (a, b), and Eastland Port (c) with the locations used in the present study. Both offshore disposal and shipping channel are indicated on top of the bathymetry in (d).

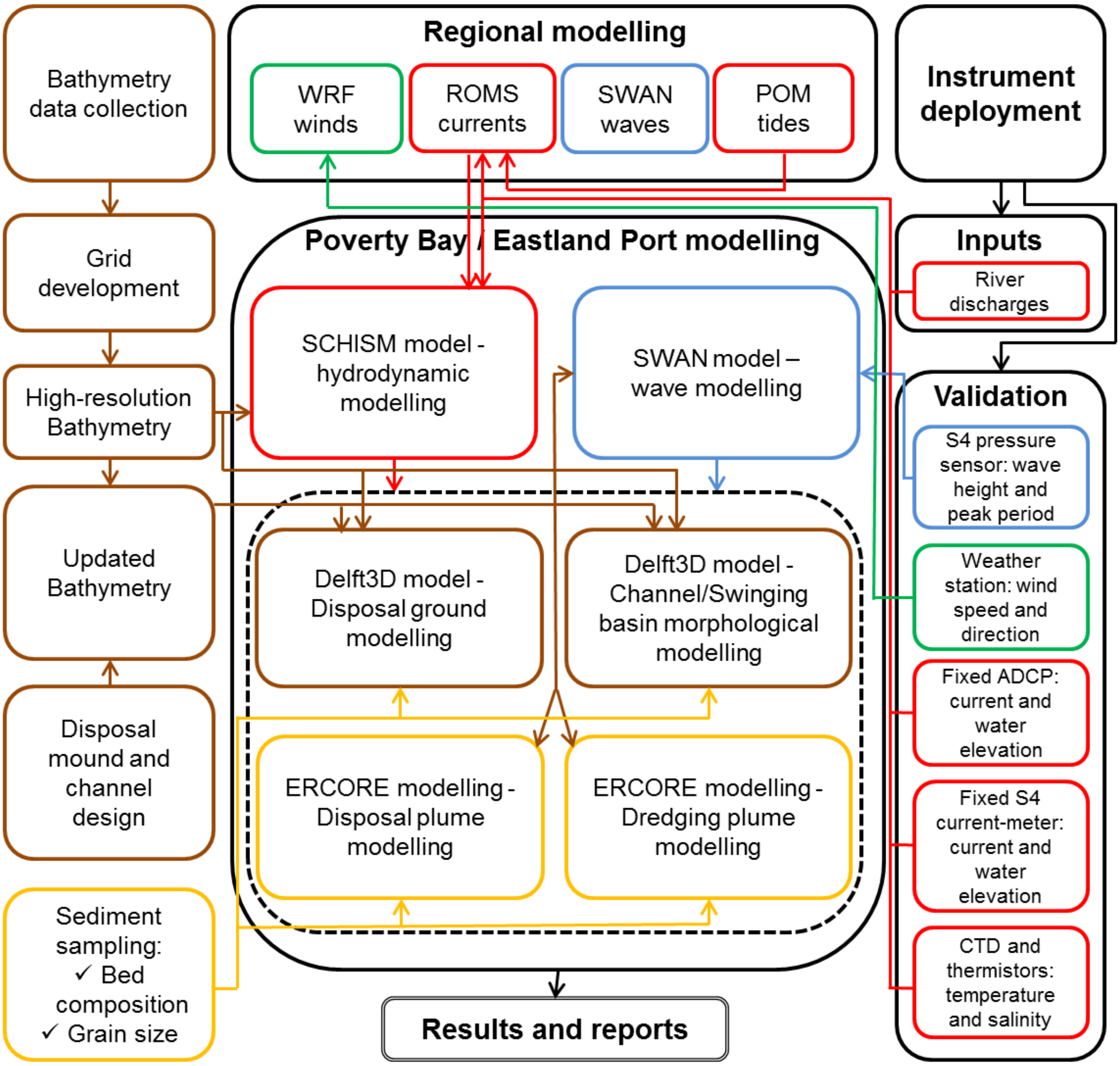

Figure 1.2 Flow chart showing the numerical modelling process for the study. Red lines indicate hydrodynamics; blue indicate waves; green indicate wind; brown indicate bathymetry; and yellow lines indicate sediments.

2. METHODS

The primary objective of the study was to capture the existing sediment dynamics and morphology at Eastland Port and the adjacent navigation channel with the use of a numerical model. To meet this objective, the focus was first on establishing a suitable modelling approach to accurately predict the annual infilling rates observed over time within the existing channel and inner basin. We detail in the present section the methods applied to implement, run and validate our numerical modelling.

2.1. Bathymetry

Bathymetry is an essential requirement for coastal numerical modelling. MetOcean Solutions has compiled an extensive national and regional bathymetric dataset derived from Electronic Navigation Charts (ENC). These datasets were updated with hydrographic surveys carried out within Eastland Port and the surroundings. Note that GEBCO data (Becker et al., 2009) was also used to characterise the deepest areas. Specialist data manipulation tools have been used to allow the merging, interpolation and quality assurance (QA) of raw bathymetry data when establishing numerical model domains.

Water depth in the regional hydrodynamic models was derived from a 500 m gridded bathymetry shown in Figure 2.1 (top). A 5 x 5 m gridded bathymetry displayed in Figure 2.1 (bottom panel) was specifically created over Poverty Bay to interpolate water depths to the computational grids in the Delft3D system.

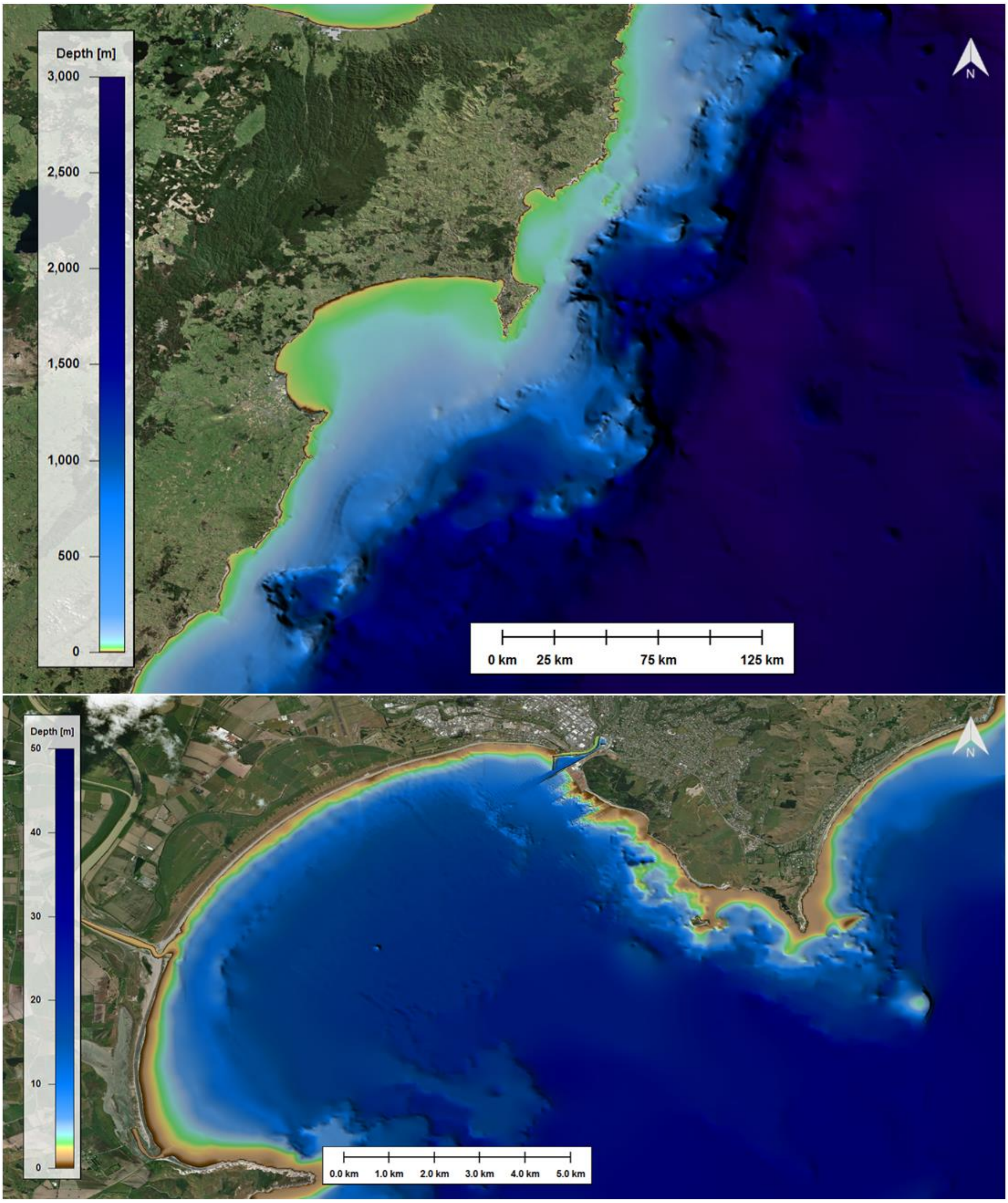

Figure 2.1 Map showing both the 500 x 500 m (top) and the 5 x 5 m (bottom) gridded bathymetries used to interpolate the water depth to the computational grids in Delft3D.

2.2. Delft3D system description

The modelling system Delft3D (Lesser et al., 2004) was used to set up and run high-resolution process-based morphodynamic models. The software is based on interlinking three separate components (Delft3D – WAVE, Delft3D – FLOW and Delft3D – MOR) that together simulate flows, waves and sediment transport. The three components are fully coupled to simulate morphodynamic feedbacks.

Delft3D has been specifically developed to simulate the dynamics of complex coastal regions controlled by a wide range of physical and morphological process interactions.

Delft3D has been successfully applied internationally and within New Zealand for a large range of coastal studies. Applications within New Zealand include for Port Otago (Weppe et al., 2015), Tauranga Harbour (Ramli et al., 2015) and Rees River (Williams et al., 2016).

The present sub-section gives a brief description of the different Delft3D modules used to replicate the coastal dynamics over northern Poverty Bay and Eastland Port.

2.2.1. Delft3D – FLOW

The hydrodynamic module Delft3D – FLOW is a multi-dimensional (2D or 3D) hydrodynamic model which calculates non-steady flows and transport phenomena. Delft3D – FLOW solves the Navier – Stokes equations on a staggered model grid for an uncompressible fluid under the shallow water and Boussinesq assumptions. The system solves the horizontal equations of motion, the continuity equation, the transport equations for conservative constituents and a turbulence closure scheme. The details of equations and associated sub-modules are fully described in Lesser et al. (2004) and Deltares (2017b).

2.2.2. Delft3D – WAVE

The third-generation SWAN model (Simulating WAves Nearshore) was used as the wave module (Booij et al., 1999; Ris et al., 1999). SWAN computes the evolution of random, short-crested waves in coastal regions with deep, intermediate and shallow water depths. The SWAN model accounts for (refractive) propagation due to depth and current and can represent the processes of wave generation by wind, dissipation due to while-capping, bottom friction and depth-induced wave breaking, and non-linear wave-wave interactions explicitly with state-of-the-art formulations (Deltares, 2017b). Wave forces computed by the wave model on the basis of the radiation shear stress gradients can be used as a driving force to compute the wave-induced currents and set-up in the flow module. More details on the coupling between SWAN and Delft3D – FLOW are given in Deltares (2014).

2.2.3. Delft3D – MOR

The Delft3D – MOR module integrates the effects of waves, currents and sediment transport on the morphological development. At each computational time step the model computes both the bed-load and the suspended-load sediment transport components over the domain. The bed level is then updated as a result of the sediment sink and sources terms and computed transport gradients. Delft3D – MOR is designed to simulate wave propagation, currents, sediment transport and morphological developments in coastal, river and estuarine areas (Deltares, 2014). The model is able to simulate the sediment dynamics associated with both non-cohesive (sandy) and cohesive (silt) sediments mixed layers or layered bed stratigraphy approaches.

The transfer of sediment between the bed and the flow is modelled using sink and source terms acting on the near-bottom layer. Bed-load and equilibrium suspended-load transport resulting from the combined effect of waves and currents can be modelled by a range of formulations, among which are Engelund-Hansen, Meyer-Peter-Muller, Bijker, Bailard and Van Rijn. The streamwise and transverse bed slope effects on the magnitude and direction of transport are also included in the model.

The modelling and transport of cohesive sediment requires an approach that is fundamentally different to mobile sand transport. For very fine sediment size (i.e. silt or clay-sized), the inter-particles forces due to ionic charges becomes significant relative to the gravitational forces which strongly dominate the sand transport processes. As a result, processes including flocculation, hindered settling, and bed consolidation have important roles in the movement of cohesive particles. An extensive description of the associated sub-models in Delft3D is given in Deltares (2017b).

In Delft3D – MOR the cohesive sediment transport is calculated by solving the advection-diffusion equation for the suspended sediment (Eq. 2.1). Note that no bed load transport is considered for cohesive sediments.

$$\frac{\partial C}{\partial t}+\frac{\partial uC}{\partial x}+\frac{\partial vC}{\partial y}+\frac{\partial (w-w_s)C}{\partial z}= \frac{\partial}{\partial x}\left(\varepsilon_{s,x}\frac{\partial C}{\partial x}\right)+\frac{\partial}{\partial y}\left(\varepsilon_{s,y}\frac{\partial C}{\partial y}\right)+\frac{\partial}{\partial z}\left(\varepsilon_{s,z}\frac{\partial C}{\partial z}\right)$$

(Eq. 2.1)

where,

E	Mass concentration [kg.m^{-3}]
u, v, w	Velocity components [m.s^{-1}],
$\varepsilon_{s-\,x,y,z}$	Eddy diffusivities in the x,y,z directions [m^2.s^{-1}],
w_s	Sediment settling velocity [m. s^{-1}].

Sediment fluxes between the water phase and the bed are calculated using the Partheniades-Krone formulations (Partheniades, 1965).

$$E = M.S(\tau_{cw}, \tau_{cr,erosion}) \quad \text{(Eq. 2.2)}$$

$$D = w_s.c_b.S(\tau_{cw}, \tau_{cr,deposition}) \quad \text{(Eq. 2.3)}$$

$$c_b = c(z = \frac{\Delta z_b}{2}, 2) \quad \text{(Eq. 2.4)}$$

where,

E	Erosion flux [kg.m^{-2}.s^{-1}]
M	User-defined erosion parameter [kg.m^{-2}.s^{-1}]
$S(\tau_{cw}, \tau_{cr,erosion})$	Erosion step function:

$$S(\tau_{cw}, \tau_{cr,erosion}) = \left\{ \begin{matrix} \left(\frac{\tau_{cw}}{\tau_{cr,erosion}} - 1 \right), & when\, \tau_{cw} > \tau_{cr,erosion} \\ 0 & , when\, \tau_{cw} < \tau_{cr,erosion} \end{matrix} \right\}$$

(Eq. 2.5)

D	Deposition flux [kg.m^{-2}.s^{-1}]
M	User-defined erosion parameter [kg.m^{-2}.s^{-1}]
w_s	Sediment settling velocity [m. s^{-1}].
c_b	Average sediment concentration near bottom [kg.m^{-3}]

$$S(\tau_{cw}, \tau_{cr,deposition}) = \left\{ \begin{matrix} \left(\frac{\tau_{cw}}{\tau_{cr,deposition}} - 1 \right), & when\, \tau_{cw} > \tau_{cr,erosion} \\ 0 & , when\, \tau_{cw} > \tau_{cr,erosion} \end{matrix} \right\}$$

(Eq. 2.6)

τ_{cw}	Maximum bed shear stress due to current and waves.
$\tau_{cr,erosion}$	User defined critical erosion shear stress [N. m^{-2}]
$\tau_{cr,deposition}$	User defined critical deposition shear stress [N. m^{-2}]

Erosion and deposition terms are finally used as bed boundary conditions;

$$-w_s . C - \varepsilon_{s,z} \frac{\partial C}{\partial z} = D - E\,,\ at\, z = z_b \qquad \text{(Eq. 2.7)}$$

The formulation requires the specification of erosion and deposition shear stresses.

2.3. Delft3D model setup

This section provides an overview of the settings used to undertake the sediment transport modelling. The model configuration established for this study is the result of the physical and computational priorities. Although not detailed here, a long process of calibration was required to reach agreement or, at least, consensus with the morphological patterns described in the literature and depicted within the surveyed bathymetric changes.

2.3.1. Hydrodynamic model

Poverty Bay is characterised by moderate to highly stratified waters due to important fresh water discharges from the Waipaoa and Turanganui Rivers. Therefore, we used the 3D mode in Delft3D to replicate both the baroclinic and the barotropic dynamics within Poverty Bay. Similar baroclinic modelling approaches have previously been carried out in Black et al. (1997) and Moriarty et al. (2015). The model grid consisted in ten *sigma* layers (scaled pressure levels) in the vertical direction focused on both the surface and the near-bottom levels to better reproduce wave – current interactions and sediment transport processes.

The model curvilinear grid given in Figure 2.2, and includes northern Poverty Bay from the Wherowhero lagoon to south Titirangi Park near Tuaheni Point. The model resolution ranged from 7 m to 120 m, with higher resolution around Eastland Port and the Waipaoa River mouth. The deepest area over the domain was located along the south-eastern section of the seaward boundary and did not exceed 25 m (Figure 2.3).

Bed shear stresses were computed in the model using a quadratic friction law. The non-linear enhancement of the bed shear stresses in the presence of waves was taken into account by means of the wave-current interaction model of Fredsøe (1984). 3-Dimensional turbulence effects were modelled using a k-Epsilon scheme. The optimal value of the background horizontal and vertical viscosity coefficients depends essentially on the model grid and the hydrodynamics of the studied region (Deltares, 2017a). The background vertical viscosity coefficient is generally much lower than the background horizontal viscosity coefficient. For region with strongly stratified flow such as Poverty Bay, using a background vertical viscosity allows damping out short-period oscillations generated over the domain (Giardino et al., 2011). Here, we determined that background horizontal and vertical coefficients set to 0.14 $m^2.s^{-1}$ and 0.0001 $m^2.s^{-1}$, respectively, provided satisfactorily results.

The bottom roughness distribution was defined following the depth-dependant Manning's formulation. The Manning coefficients of roughness for the longitudinal and transverse components typically range from 0.01 for a clean and smooth bed to 0.06 for a rocky sea bed with debris and/or vegetation. Constant value of 0.018 for both components showed reasonable results when comparing the near-bottom current velocities in the model against measurements. The results of the hydrodynamic validation are provided in Section 3.1.

In the absence of dominant tidal flows over Poverty Bay, we preferred applying weakly reflective Riemann boundary conditions (Engquist and Majda, 1977, 1979; Verboom and Slob, 1984; Verboom and Segal, 1987) rather than water elevation or current conditions at boundaries. The Riemann boundaries typically improve the model stability when feeding the hydrodynamic model with the wave forces computed by SWAN, and limit the propagation of artificial disturbances over the model domain. The formulation of the Riemann boundaries are detailed in Deltares (2017a).

Salinity was explicitly prescribed to the model as it dominates vertically the density structure (Black et al., 1997; Stephens et al., 2001; Beamsley, 2003). Although the thermocline tends to reduce somewhat water mixing near the river mouths, the effect of the temperature in Poverty Bay is secondary (Black et al., 1997). We thus considered that the non-inclusion of temperature into the model was coherent, since the effect of temperature gradients on the hydrodynamics was implicitly taken into account through the flow conditions prescribed at boundaries. The background horizontal and vertical diffusivity coefficients were set to 1.8 $m^2.s^{-1}$ and 0.001 $m^2.s^{-1}$, respectively.

The wind-driven circulation was included in the model through the boundary conditions extracted from the SCHISM hindcast described in MetOcean Solutions (2017a). No explicit wind fields were prescribed at the model atmospheric – ocean interface given the limited extent of the domain.

The set value for the numerical time step was 2.4 s based on a Courant stability criterion lower than 10 in Delft3D (Deltares, 2017a). A smoothing time of 30 min was used to prevent introduction of short wave disturbances into the model during the spin-up phase.

A summary of the Delft3D settings applied for this study is provided in Section 2.3.4.

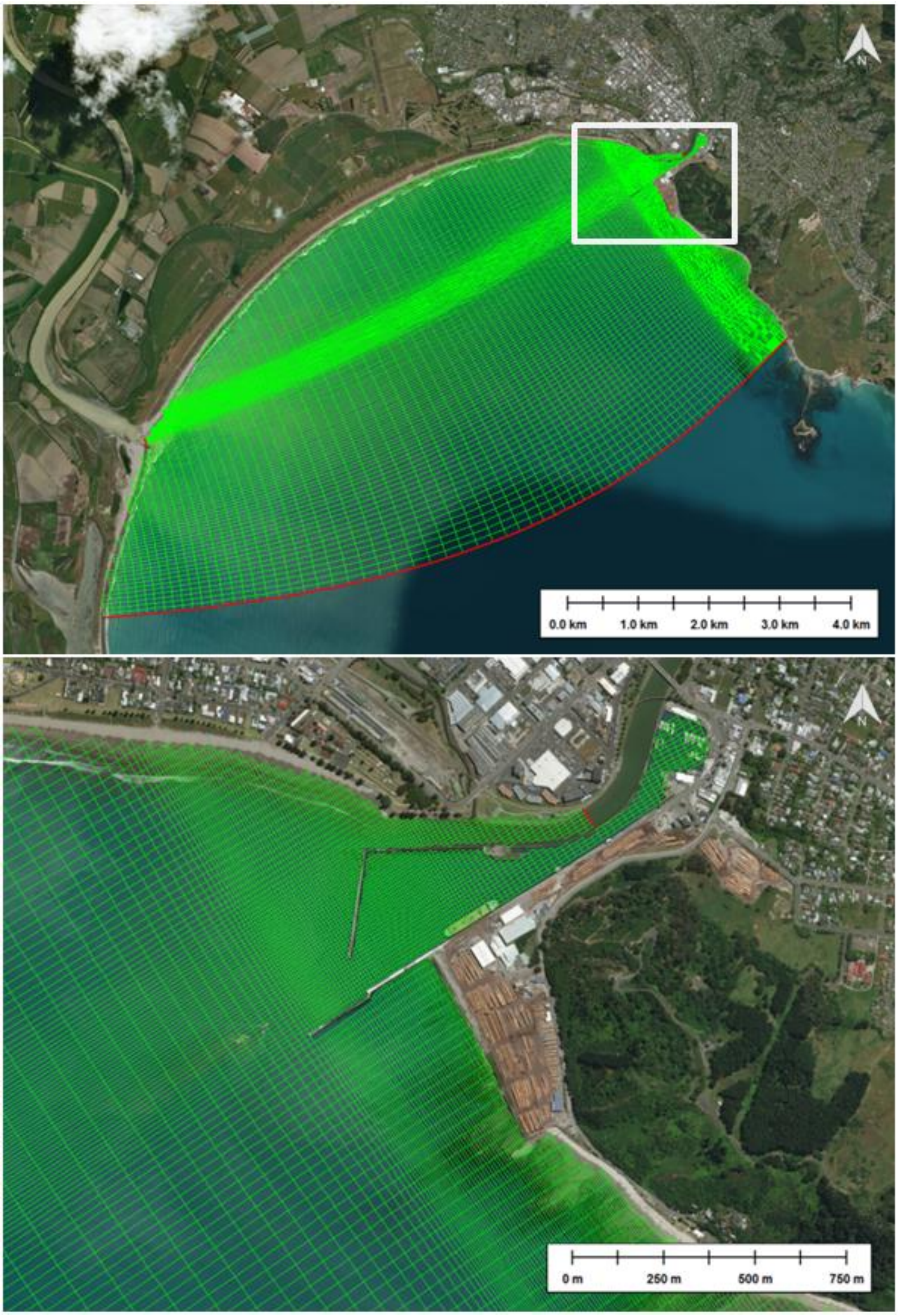

Figure 2.2 Map showing the Delft3D – FLOW and MOR grids used to replicate the hydro- and morpho-dynamics over northern Poverty Bay and Eastland Port. The resolution of the grid ranged from 7 m to 120 m. Model open boundaries characterised by inflows and sediment discharges are indicated by red lines.

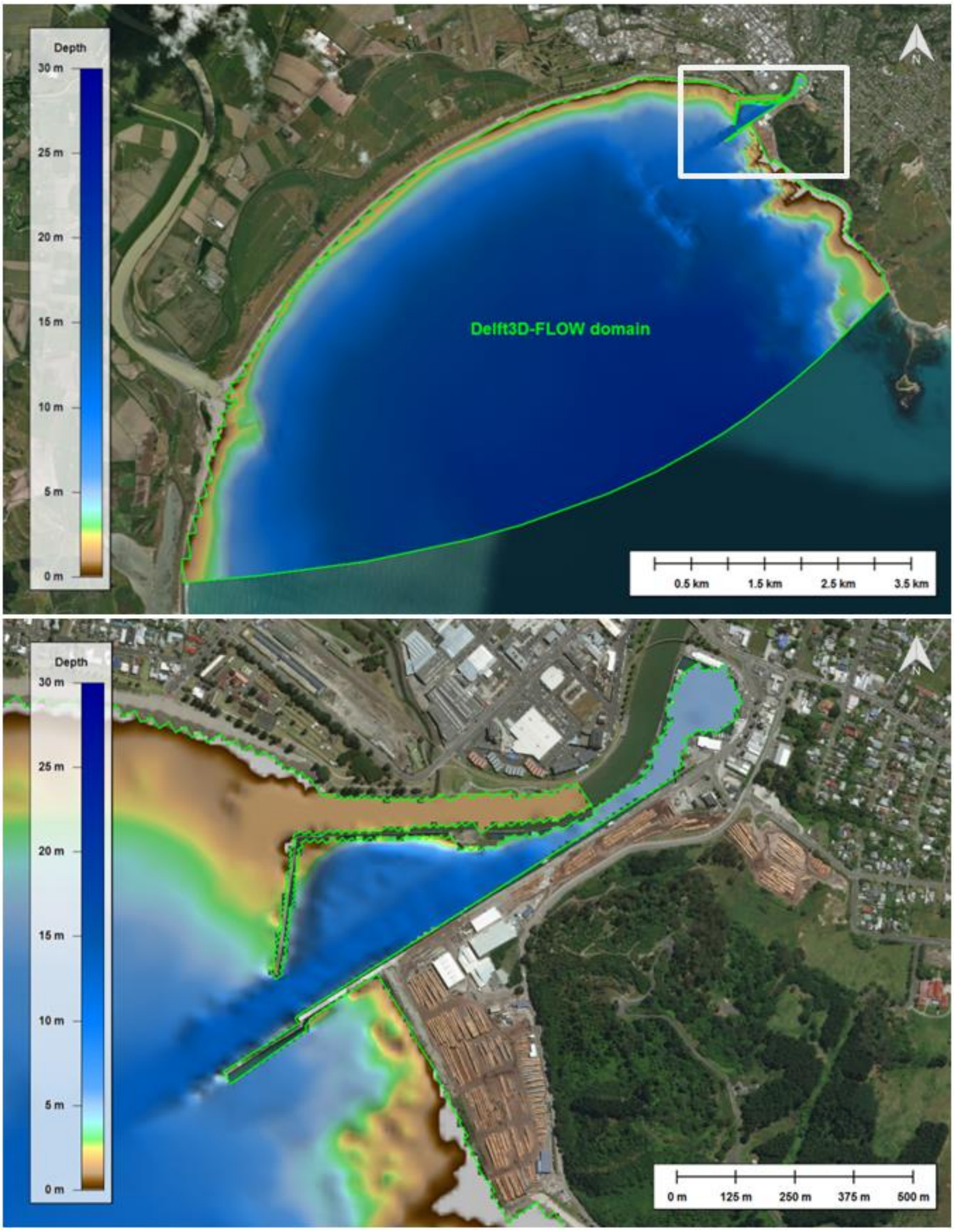

Figure 2.3 Map showing the Delft3D – FLOW bathymetry used to simulate the morphological dynamics at Eastland Port. The green polygon delimits the Delft3D – FLOW model domain

2.3.2. Wave model

For the medium-term morphological modelling, we applied a three-level nesting approach allowing the retention of spatial variability in the incident wave field due to large scale regional refraction and sheltering effects. Open-boundary conditions were prescribed using constant wave parameters (significant wave height, peak period, peak direction and directional spreading) associated with each simulated scenario. The regional wave grid extended approximately 120 km offshore from Hawkes Bay (southern boundary) to Waiharehare Bay (northern boundary) with resolutions ranging from 600 m to 6000 m (Figure 2.4). The intermediate grid characterised by resolutions in the range 60 m to 200 m covered the entire Poverty Bay.

At the same time, a short-term historical simulation was also performed combining a two-level nesting approach with 2D spectral conditions provided hourly by the embedded wave model described in MetOcean Solutions (2017b). This coincided with the interval of the sequential two-way coupling between SWAN and Delft3D – FLOW that allows the exchange of relevant parameters on curvilinear model grids via a communication file. Wave parameters and forcing terms associated with the wave radiation stresses computed by SWAN were read by the Deflt3D – FLOW module to model the hydrodynamic conditions. At the end of each assigned 60 minutes runtime, bottom elevation, water level and current fields were used as input into SWAN. The model looped through these sequential module applications until the end of the complete simulation. Morphodynamic modelling was thus performed through the implementation of a fully coupled wave – hydrodynamic system based on wave and current interactions.

Bottom friction was modelled using the formulation of Collins (1972) with a coefficient of 0.015. The depth induced breaking followed the formulation of Battjes and Janssen (1978) with the coefficients *Alfa* = 1 and *Gamma* = 0.73 (default values). Diffraction typically makes the SWAN model unstable for very fine resolutions (Enet et al., 2006) and as such diffraction was not accounted for. The exclusion of diffraction is only likely to be relevant within the swinging basin, but is not expected to significantly alter the modelled outcomes as infilling processes within Eastland Port are essentially controlled by current-induced sediment transport and diffusion processes.

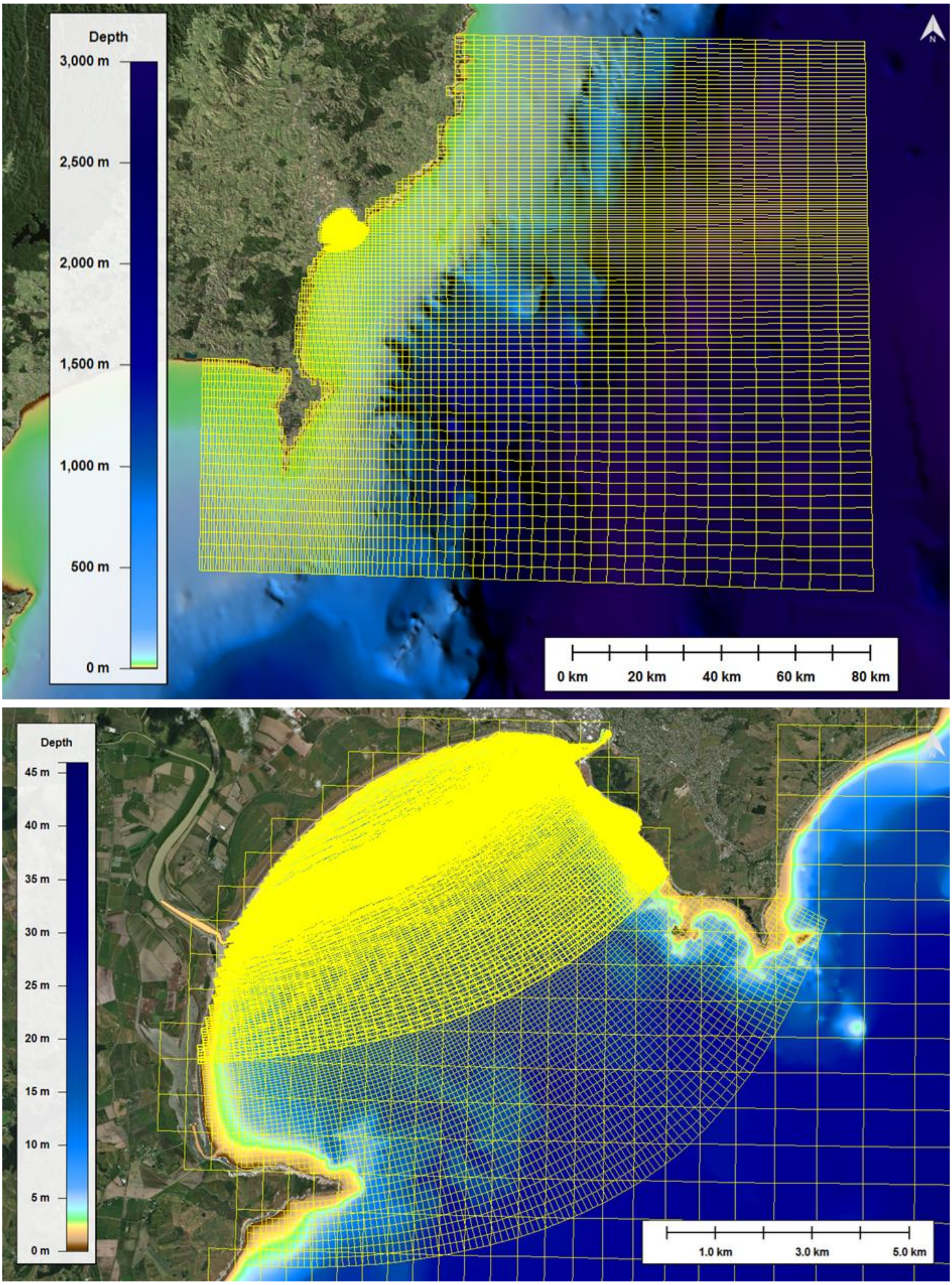

Figure 2.4 Map showing the three-level nesting strategy applied in SWAN (Delft3D – WAVE) to replicate the wave dynamics over Poverty Bay and Eastland Port. The resolution of the finest grid ranges between 7 and 120 m, with a particular focus on Eastland Port. The intermediate and coarse grid resolutions range between 60 – 200 m and 600 - 6000 m, respectively.

2.3.3. Morphological model

Morphological modelling approach

Two strategies are generally considered when applying process-based morphodynamic models in coastal regions. The first approach is based on dynamic equilibrium and consists in initialising the sediment availability and bed composition imposed by hydrodynamics. A bed stratigraphy scheme is used to redistribute a range of grain size fractions vertically between layers (i.e. Van der Wegen et al., 2011). This strategy is generally used for long-term process studies (decades to centuries) to limit unrealistic divergence that can occur due to uncorrected non-linear feedbacks between waves, currents and morphology.

For the second approach the sediment availability and characteristics are “manually” defined over the domain using *in situ* data. This approach may lead to unrealistic divergences between the hydrodynamic conditions and the sea bed composition. The erosion rate can become the limiting factor regarding the overall sediment dynamics, particularly for fine-sized particles. To ensure realistic erosion rates of material in shallow waters, a careful process of calibration is required to limit the formation of unrealistic morphological patterns over time, particularly when using thick surficial sediment layers.

The considerable efforts undertaken over the last decades to investigate the sediment dynamics within Poverty Bay allowed gathering a large amount of information related to the coastal characteristics. This information has been fully exploited here to initialise the morphological model as realistically as possible, dealing with constraints imposed by limited computational resources. In this context, the second approach proved valuable for replicating realistic morphological patterns near Eastland Port.

Multi-grain-size model

Poverty Bay is characterised by five surficial sediment textural types described in Beamsley (2003) as follows:

- Well sorted sands near the beaches
- Moderately well sorted silty-sands covering most of the bay
- Moderately well-sorted silty-sands with more clay in the southern corner of Poverty Bay
- A patch of finer sediment near Young Nick’s Head
- Poorly sorted material in and adjacent to the dredge spoil mound

Surficial sediments are comprised of predominantly fine sand and mud (silt and clay) in the bay and Eastland Port, while medium to coarse sands are found near the Waipaoa river mouth and beaches. A silt-mud blanket with percentage of mud higher than 50% is found at 15 m deep in Poverty Bay and extends offshore to the continental shelf margin (Miller, 1981; Kensington, 1990; Sander, 1993; Foster and Carter, 1997; Beamsley, 2003).

Here, we set up the morphological model using mud, fine-grained and medium-grained sand sediment classes. The spatial distribution of the sediments initialised in the morphological model are given in Figure 2.5, Figure 2.6 and Figure 2.7. The exclusion of both the clay and the coarse-grained sand classes from the morphological modelling, which aimed to economize computational run-time, was motivated by their relative low availability over the domain. Note however that the consolidation effect that clay particles provide to the surficial sediment layer was indirectly taken into account through the critical bed shear stress calculation. Moreover, most of the riverine suspended-clay load is transported away from the bay as shown in Moriarty et al. (2015). Limitations due to the initial seabed composition are discussed in Section 3.

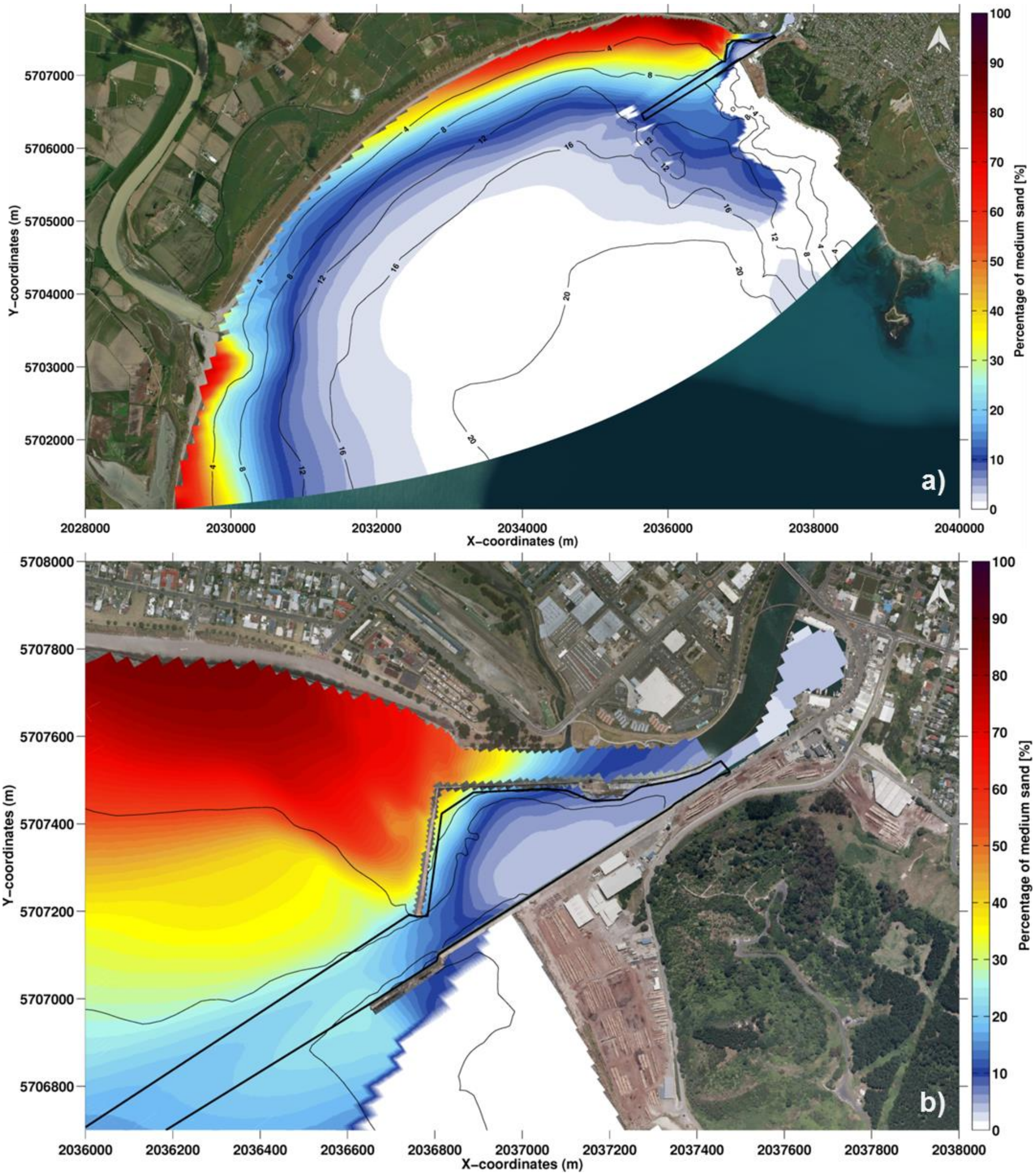

Figure 2.5 Initial spatial distribution of the percentages of medium sand (D50 set to 250 µm) contained in the surficial bed layer over Poverty Bay (a) and Eastland Port (b) in the model. The black polygon delimits the area used to estimate the infilling rate after one year.

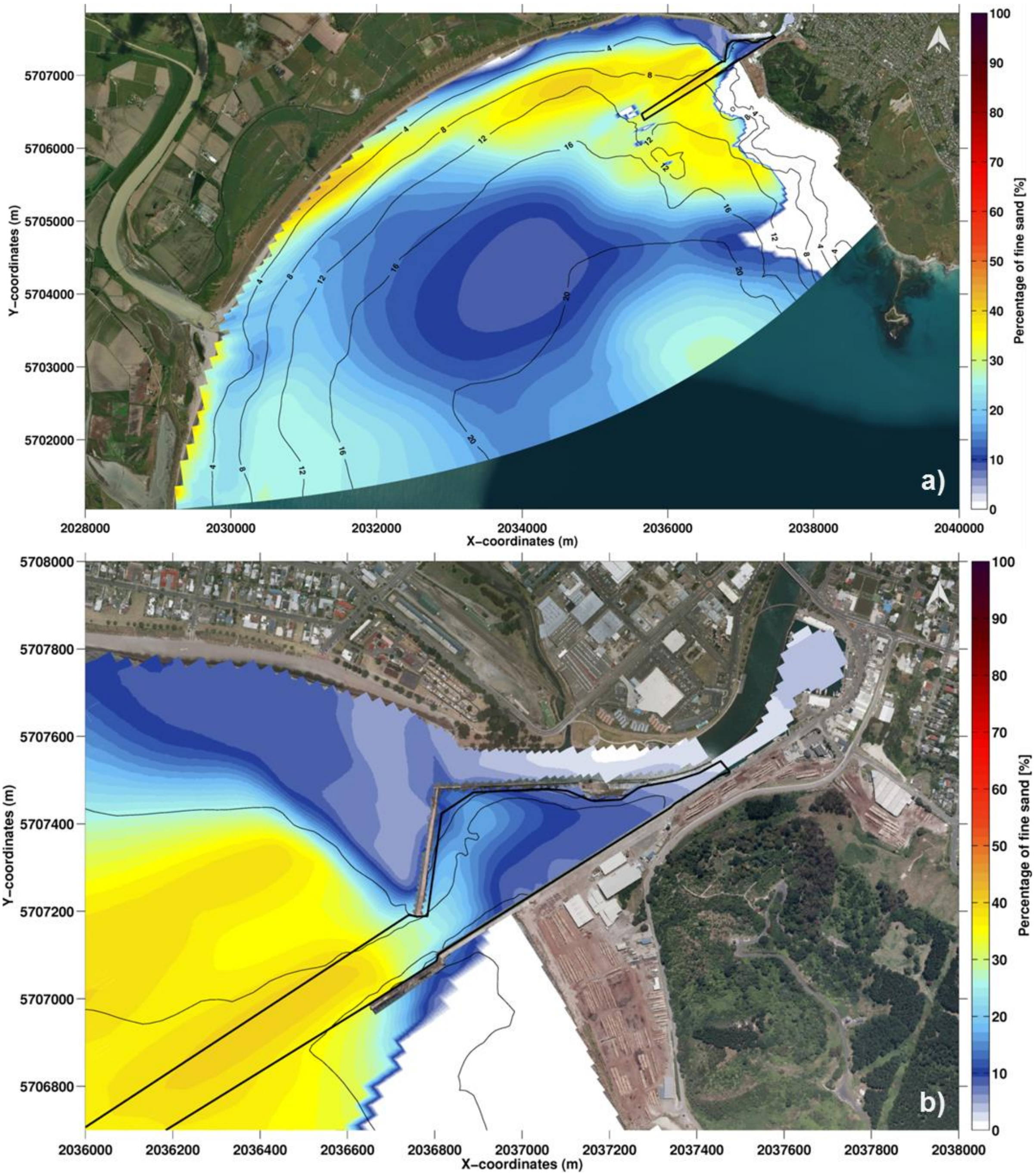

Figure 2.6 Initial spatial distribution of the percentages of fine sand (D50 set to 140 µm) contained in the surficial bed layer over northern Poverty Bay (a) and Eastland Port (b) in the model. The black polygon delimits the area used to estimate the infilling rate after one year.

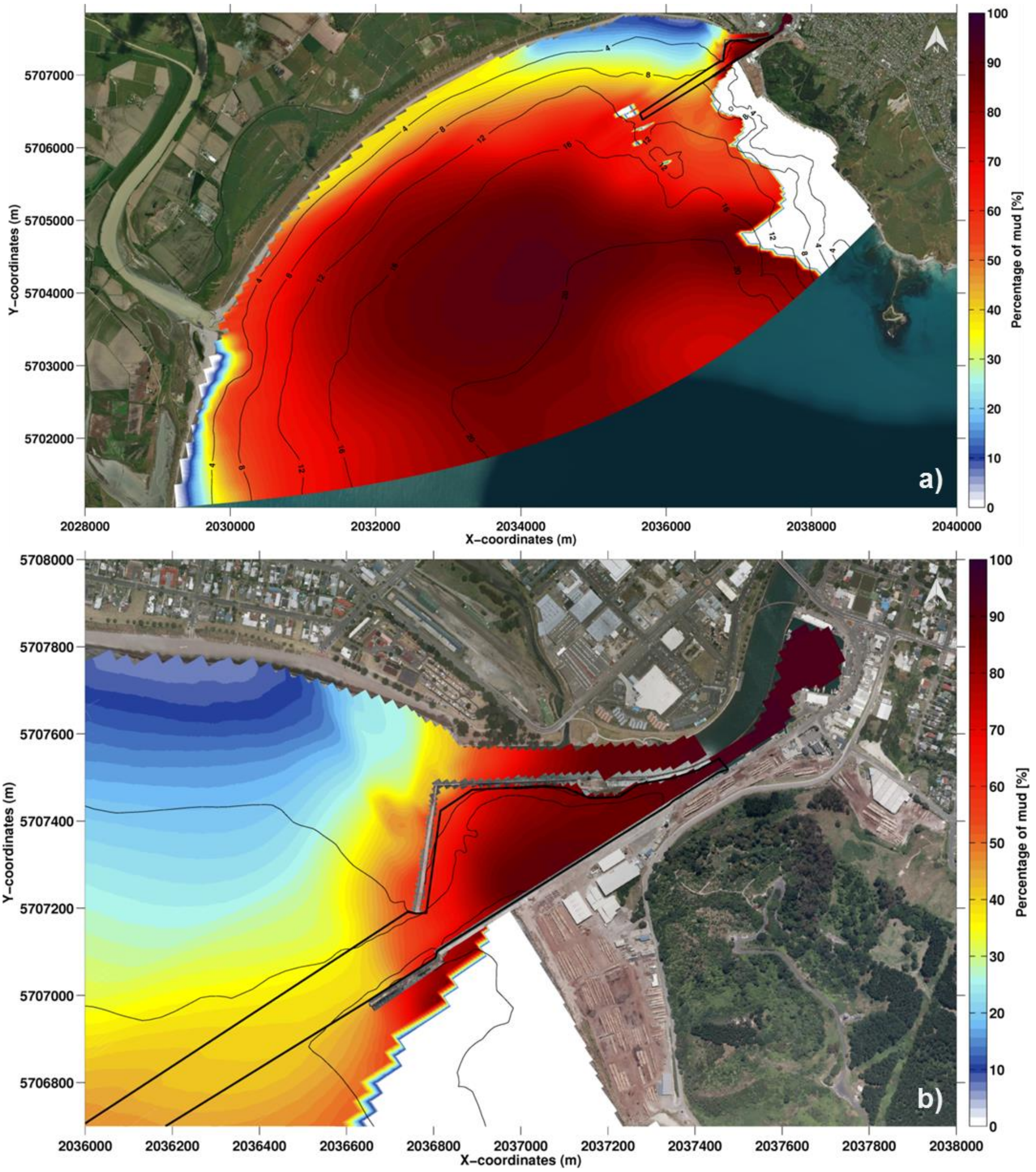

Figure 2.7 Initial spatial distribution of the percentages of cohesive mud contained in the surficial bed layer over northern Poverty Bay (a) and Eastland Port (b) in the model, white areas delineates the approximate rocky reef substrate. Fresh and saline settling velocities were set to 0.05 mm.s^{-1} and 0.65 mm.s^{-1}, respectively. The black polygon delimits the area used to estimate the infilling rate after one year.

Transport of non-cohesive and cohesive sediments

For non-cohesive sediments, the TRANSPOR2004 sediment transport predictor described in Van Rijn et al. (2004) was used rather than the default predictor (Van Rijn, 1993) due to recalibration against new data and the extension of the model to incorporate the wave zone. The computed sediment transport vectors were then relocated from water level points to velocity points using an upwind computational scheme to ensure numerical stability.

The formulation of Bagnold (1966) was applied for resolving the longitudinal slope effect. Following the Delft3D guideline, we set the bed gradient factor (*AlfaBs*) to 1 (default). The formulation of Ikeda (1982, 1988) presented by Van Rijn (1993) was used to simulate the transverse bed slope effect. *AlfaBs* was of lesser importance in model calibration compared with the transverse bed gradient factor *AlfaBn* which can cause unrealistic incision of channels (Van der Wegen and Roelvink, 2008; Dastgheib, 2012; Dissanayake et al., 2012). The default value (*AlfaBn* = 1.5) commonly leads to unrealistic channel slope with gradients larger than the angle of repose. Therefore, we preferred to set the transverse bed gradient factor to 50 as validated in Walstra et al. (2004).

The transfer of cohesive sediments at the water – sea bed interface was calculated using the Partheniades – Krone formulations (Partheniades, 1965). These formulations depend on numerous parameters that need to be carefully set up. While some of them can be transposed from one study to the other, others are inherent to the current system and have to be carefully calibrated.

The reference density (for hindered settling), the specific density and the dry bed density specific to silt particles were set to 1600, 2650 and 500 kg.m^{-3}, respectively. These values are commonly used assuming equivalent quartz density with a porosity of 0.4 and a light sandy mud.

We calibrated the erosion parameter (*E*) used in the Partheniades (1965) – Krone formulations comparing the estimated and the predicted channel infilling rates. The best model performance was reached for *E* set to 0.0045 kg.m^{-2}.s^{-1}.

The erosion of dry cells was turned on (*ThestSD = 0.5)* allowing the dry beach to partially erode when there is erosion just underwater. Several values for the total and wave-related suspended and bed-load transport factors (*Sus*, *Bed*, *SusW*, *BedW*) were tested. The morphological model showed coherent results for values of *Sus*, *Bed*, *SusW*, *BedW* set to 1, 1, 0.5 and 0.5, respectively. The choice of *Bed* and *BedW* had little influence on the model outcomes due to the cohesive sediment tractions not being subjected to bed-load transport in Delft3D.

Sediment supplies

The Waipaoa and Turanganui rivers drain tertiary and mudstone hill-country catchments of 2200 km^2 and 220 km^2, respectively (Griffiths and Glasby, 1985; Smith, 1988). The fluvial load of both rivers is primarily silt mud (Hicks et al., 2004; Orpin et al., 2006). The sandy bed load was estimated to be about 1% of the suspended load of the Waipaoa River (Healy et al., 2002). No information related to the suspended load composition of the Turanganui River is available. Both catchments areas have similar substrate compositions and terrain characteristics; therefore, it is likely that the suspended load composition will be similar for both rivers.

.

It is estimated that the Waipaoa and Turanganui rivers deliver an total of $12.1\text{x}10^6$ tonnes.year^{-1} and $0.69\text{x}10^6$ tonnes.year^{-1} of suspended sediment into Poverty Bay, respectively (Griffiths and Glasby, 1985; Gisborne District Council, 1994; Beamsley, 2003). The amount of discharged sediments by bed load is estimated to be approximately $0.2\text{x}10^6$ tonnes.year^{-1} and $1.25\text{x}10^6$ tonnes.year^{-1} for both rivers in summer and winter, respectively (Foster and Carter, 1997). In the absence of continuous measured suspended-sediment concentrations (*SSC*), empirical relationships between river discharges (*Q*) and suspended-sediment concentrations (SSC) described in Hicks et al. (2000) and Beamsley (2003) were applied to estimate the Waipaoa and Turanganui river loads (Figure 2.8). The respective time-series of estimated SSC are given in Figure 2.9. The sediment discharge associated with both rivers consisted in 99% of mud and 1% of sand consistent with the numerical modelling carried out by Moriarty et al. (2015). The supplied sand fraction was equally divided into medium and fine grain sizes. Beamsley (2003) estimated the background ambient SSC from 0.06 to 0.1 kg.m-3 over northern Poverty Bay. To preserve the model from unrealistic accretion processes, inputs of mud particles were prescribed along the model seaward boundary based on a background ambient SSC of 0.02 kg.m-3. This assumes that the majority of turbid water is derived from fluvial inputs within the bay. Although coastal erosion processes generate a suspended-transport of sand particles, the input of sand particles were not included in the present study.

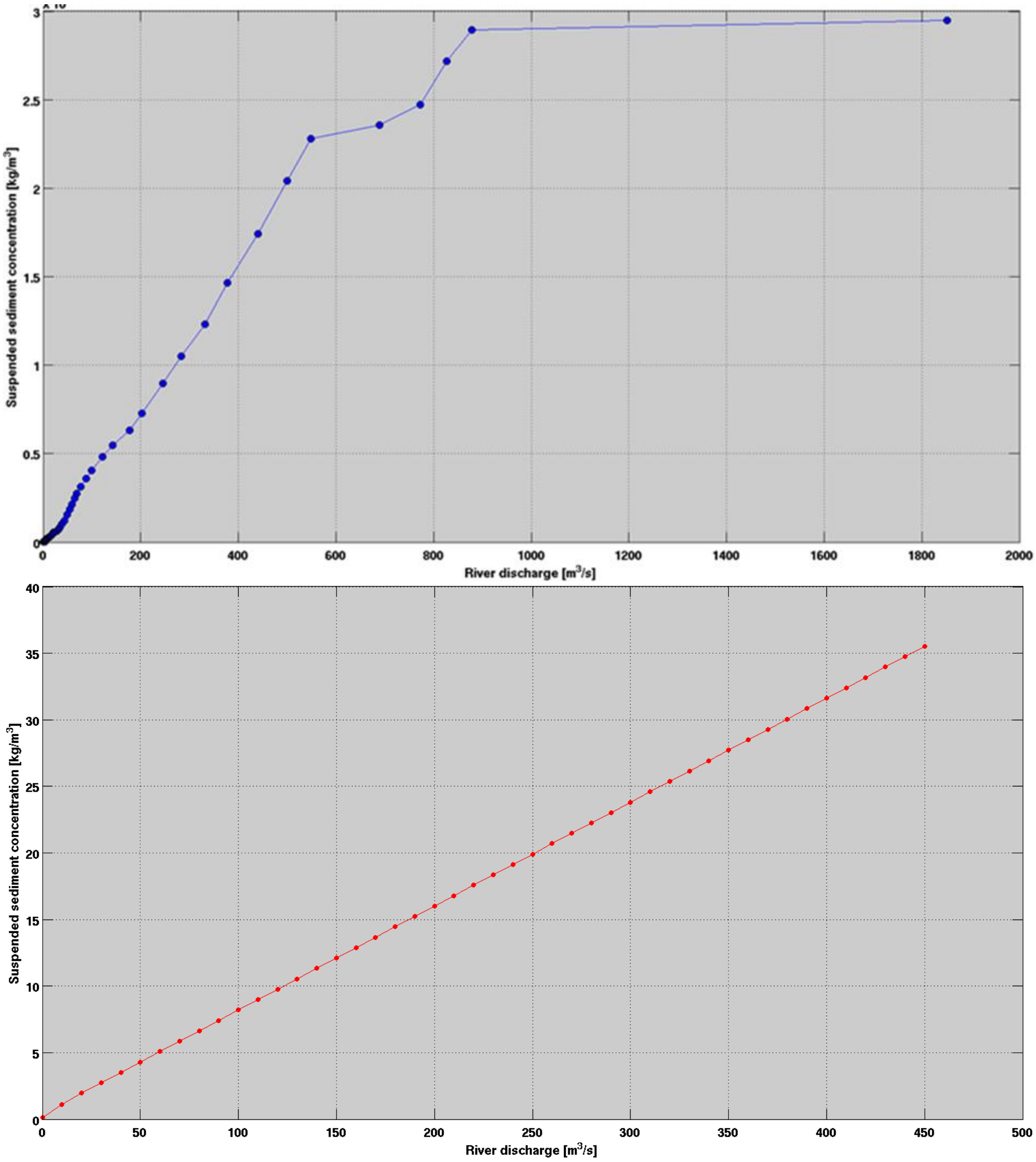

Figure 2.8 Empirical relationship between river discharges (Q) and suspended-sediment concentrations (SSC) associated with the Waipaoa (top) and Turanganui rivers (bottom) as described in Hicks et al. (2000) and Beamsley (2003).

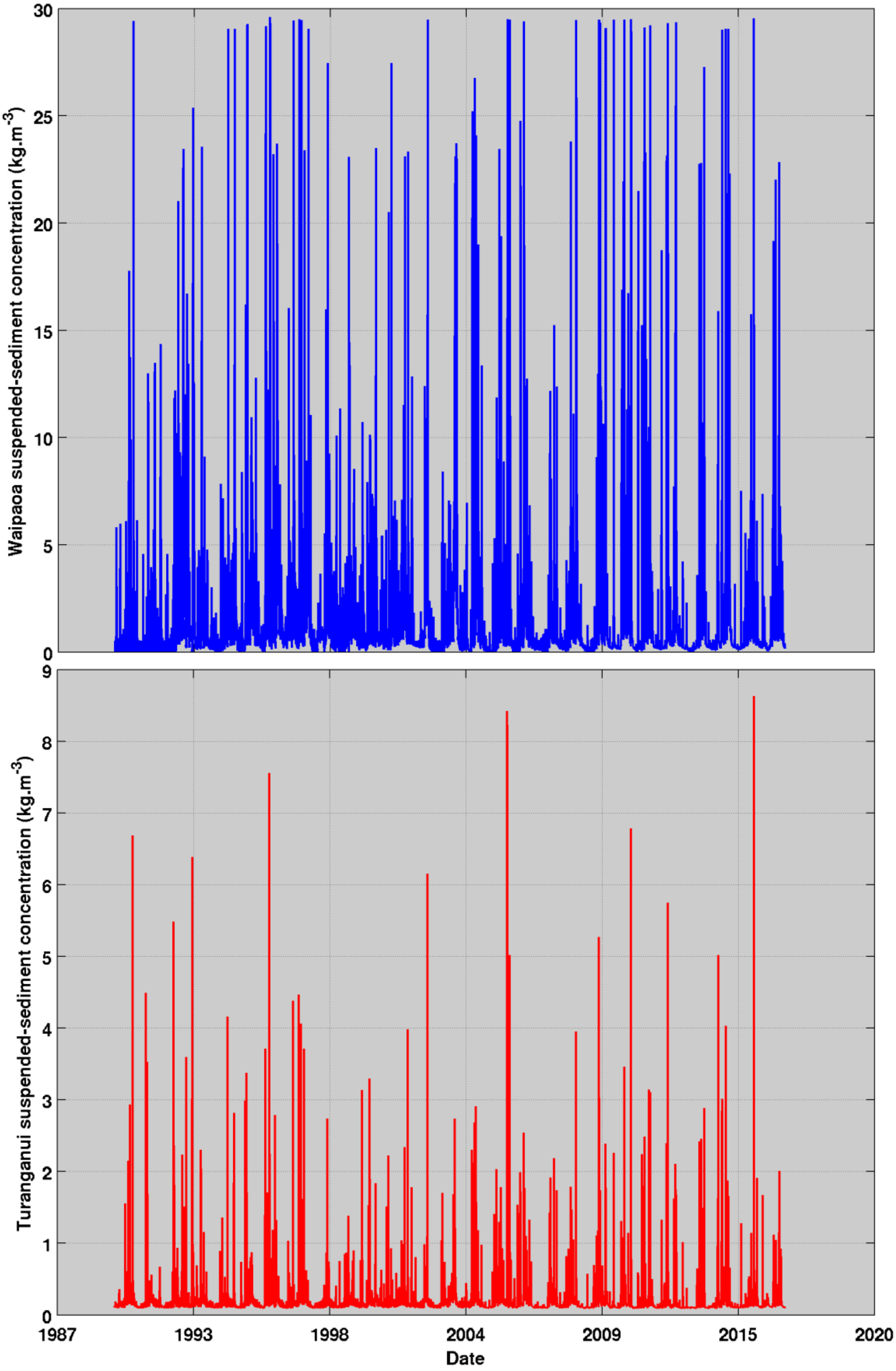

Figure 2.9 Time series of the estimated suspended-sediment concentrations (SSC) associated with the Waipaoa (top) and Turanganui rivers (bottom). The empirical relationships described in Hicks et al. (2000) and Beamsley (2003) between the rivers discharges and the SSC were used for the estimation.

Critical shear stress and settling velocity for cohesive sediment

Cohesive sediment transport and deposition are not only influenced by the combined effect of waves and currents but also by space- and time-varying sediment properties. Flocculation and consolidation of mud-sand mixtures make the prediction of sediment dynamics particularly challenging. While flocculation leads to increasing settling velocities of aggregated particles through the water column, sea bed consolidation mechanisms also increase the critical shear stress for erosion of surficial sediments.

Northern Poverty Bay is characterised by mud-sand mixtures resulting from the fluvial discharges. Beamsley (2003) highlighted notable disparities in the surficial sediments shear strength depending on the distance from sediment sources (Turanganui River mouth or centre of dredge spoil ground), water depth, percentage of organic content and ratio between fine-grained sand and mud fractions. In this context, we found that using a spatially-varying critical bed shear-stress for erosion (τ_{ce}) specific to the mud class allowed balancing the erosion rates over the domain. The model critical bed shear stress was defined as a function of the water depth, the distance from the river mouths and the ratio of percent mud to sand (Eq. 2.8) as follows.

$$\tau ce_{(i,j)} = \left(\left(\tau ce_{firm} - \tau ce_{weak} \right) * \frac{dist_{(i,j)} + depth_{(i,j)}{}^{2}}{dist_{max} + depth_{max}{}^{2}} \right) + \tau_{weak} \qquad \text{(Eq. 2.8)}$$

where τce_{firm}, τce_{weak} were determined using Van Rijn (2016) as shown in Figure 2.10 (green solid and dash lines) for specific percentages of mud and fine-grained sand; In Eq. 2.8, $dist_{(i,j)}$ corresponds to the sum of distances from both river mouths and $depth_{(i,j)}$ corresponds to the water depth. The inclusion of the stabilising effect provided by organic contents in the model was not implemented due to both the lack of understanding around this mechanism and the constriction of data to the near-port areas. Figure 2.11 exhibits the initial critical bed shear stress field for erosion applied to the mud particles in Delft3D – MOR. Note that the calculation of this parameter was updated at the beginning of each medium-term modelling simulation. No update was implemented in the short-term historical simulations.

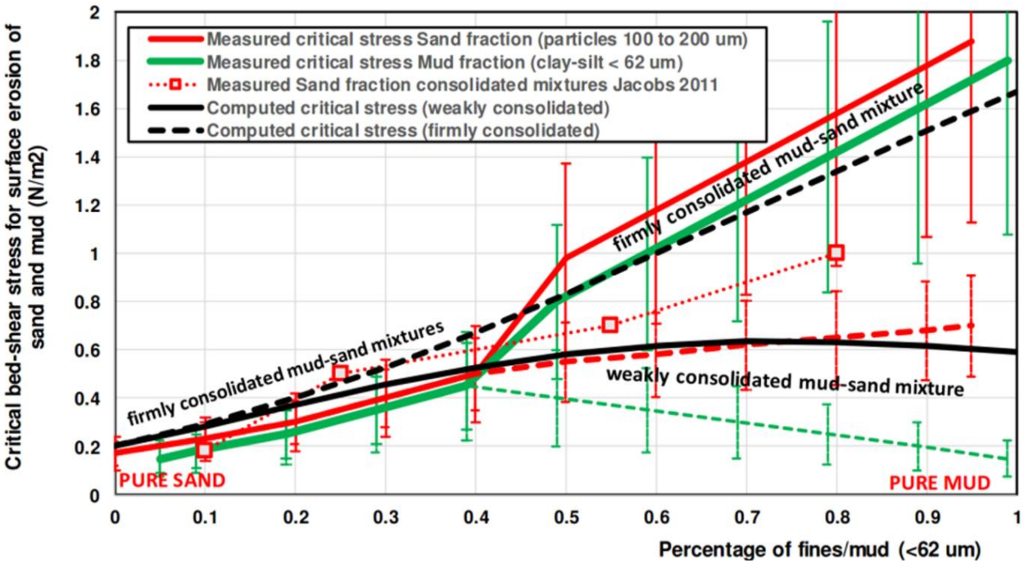

Figure 2.10 Empirical relationship between critical bed-shear stress for surface erosion and percentage of fine-grained sand/mud as described in Van Rijn (2016).

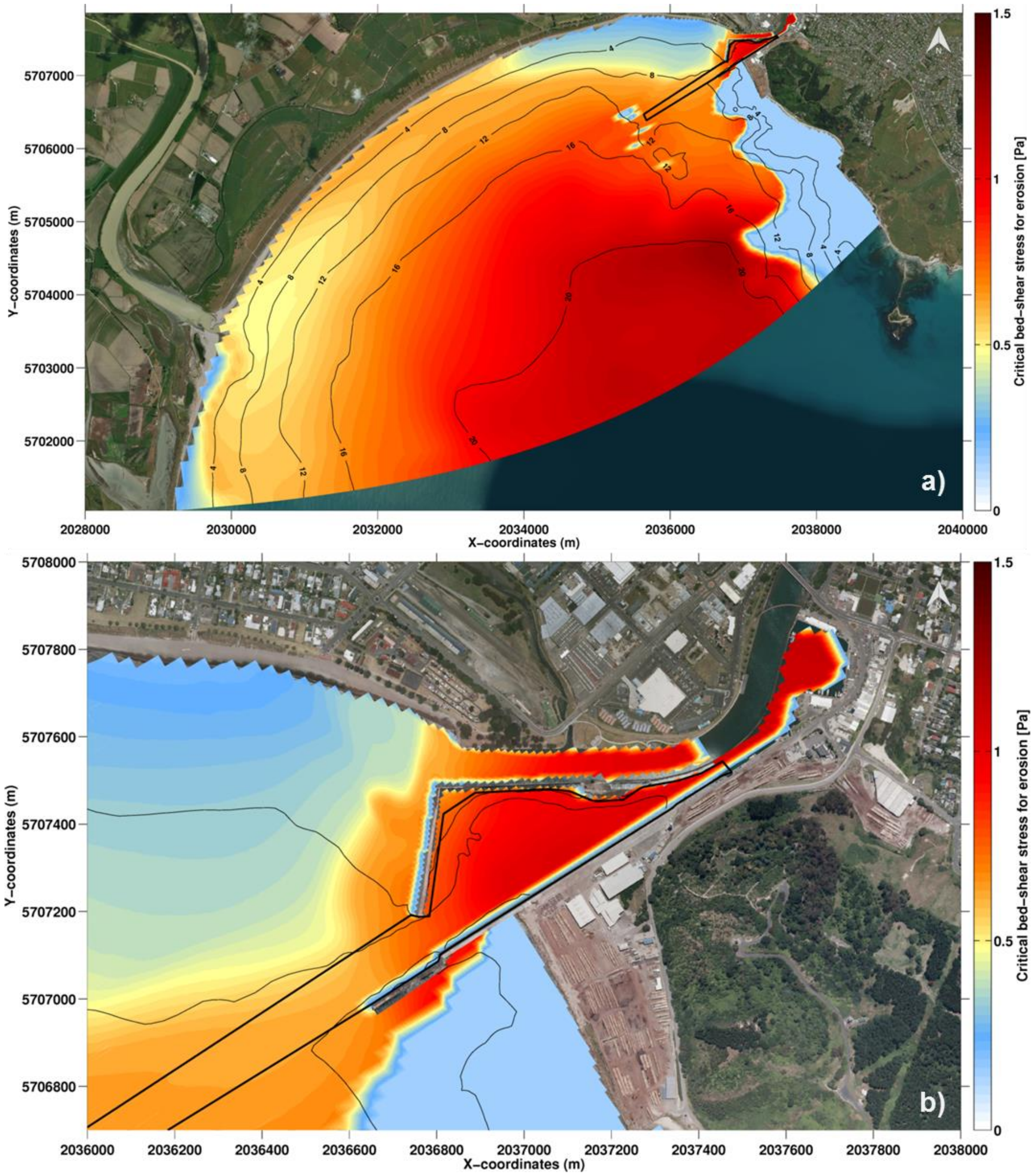

Figure 2.11 Initial critical bed-shear stress for erosion over northern Poverty Bay (a) and Eastland Port (b) applied to cohesive mud particles in the model. The black polygon delimits the area used to estimate the annual volumetric infilling rate in the channel.

The deposition of sediments is a process by which a sediment particle or floc settles to the seabed (Krone, 1993). While the existence of the critical shear stress for erosion (τ_{ce}) is largely accepted in the scientific community, the existing of the critical shear stress (τ_{cd}) for deposition is still being debated. In Delft3D, the critical shear-stress value for deposition is generally set to 1000 N.m^{-2} to avoid any depositional restriction. Recent studies using advanced instruments (Andersen et al., 2007; Shi et al., 2015) allowed determining values of *in situ* critical shear stress associated with the deposition (τ_{cd}) under natural environment. In these studies, τ_{cd} was typically ranging between 0.08 N.m^{-2} and 0.10 N.m^{-2}. Similar values were therefore tested during the model calibration. However, it is likely that limiting the deposition of material was not well adapted to the input reduction approach as suspended-sediments are reset at the end of each tidal cycle. For this reason, depositional restrictions were removed from the model settings. The critical bed shear stress for deposition was set to 1000 $N.m^{-2}$ as advised in the Delft3D guideline.

Estimating the settling velocity of sediment particles through the water column is a fundamental requirement when modelling sediment transport in coastal environments. While a large number of relationships for non-cohesive particles exist in the literature, estimating the settling velocity associated with cohesive particles remains extremely complex. Turbulence-induced aggregation and flock breakup processes induces great variations in time and space of the settling velocity. Many factors may influence these processes, such as salinity, *SSC*, proprieties of the mud-sand mixture etc.

A well-known technique for the numerical modelling of cohesive sediment transport is to define a large range of cohesive sediment classes characterised by different settling velocities. The main issue is therefore the important computational time that such approach requires, particularly for high-resolution 3D domains. For this reason, such an approach is generally implemented for 2-dimensional numerical modelling.

Here, we defined a unique cohesive sediment class characterised by settling velocities ranging between 0.05 $mm.s^{-1}$ and 0.65 $mm.s^{-1}$. These values were defined for salinity ranging between 0 and 35 PSU based on the results provided in Portela et al. (2013). The model was therefore able to partially simulate flocculation processes of suspended fine-grained sediments when salinity increases. Note however that many mechanisms affecting the settling velocity of flocculated particles are still poorly understood and were therefore excluded from the sediment transport modelling.

2.3.4. Summary of Delft3D model settings

The input parameters used in Delft3D – FLOW, WAVE and MOR (version 6.02.13.7545, 13 September 2017) to predict the sediment dynamics and morphology over northern Poverty Bay are summarised in Table 2.1 and Table 2.2. Note that many parameters existing in Delft3D are not explicitly defined in these tables. For these parameters, no calibration process was undertaken as they generally do not significantly influence the model results. Default values were therefore applied.

Table 2.1 Delft3D – FLOW and WAVE parameters used for the morphological modelling over northern Poverty Bay.

Parameter	Description	Value
Wave		
BedFriction	Seabed friction formulation	Collins (1972)
BedFricCoef	Collins's frictions coefficient	0.015
Breaking	Depth induced breaking model	TRUE (Battjes and Janssen, 1978)
BreakAlpha	Rate of dissipation	1
BreakGamma	Breaker parameter Hmax/h	0.73
WaveSetup	Wave-induced setup model	TRUE
Whitecapping	Dissipation by whitecapping	TRUE (Van der Westhuysen et al., 2007)
Hydrodynamics		
Dt	Computational time step [s]	2.4
DryFlc	Minimum depth for drying/flooding [m]	0.1
Vicouv	Horizontal background eddy viscosity [$m^2.s^{-1}$]	0.14
Dicouv	Horizontal background eddy diffusivity [$m^2.s^{-1}$]	1.8
Vicoww	Vertical background eddy viscosity [$m^2.s^{-1}$]	1.00E-04
Dicoww	Vertical background eddy diffusivity [$m^2.s^{-1}$]	1.00E-03
Rouwav	Model for bottom stress formulation due to combined wave and current action	#FR84# (Fredsoe, 1984)
Roumet Ccofu,Ccofv	Manning Coefficient [-]	#M# 0.018
Thick	Layer thicknesses [%]	[2 ; 3.5 ; 7 ; 12 ; 25 ; 25 ; 13 ; 7 ; 3.5 ; 2]

Table 2.2 Delft3D – MOR parameters used for the morphological modelling over northern Poverty Bay.

Parameter	Description	Value
Sediment transport		
Non – Cohesive Sediment (Sand)		
RhoSol	Sediment density [kg/m3]	2650
SedTyp	Sediment type	Sand
SedDia	Median sediment diameter (D50) [m]	1.4E-04 2.5E-04
CDryB	Dry bed density [kg.m^{-3}]	1600
IFORM	Sediment transport formulation	(TR2004, Van Rijn et al., 2004)
Cohesive Sediment (Mud)		
RhoSol	Sediment density [kg.m^{-3}]	2650
SedTyp	Sediment type [-]	Mud
WS0	Settling velocity in fresh water [m.s^{-1}]	5.0E-05
WSM	Settling velocity in saline water [m.s^{-1}]	6.5E-04
SalMax	Salinity for settling velocity [ppt]	35
TcrSed	Critical bed shear stress for sedimentation [N.m^{-2}]	1.0E+03
TcrEro	Critical bed shear stress for erosion [N.m^{-2}]	Space varying
EroPar	Erosion parameter [kg.m^{-2}.s^{-1}]	3.8E-03
Morphology		
AlfaBs	Streamwise bed gradient factor for bed load transport [-]	1
AlfaBn	Transverse bed gradient factor for bed load transport [-]	50
Sus	Multiplication factor for suspended sediment reference concentration [-]	1
Bed	Multiplication factor for bed-load transport vector magnitude [-]	1
SusW	Wave-related suspended sediment transport factor [-]	1
BedW	Wave-related bed-load sediment transport factor [-]	1
SedThr	Minimum water depth for sediment computations [m]	0.1
ThetSD	Factor for erosion of adjacent dry cells [-]	0.5

2.4. Numerical modelling scenarios

The main challenge when applying process-based models to predict coastal dynamics is that the morphology of coastal systems generally develops over time scales several orders of magnitude larger than the time scale of the hydrodynamic fluctuations driving the sediment transport (i.e. hours to days versus years to decades and more). This means that a model system that is able to predict the time series of instantaneous hydrodynamics and sediment transport will require a considerable computation runtime. Luijendijk et al. (2017) followed this approach simulating historical morphological changes over 1 year with Delft3D set up in depth-averaged mode (2-dimensional). Here, we expected unfeasibly long period of time using the 3-dimensional mode in Delft3D, not including the calibration process.

As an alternative, several strategies are commonly used to simplify and accelerate the modelling of medium to long term morphological evolution (i.e. De Vriend et al., 1993; Roelvink, 2006). The approach employed here combined the reduction of the input forcing with the use of morphological acceleration factors, which is one of the most commonly applied methods.

The accelerated morphological simulations were supplemented by a historical short-term simulation featuring storm conditions and high river discharges. Such historical simulation aimed to examine the variations in sediment fluxes due to high energy waves and river discharges. This allowed taking into account the non-linearity of the morphological patterns associated with the interactions between waves, currents and sediments. This also provided a basis to verify the reduced models overall robustness in terms of predicted net transport patterns and morphology.

2.4.1. Medium-term morphological modelling

The medium-term morphological modelling was performed based on the reduction of waves, tides, shelf flows and river discharges over two periods of 365 days. Input reduction essentially means selecting a limited number of representative forcing conditions that will reproduce the medium-term residual sediment transport patterns and associated morphological evolution (De Vriend et al., 1993). The morphological factor is a technique to improve computational efficiency by accelerating computed morphological evolution.

The selected periods extended from June 1998 to May 1999 and from June 2002 to May 2003 and were characterised, respectively, by 'La Niña' and 'El Niño' phases of 'El Niño – Southern Oscillation' (ENSO). 'El Niño' events typically strengthen the westerly flow over New Zealand increasing the chance of drought in the Gisborne region. By contrast, winds from the northeast often bring rain to the east coast during 'La Niña' phases. We considered appropriate modelling relatively low and high river discharge periods associated with 'El Niño' and 'La Niña' events to bracket the likely infilling that may occur at Eastland Port.

Tidal input reduction

Astronomical tides are deterministic and can therefore be accurately predicted for any period of time. However tidal oscillations exhibits significant long-term modulations (e.g. spring/neap, yearly and nodal cycles), which make chronological simulations of such cycles computationally demanding.

The basis for tidal input reduction is to find a representative tide that most closely reproduce the net and gross sediment transport as the naturally varying tides over the region of interest and for the time period considered. In the present study, the 'representative' tide was determined following the approach of Latteux (1995), which is commonly applied (e.g. Grunnet et al., 2004; Brown and Davies, 2009; Dastgheib, 2012).

Given the duration of the simulations (i.e. 1 year), the main concern was to capture the residual effects of the spring-neap oscillations, so a time period of 12 cycles (~1 year) or longer was considered necessary.

Tidal signals at a reference point located near the Eastland Port entrance were generated from a high resolution tidal constituents grid extracted from SCHISM, and time series of sediment transport were estimated using a simple power law $Q=A.u^{b}$ (*Q* is the transport flux, *A* is a constant factor, *u* is current velocity, *b*=5 following Engelund and Hansen (1967). The single tide best reproducing the net and gross transport magnitude was identified and used in the accelerated simulations. The representative tide is compared to M2 tidal signals in Figure 2.12.

Note that a four hour spin-up at flood stage with no morphological update was applied to initialise the 3-dimensional hydrodynamic conditions over the domain.

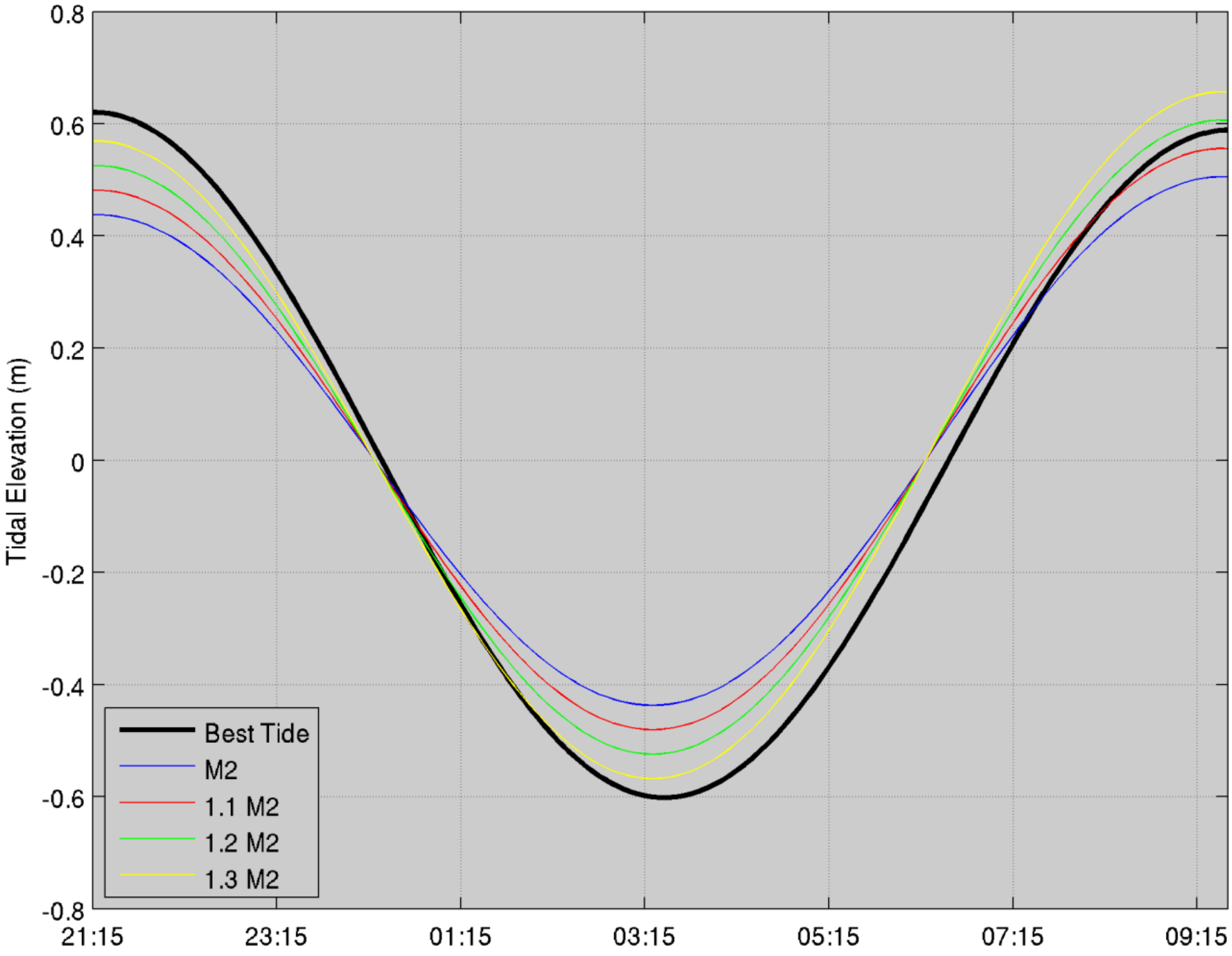

Figure 2.12 Comparison between the best representative tide, pure M2 tide, 1.1 M2, 1.2 M2 and 1.3 M2 tide curves at the control site located near the entrance to Eastland Port.

Wave input reduction

The objective of the wave input reduction was to define a set of offshore wave boundary conditions which reproduced the same residual sediment transport patterns and morphological evolution as the real time forcing over a given time period. The approach employed here followed the input reduction framework provided in Lesser (2009) and Walstra et al. (2013).

The first step was the selection of a reduction period, which is the length of real-time wave time series that is used to define the representative conditions. This is typically governed by the time scale of the morphological evolution of interest (e.g. monthly, seasonal, annual behaviour). In the present study, the reduction was undertaken based on a 1 year hindcast wave climate obtained from SWAN simulations to define an average annual wave climate. The wave conditions time-series was extracted at the middle of the eastern boundary of the coarse wave model domain.

In a second step, a set of representative wave classes was defined by distributing the discrete wave data points into a finite number of height and direction bins, and computing a representative value for each bin.

The basic method to determine a representative value within a bin is to use a weighted average of the data points by their frequency of occurrence:

$$F_{rep,j} = \frac{\sum_{i=1}^{n} f_i . F}{\sum_{i=1}^{n} f_i} \qquad \text{(Eq. 2.9)}$$

where *F* represents the wave height, period or direction, *f* is the frequency of occurrence of the wave condition *i* and *n* is the number of data points within a bin.

To account for the non-linear dependence of sediment transport on wave height, an additional weighting can be applied for the computation of the representative height:

$$H_{s,rep,j} = \left(\frac{\sum_{i=1}^{n} f_i . H_{s,i}^{p}}{\sum_{i=1}^{n} f_i}\right)^{1/p} \qquad \text{(Eq. 2.10)}$$

where *p* is the power to which the sediment transports are assumed to be related to the wave height. Typically *p* is set to 2 to 3. The exponent ensures that larger waves will have a relatively greater contribution in the computation of the representative wave height.

Here Eq. 2.10 was solved with a value of *p* = 2.5 which corresponds to the CERC formula for longshore transport (CERC, 1984) and is frequently used to estimate the morphological impact of waves. Associated representative periods and directions were determined using the same weighting as the wave height.

The initial wave data binning is relatively arbitrary and can be equidistant or non-equidistant (i.e. varying bin size). In the non-equidistant case, bins can be defined following either (subjective) scientific judgment or more objective approaches. Here, the height and direction bins were defined so that the relative “morphological impact of waves” was similar in each bin (Lesser, 2009; Dastgheib, 2012).

The morphological impact of waves of a given wave class was estimated according to:

$$M_j = p_j \,.\, H_{s,rep,j}^{2.5} \tag{Eq 2.11}$$

where p_j is the probability of occurrence of the bin j, and $H_{s,rep,j}$ the representative wave height of that bin (Lesser, 2009). Note that this is equivalent to “potential sediment transport” indicator used in Dastgheib (2012). To automate the determination of bin limits, this indicator was initially computed for a joint probability of wave height and direction with very fine equidistant bins (ΔH = 0.1 m, ΔDir = 2 deg.). Based on the number of directional and wave height bins to be used for the classification, the directional bin limits were determined first, in a way that the sum of the morphological impact of waves M_j within each bin was (approximately) equal. The same principle was then used within each of these directional bins to define the wave height bin limits. This way, the “morphological impact of waves” was similar in each bin.

The wave climate classification used in the following morphological simulations was defined using 2 directional bins and 3 wave height bins (Figure 2.13). The general classification obtained for the average annual wave climate at the reference site reproduced the two main groups of wave events from the south and southwest directions experienced at the site. Note that low-frequent swell events coming from the north and northwest octants were not considered in the medium-term morphological modelling. This is not expected to influence the morphological modelling results as the East Cape coastline orientation provides significant sheltering to Poverty Bay from northerly incident waves.

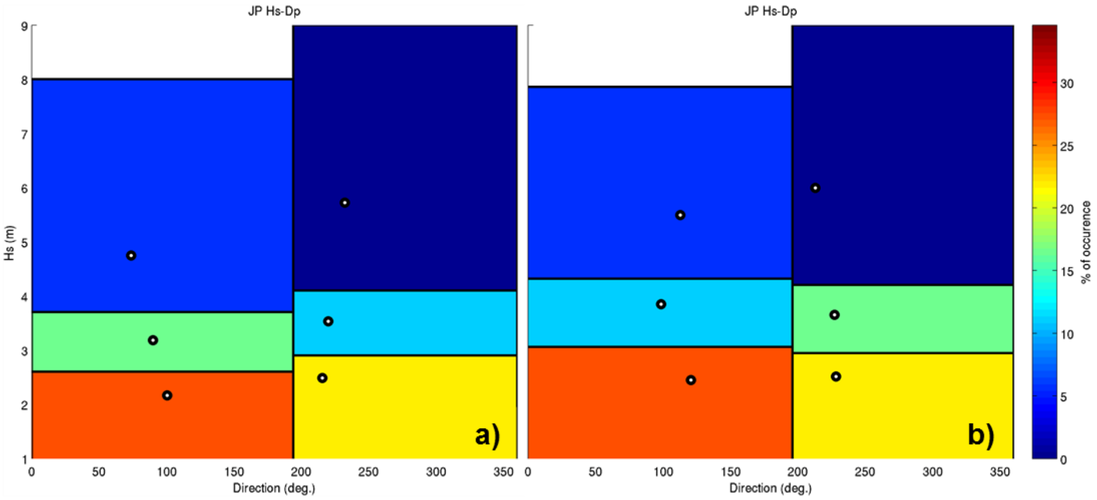

Figure 2.13 Reduced average annual wave climate based on the 1-year wave hindcast between June 1998 and May 1999 (La Niña; a), and between June 2002 and May 2003 (El Niño; b). The wave reduction was performed using two directional bins and three wave height bins (i.e. six wave classes). Colours indicate the probability of occurrence of a given class. The white dots are the representative wave condition of each wave class.

Shelf flow and river discharge reductions

The influence of the shelf currents on the inner Poverty Bay circulation has been largely described in Black et al. (1997) and Stephens et al. (2001). Northerly and southerly flowing shelf currents induce, respectively, clockwise and anticlockwise gyres in the bay during weak Waipaoa River discharge events. The ROMS model applied for the numerical modelling of the regional circulation showed good skills in replicating these patterns (MetOcean Solutions, 2017a).

From a morphological perspective, the shelf currents greatly influence the alongshore component of the sediment transport toward Eastland Port. During large river discharges and/or high energy wave events, important amounts of suspended-sediments may be released through the water column. Residual suspended-sediment transport fluxes are therefore mainly driven by the inner circulation and may lead to significant accretion of sediments into the channel over a relative short time period. Black et al. (1997) estimated the infilling rate from 690 to 2,000 $m^3.day^{-1}$ during storm to sever conditions, respectively.

The input reduction was extended to the shelf currents and river discharges to account for the range of physical processes that influence the sediment dynamics within Poverty Bay.

Time series of co-temporal shelf current directions and speeds to each representative wave condition periods were extracted from ROMS (MetOcean Solutions, 2017a) at a reference site (178.1897 E; 38.7837 S) located over the margin of the continental shelf. Periods characterised by southerly and northerly flowing shelf currents were identified and used to average the residual component of the currents in the SCHISM model (MetOcean Solutions, 2017a) at the Delft3D open-boundaries. At this stage, the input reduction approach consisted of twelve representative scenarios with specific wave and shelf-flowing currents patterns.

Smith (1988), Foster and Carter (1997), Hicks et al. (2000), Kniskern (2007) and Moriarty et al. (2015) showed that the Waipaoa River drains important amounts of sediments into Poverty Bay and over the adjacent continental shelf margin. The resultant influx of new fluvial material causes a progradation of the beaches into the bay. Although that influxes of fluvial material from the Turanganui river plays a major role in infilling the navigation channel (Beamsley, 2003), the input reduction was performed based on the time series of the Waipaoa river discharge (Q). We found this approach appropriate here since the correlation between the variations of both river discharges was approximately 81% over the simulated period.

Reduced-river discharges specific to each wave and shelf-current scenario were determined as follows:

- Low Waipaoa river discharge periods defined by Q lower than the 50th percentile of the discharge distribution.

- Moderate Waipaoa river discharge periods defined by Q higher than the 50th percentile and lower than the 98th percentile of the discharge distribution.

- High Waipaoa discharge periods defined by Q higher than the 98th percentile of the discharge distribution.

Note that the percentiles used for the identification of the low, moderate and high discharge periods were chosen arbitrary. In contrast to the wave-driven sediment transport, the effect of the river discharges on the model morphodynamic was relatively linear since no flocculation effect associated with *SSC* was included in the numerical modelling. In this context, the choice of the thresholds for the river input reduction was not expected to greatly affect the results.

At the end of the overall reduction process, thirty-six representative scenarios were finally generated to simulate the annual depth changes over northern Poverty Bay. Waves, shelf currents, river discharges, percentages of occurrence corresponding to each scenario are summarised in Table 2.3.

Morphological acceleration factor

The morphological acceleration factor (MORFAC) is a technique to bridge the gap between hydrodynamic and morphological timescales (Lesser et al., 2004). This technique consists in multiplying the calculated depth changes over a hydrodynamic time step $\Delta t_{hydrodynamic}$ by a constant factor f_{MOR}, effectively predicting morphological changes over a given period:

$$\Delta t_{morphology} = \Delta t_{hydrodynamic} \cdot f_{MOR} \qquad \text{(Eq. 2.12)}$$

Such an approach obviously has limits and involves many implicit assumptions. However it has been successfully applied on many studies to estimate medium-term morphological evolutions of tidal (e.g. Van der Wegen and Roelvink, 2008) and mixed tide and wave environments (e.g. Grunnet et al., 2004; Reniers et al., 2004; Lesser, 2009). This acceleration method was combined with the reduced tide and wave forcing outlined above to simulate the morphological evolution of the study area over an annual period (i.e. 365 days).

To account for the random phasing between waves, currents, river discharges and tides that occurs naturally, each of the representative conditions was simulated for the duration of one complete tidal cycle. A morphological acceleration factor specific to each class was defined so that the morphological duration of the class matches its probability of occurrence within the period considered.

The model system was run for each different class, one after the other, over a complete tidal cycle using the appropriate morphological factor (see Table 2.3). The final bathymetry, sediment fractions and bed thickness produced in the model outputs at the end of each simulation were used as initial inputs for the next simulation. Running each class separately rather than using time-varying forcing and *MORFAC* over a single continuous simulation suppresses any risk of discontinuities that can potentially develop in suspended sediment concentrations when the *MORFAC* are changed after a given class simulation (Lesser, 2009).

Table 2.3 Wave, shelf-current, river discharge, river suspended-sediment concentration, percentage of occurrence and morphological acceleration factor parameters specific to each simulated representative case from June 1998 to May 1999 (La Niña phase).

June 1998 – May 1999 (La Niña)											
Cases	H_s	D_p	T_p	**SPD$_{shelf}$**	**DIR$_{shelf}$**	**Q$_{Waip}$**	**SSC$_{Waip}$**	**Q$_{Turang}$**	**SSC$_{Turang}$**	**Occ.**	**MORFAC**
	m	**deg.**	**s**	**m.s^{-1}**	**deg.**	**m^3.s^{-1}**	**kg.m-^{3}**	**m^3.s^{-1}**	**kg.m^{-3}**	**%**	**-**
C1	2.16	100.42	10.02	0.12	70.48	130.77	5.11	6.79	0.72	9.59%	67.64
C2	2.16	100.42	10.02	0.12	70.48	125.96	4.97	6.81	0.72	9.20%	64.89
C3	2.16	100.42	10.02	0.12	70.48	202.73	7.30	9.50	1.05	0.39%	2.74
C4	2.16	100.42	10.02	0.13	229.36	121.60	4.82	6.78	0.72	9.43%	66.51
C5	2.16	100.42	10.02	0.13	229.36	151.70	5.71	6.86	0.73	9.05%	63.84
C6	2.16	100.42	10.02	0.13	229.36	285.73	10.59	18.59	1.84	0.38%	2.66
C7	3.18	89.86	10.56	0.14	79.69	49.82	1.53	5.06	0.50	3.73%	26.31
C8	3.18	89.86	10.56	0.14	79.69	46.86	1.37	5.74	0.58	3.58%	25.26
C9	3.18	89.86	10.56	0.14	79.69	29.35	0.69	6.80	0.72	0.15%	1.05
C10	3.18	89.86	10.56	0.22	209.19	28.31	0.65	6.78	0.72	3.16%	22.28
C11	3.18	89.86	10.56	0.22	209.19	55.89	1.90	5.12	0.51	3.03%	21.39
C12	3.18	89.86	10.56	0.22	209.19	37.54	1.01	1.16	0.17	0.13%	0.89
C13	4.75	73.67	10.44	0.28	59.95	63.67	2.42	6.79	0.72	1.33%	9.36
C14	4.75	73.67	10.44	0.28	59.95	23.14	0.57	6.78	0.72	1.27%	8.96
C15	4.75	73.67	10.44	0.28	59.95	16.64	0.38	2.93	0.28	0.06%	0.40
C16	4.75	73.67	10.44	0.38	213.35	21.62	0.52	6.78	0.72	1.28%	9.04
C17	4.75	73.67	10.44	0.38	213.35	54.14	1.82	6.81	0.72	1.24%	8.72
C18	4.75	73.67	10.44	0.38	213.35	33.09	1.05	6.99	0.75	0.05%	0.32
C19	2.49	215.40	11.98	0.13	46.61	92.56	3.77	6.78	0.72	6.90%	48.67
C20	2.49	215.40	11.98	0.13	46.61	130.10	5.08	6.78	0.72	6.63%	46.73
C21	2.49	215.40	11.98	0.13	46.61	310.30	11.50	34.90	3.12	0.27%	1.94
C22	2.49	215.40	11.98	0.13	221.64	103.90	4.19	5.48	0.55	6.54%	46.09
C23	2.49	215.40	11.98	0.13	221.64	124.78	4.92	6.84	0.73	6.27%	44.23
C24	2.49	215.40	11.98	0.13	221.64	127.59	5.02	4.64	0.45	0.26%	1.86
C25	3.53	219.84	12.01	0.21	21.50	24.19	0.58	6.78	0.72	2.24%	15.82
C26	3.53	219.84	12.01	0.21	21.50	77.40	3.07	5.06	0.50	2.15%	15.17
C27	3.53	219.84	12.01	0.21	21.50	52.52	1.70	2.30	0.23	0.09%	0.65
C28	3.53	219.84	12.01	0.13	198.75	41.28	1.13	6.78	0.72	3.87%	27.28
C29	3.53	219.84	12.01	0.13	198.75	58.52	2.06	4.74	0.46	3.71%	26.15
C30	3.53	219.84	12.01	0.13	198.75	28.79	0.66	0.94	0.16	0.16%	1.13
C31	5.72	232.19	12.05	0.47	24.62	10.95	0.25	6.78	0.72	0.54%	3.79
C32	5.72	232.19	12.05	0.47	24.62	13.27	0.31	6.87	0.73	0.52%	3.63
C33	5.72	232.19	12.05	0.47	24.62	5.29	0.10	4.59	0.44	0.02%	0.16
C34	5.72	232.19	12.05	0.31	142.05	41.80	1.15	6.85	0.73	1.36%	9.60
C35	5.72	232.19	12.05	0.31	142.05	25.57	0.60	6.45	0.68	1.30%	9.20
C36	5.72	232.19	12.05	0.31	142.05	14.20	0.33	2.19	0.23	0.06%	0.40

Table 2.4 Wave, shelf-current, river discharge, river suspended-sediment concentration, percentage of occurrence and morphological acceleration factor parameters specific to each simulated representative case from June 2002 to June 2003 (El Niño phase).

June 2002 – May 2003 (El Niño)											
Cases	H_s	D_p	T_p	**SPD$_{shelf}$**	**DIR$_{shelf}$**	**Q$_{Waip}$**	**SSC$_{Waip}$**	**Q$_{Turang}$**	**SSC$_{Turang}$**	**Occ.**	**MORFAC**
	m	**deg.**	**s**	**m.s^{-1}**	**deg.**	**m^3.s^{-1}**	**kg.m^{-3}**	**m^3.s^{-1}**	**kg.m^{-3}**	**%**	**-**
C1	2.27	120.72	10.28	0.13	66.00	113.52	4.55	9.62	1.06	8.18%	57.71
C2	2.27	120.72	10.28	0.13	66.00	74.32	3.00	8.48	0.93	7.85%	55.37
C3	2.27	120.72	10.28	0.13	66.00	161.43	5.93	7.93	0.87	0.33%	2.34
C4	2.27	120.72	10.28	0.13	234.42	98.85	4.02	9.39	1.04	9.11%	64.25
C5	2.27	120.72	10.28	0.13	234.42	113.34	4.54	11.29	1.23	8.74%	61.66
C6	2.27	120.72	10.28	0.13	234.42	70.01	2.79	7.18	0.77	0.37%	2.58
C7	3.49	98.39	10.80	0.22	40.86	24.77	0.59	6.80	0.72	2.54%	17.92
C8	3.49	98.39	10.80	0.22	40.86	54.61	1.83	5.14	0.51	2.44%	17.19
C9	3.49	98.39	10.80	0.22	40.86	22.93	0.57	6.81	0.72	0.10%	0.73
C10	3.49	98.39	10.80	0.17	251.44	18.70	0.45	4.64	0.45	2.83%	19.94
C11	3.49	98.39	10.80	0.17	251.44	62.38	2.31	6.40	0.67	2.71%	19.13
C12	3.49	98.39	10.80	0.17	251.44	23.01	0.57	4.08	0.39	0.11%	0.81
C13	4.93	112.83	12.22	0.24	28.63	12.84	0.29	6.80	0.72	1.09%	7.67
C14	4.93	112.83	12.22	0.24	28.63	15.73	0.35	6.80	0.72	1.04%	7.34
C15	4.93	112.83	12.22	0.24	28.63	16.85	0.38	0.29	0.13	0.05%	0.32
C16	4.93	112.83	12.22	0.23	207.42	13.14	0.30	6.80	0.72	1.35%	9.52
C17	4.93	112.83	12.22	0.23	207.42	23.97	0.58	6.80	0.72	1.29%	9.12
C18	4.93	112.83	12.22	0.23	207.42	16.74	0.38	3.00	0.28	0.06%	0.40
C19	2.32	228.24	10.44	0.14	23.98	91.42	3.72	7.63	0.83	5.86%	41.32
C20	2.32	228.24	10.44	0.14	23.98	67.64	2.64	6.80	0.72	5.63%	39.71
C21	2.32	228.24	10.44	0.14	23.98	68.38	2.70	4.62	0.45	0.23%	1.61
C22	2.32	228.24	10.44	0.10	201.06	115.91	4.63	12.23	1.32	9.98%	70.38
C23	2.32	228.24	10.44	0.10	201.06	86.95	3.54	7.52	0.81	9.58%	67.56
C24	2.32	228.24	10.44	0.10	201.06	123.62	4.89	14.78	1.54	0.40%	2.82
C25	3.32	227.08	10.67	0.22	21.57	22.57	0.56	6.60	0.70	2.47%	17.43
C26	3.32	227.08	10.67	0.22	21.57	54.09	1.80	6.80	0.72	2.37%	16.71
C27	3.32	227.08	10.67	0.22	21.57	13.81	0.31	5.59	0.56	0.10%	0.73
C28	3.32	227.08	10.67	0.14	82.13	33.70	0.83	6.80	0.72	4.30%	30.35
C29	3.32	227.08	10.67	0.14	82.13	69.38	2.76	6.18	0.64	4.13%	29.14
C30	3.32	227.08	10.67	0.14	82.13	77.67	3.14	7.71	0.84	0.17%	1.21
C31	5.37	212.81	11.71	0.34	24.02	12.70	0.29	6.80	0.72	0.80%	5.65
C32	5.37	212.81	11.71	0.34	24.02	21.50	0.55	6.81	0.72	0.77%	5.41
C33	5.37	212.81	11.71	0.34	24.02	12.91	0.30	0.23	0.13	0.03%	0.24
C34	5.37	212.81	11.71	0.32	38.81	14.03	0.32	6.80	0.72	1.45%	10.25
C35	5.37	212.81	11.71	0.32	38.81	26.31	0.61	4.63	0.45	1.40%	9.85
C36	5.37	212.81	11.71	0.32	38.81	18.02	0.42	0.29	0.13	0.00	0.40

2.4.1. Short-term morphological modelling

The medium-term morphological simulation was supplemented by a fifteen-day historical simulation characterised by high energy wave conditions and large river discharges. Details about this simulation are given in Table 2.5 and Figure 2.14-Figure 2.16.

By contrast with the medium-term modelling, 2-dimensional directional hourly wave spectra were applied here at the open-ocean boundaries to allow a full representation of both the sea and the swell components of the wave climate. For this approach, no morphological acceleration was defined (*MORFAC* set to 1). Predicted daily infilling rates were then compared to the reference values providing in the literature (Black et al., 1997; Beamsley, 2003) for average, storm and severe conditions.

Table 2.5 Wave and river characteristics during historical events at the western end of the navigation channel (178.0104 E; 38.6807 S).

Start time	**End time**	**H_s (max)**	**D_p (mean)**	**$Q_{Waip.}$ (max)**	**$SSC_{Waip.}$ (max)**	**$Q_{Turan.}$ (max)**	**$SSC_{Turan.}$ (max)**
		[m]	**[deg.]**	**[$m^3.s^{-1}$]**	**[$m^3.s^{-1}$]**	**[$m^3.s^{-1}$]**	**[$m^3.s^{-1}$]**
07/07/2002	22/07/2002	2.71	173.88	220.55	7.99	30.09	2.74

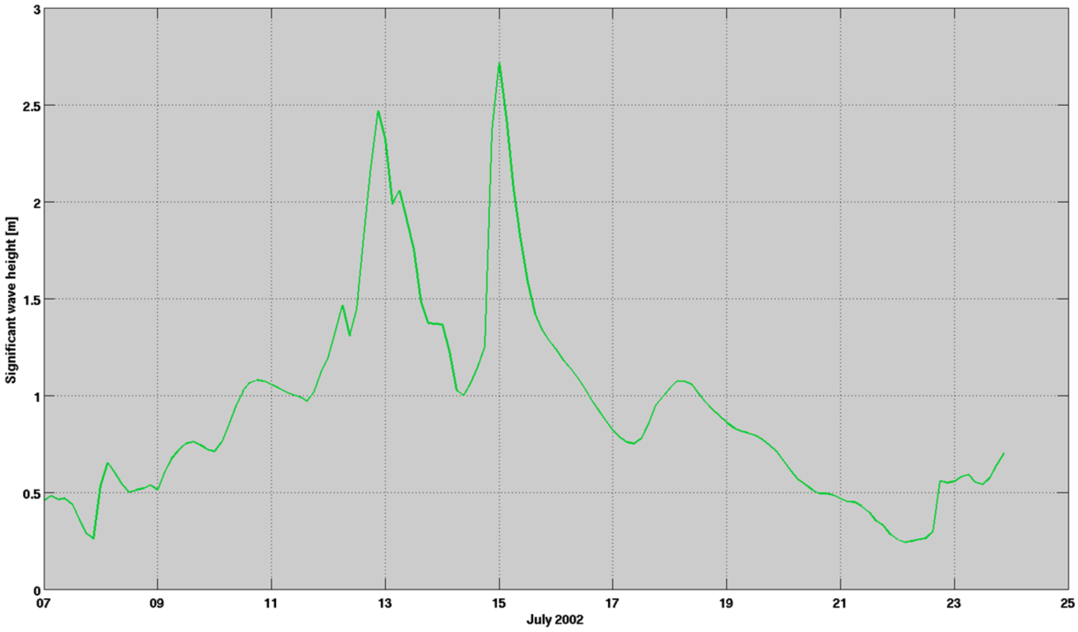

Figure 2.14 Time series of hindcast significant wave height during between 07/07/2002 and 23/07/2002 at the western end of the navigation channel (178.0104 E; 38.6807 S).

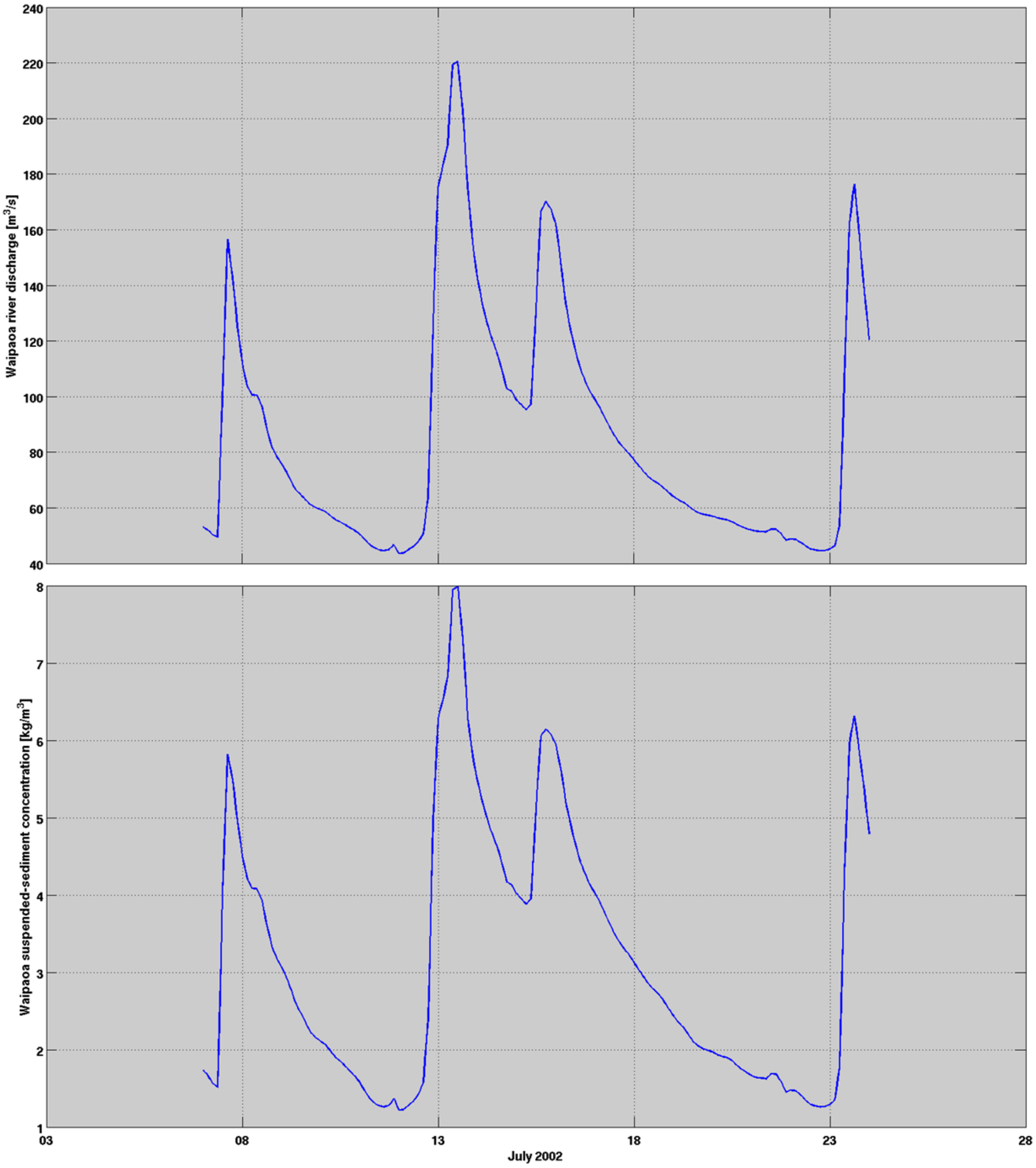

Figure 2.15 Time series of the Waipaoa river discharge (top) and suspended-sediment concentration (bottom) between 07/07/2002 and 23/07/2002 at the western end of the navigation channel (178.0104 E; 38.6807 S).

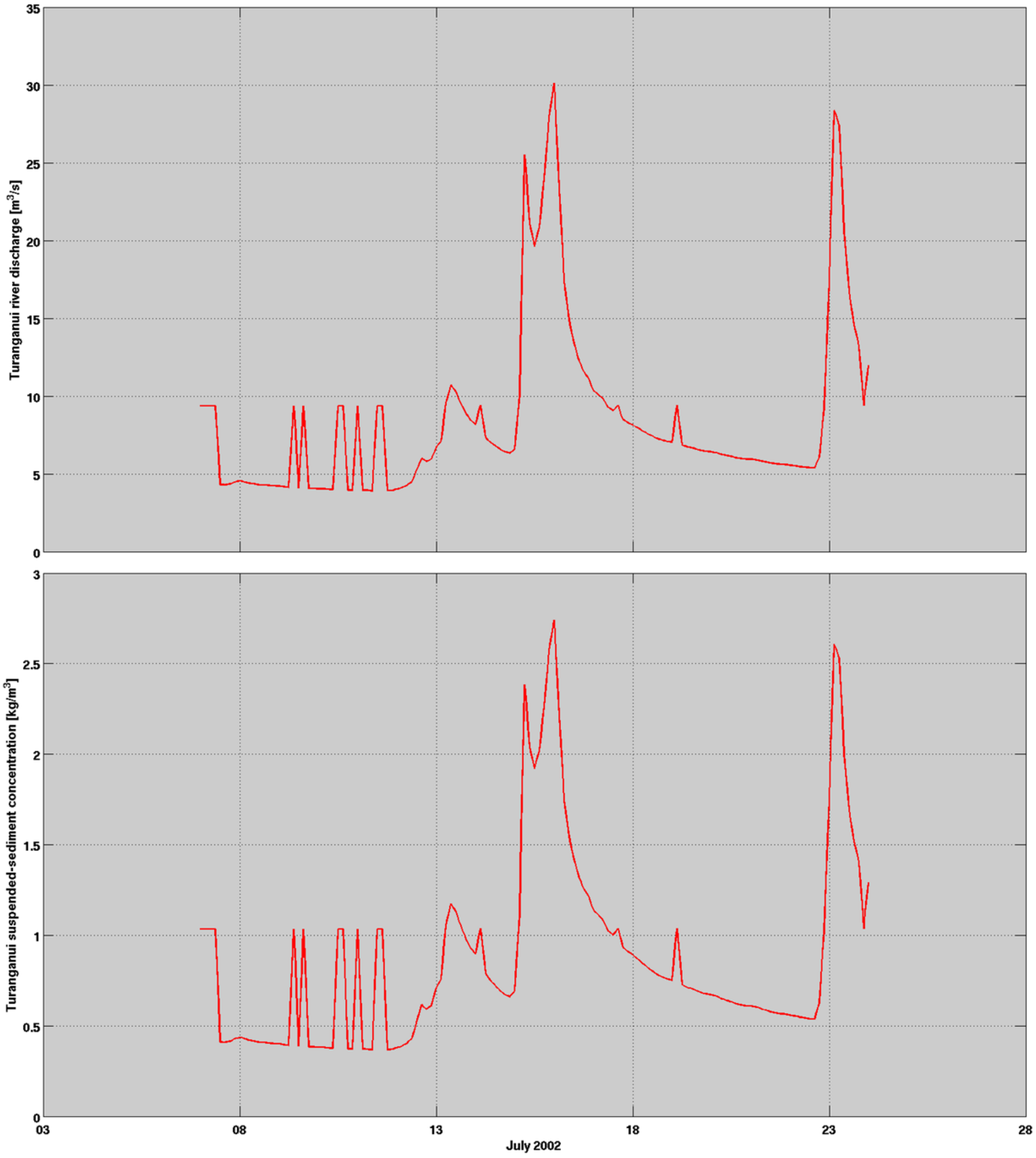

Figure 2.16 Time series of the Turanganui river discharge (top) and suspended-sediment concentration (bottom) betweem 07/07/2002 and 23/07/2002 at the western end of the navigation channel (178.0104 E; 38.6807 S).

2.5. Hydrodynamic model validation

2.5.1. Evaluation criteria

The predictive skill assessment of the Delft3D – FLOW model was evaluated based on the quantitative accuracy parameters calculated from the measured X_m and hindcast, X_h data:

Mean absolute error (MAE): $$\overline{|x_h - x_m|} \qquad \text{(Eq. 2.13)}$$

Root Mean Square Error (RMSE): $$\sqrt{\overline{(x_h - x_m)^2}}$$ (Eq. 2.14)

Mean relative absolute error (MRAE): $$\overline{\left|\frac{x_h - x_m}{x_m}\right|}$$ (Eq. 2.15)

Bias: $$\overline{x_h - x_m}$$ (Eq. 21.6)

Scatter Index (SI): $$\frac{\sqrt{\overline{(x_h - x_m)^2}}}{\overline{x_h}}$$ (Eq. 2.17)

2.5.2. Measured data

The current velocities and water elevations measured by an S4 current meter at site CM2 (Figure 2.17) were used to support the validation of the Delft3D – FLOW model.

The instrument deployments, including geographic coordinates, observational durations, record levels, and water depths, are summarised in Table 2.6. Results of the model performance assessment including accuracy measurements (Eq. 2.13 to 2.17) and plots are provided in Section 3.

Table 2.6 Geographic coordinates, observational durations, samplings, record levels and water depths of the ADCP and S4 current meter deployments over Poverty Bay and the adjacent shelf margin.

Site	**Deployment**	**Coordinates (WGS84)**		**Observational durations (dd/mm/yyyy)**		**Vertical references (m - BSL)**	
		Longitude (E)	**Latitude (N)**	**Start date**	**End date**	**Level**	**Water depth**
CM2	S4 CM - 01	178.0077	-38.6819	04/07/1996	10/08/1996	10	11
	S4 CM - 02			16/08/1996	28/08/1996		

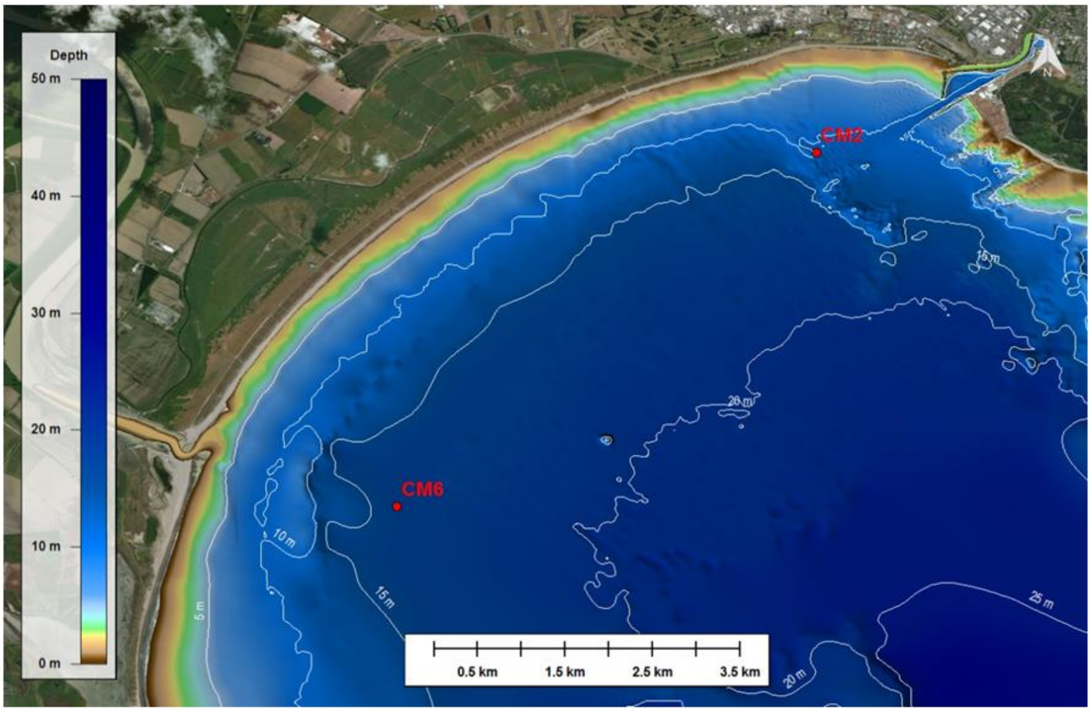

Figure 2.17 Map showing the bathymetry over Poverty Bay. The CM2 site was used to validate the Delft3D – FLOW model against currents and water elevations data measured by S4 current meter near the navigation channel in 1996.

2.6. Morphological model validation

The validation of a morphodynamic model by field observations is generally very difficult to achieve. The complexity of morphodynamic evolution in coastal environments driven by both short and long-term processes requires appropriate measured data of bathymetry, which should ideally be available at different time scales and for relatively large areas.

The validation stage can be undertaken on a storm-induced or on a medium-term bed evolution to verify the level of agreement between the measurements and the model results. Both methods provide useful information regarding the capability of the model to predict a range of morphodynamic mechanisms which control the overall coastal dynamics. Analysing storm-induced bed evolution provides both calibration and a quantitative validation of the model configuration, while a long-term bed evolution study is useful in that it qualitatively characterises the overall relevance of the model.

Here, the morphological model assessment consisted in comparing model results against annual and daily infilling rates estimated by Black et al. (1997), Beamsley (2003) and the Gisborne District Council (GDC) for averaged, storm and severe conditions. These estimates were obtained from previous numerical modelling and historical bathymetry surveys.

The quantitative validation of the predicted infilling rates was exclusively carried out in the inner basin and the outer navigation channel. The polygons displayed in Figure 2.18 delimit a total area of 137,300 m^2 used to estimate the daily and annual infilling rates. This corresponds to the same surface area used in Black et al. (1997) and Beamsley (2003) for estimating the port volumetric infilling rates.

Additionally, infilling patterns highlighted by recent bathymetry surveys were used to validate qualitatively the model results in the near-port area.

Over northern Poverty Bay, we investigated the coherency of the model results comparing the predicted morphological patterns against those described in the literature from historical aerial photographs and surveys (Pullar and Penhale, 1970; Smith, 1988; Foster and Carter, 1997).

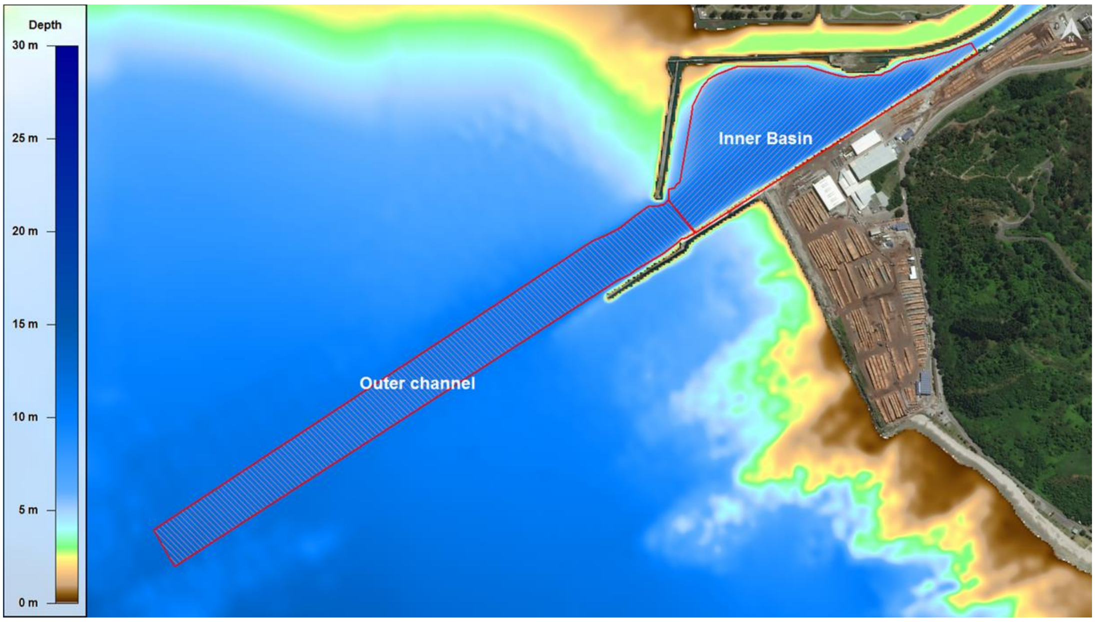

Figure 2.18 Map showing the bathymetry over Poverty Bay. The red polygon delimits the 137,300 m^2 surface area used to validate the daily and annual infilling rates predicted by the numerical model.

3. RESULTS

The key aim of the present work is to determine the degree of confidence in the numerical model that will be used to assess the morphological response to the future dredging program at Eastland Port. Results of the hydrodynamic and morphological modelling validation are presented in this section.

3.1. Validation of the hindcast current velocities and water elevation

The Delft3D – FLOW model outputs were validated against measured data recorded by an S4 current meter deployed near the navigation channel at 10 m depth. The statistical errors between measured and hindcast near-bottom current velocities are provided in Table 3.1 while the corresponding time series and Quantile-Quantile plots (QQ plots) are shown in Figure 3.1 and Figure 3.2.

The validation of the near-bottom flows at site CM2 showed reasonable model skills given the complexity of the area. The QQ plots outlined a relative good agreement between the distributions of the model and measured current velocities. This feature was particularly important as the reduction techniques used for the medium-tern morphological modelling was mainly based on statistical distributions. The analysis of the different time series pointed out some discrepancies between the hindcast and measured residual peak flow periods. This is expected to have only minor impact on the balance of the sediment fluxes represented in the input reduction modelling. The effect of uncorrelated peak flows may however be of higher importance in the short-term modelling. For this reason, we also calibrated the model for the fifteen day historical simulation.

Time series of hindcast and measured water elevations are given in Figure 3.3. While the tidal component of the water elevation was well replicated in the model, the dominant residual component was somewhat biased. The effect of biased water elevations on the model bed shear stress fields remained difficult to predict under current and wave actions. However, we addressed the lack of precision in the hydrodynamic modelling by a careful calibration of the morphological model.

Table 3.1 Accuracy measures between hindcast and measured current velocities at 10 depth at site CM2 (deployment 1 and 2) near Eastland Port.

Sites	Parameters	Level	MAE	RMSE	MRAE	Bias	Scatter Index	Number of data
CM2 – 01	**Current speed**	**10 m**	0.0216	0.0279	0.8038	-0.0094	0.7439	381
CM2 – 02	**Current speed**	**10 m**	0.0216	0.0282	1.4102	-0.0094	0.7778	285

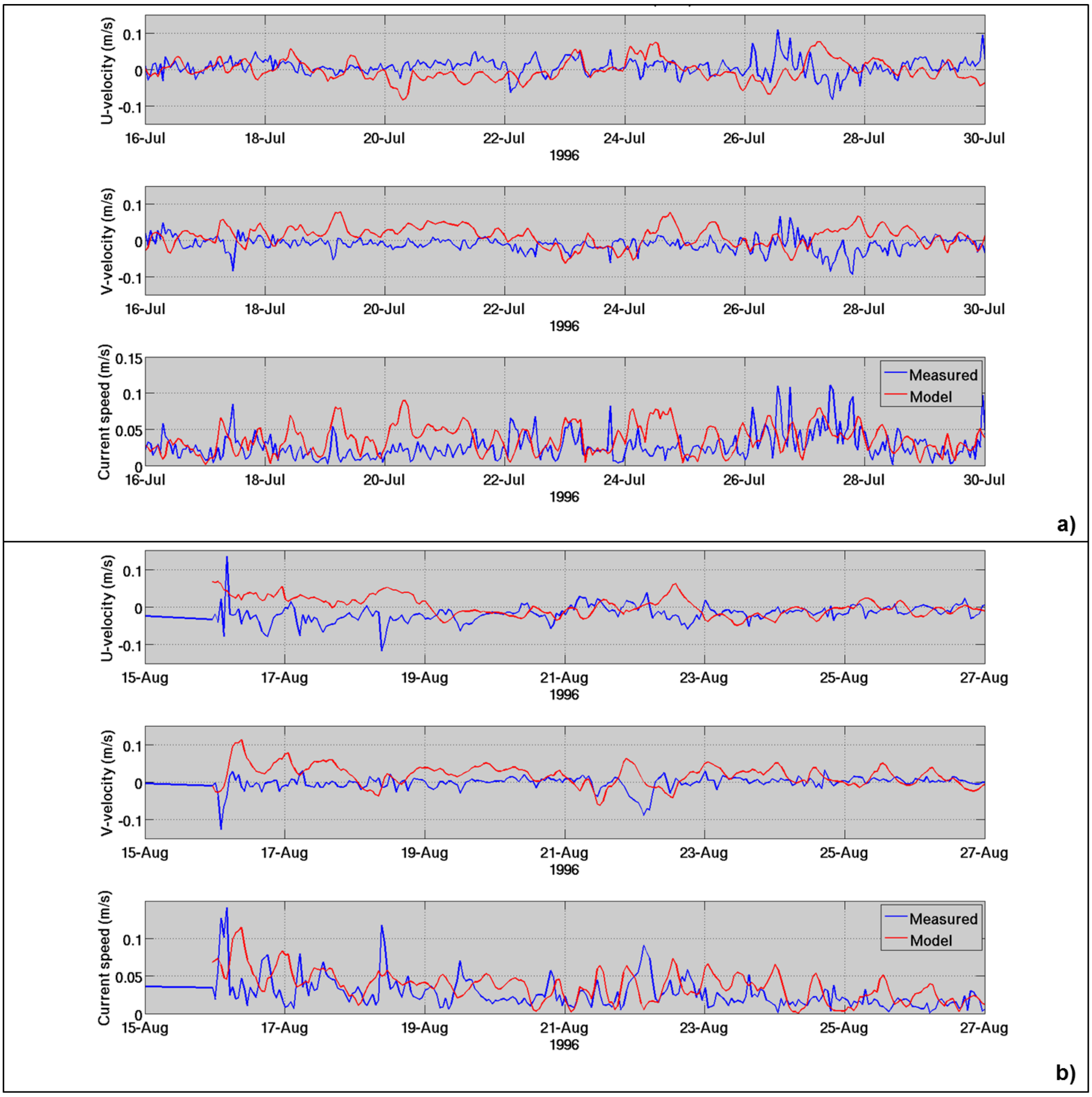

Figure 3.1 Comparison between measured and Delft3D model current time series at site CM2 at 10 m (below sea level) for the first (a) and second deployment (b).

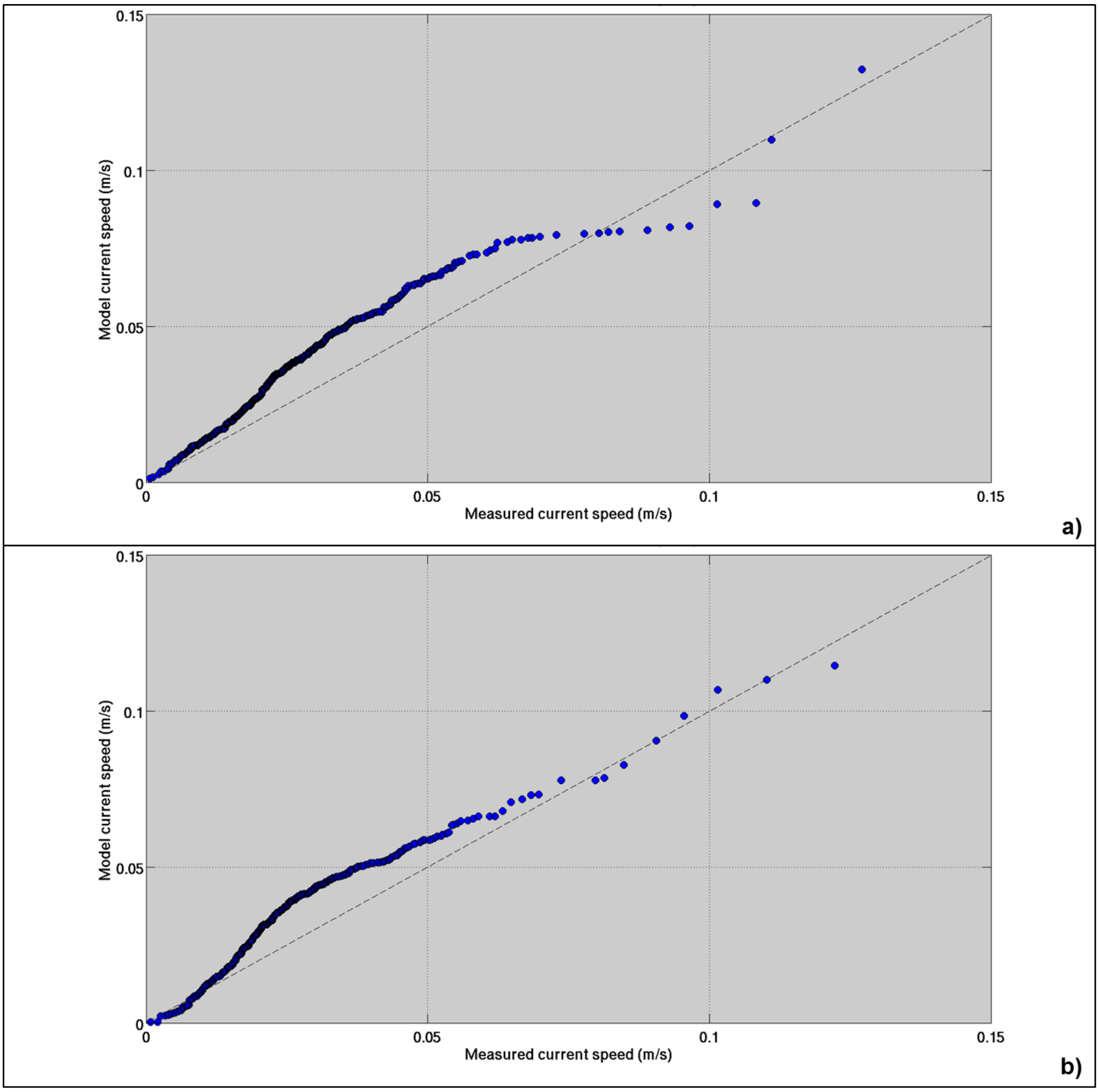

Figure 3.2 Quantile-Quantile plot created from measured and Delft3D model current time series at site CM2 at 10 m (below sea level) for two deployments. The dashed black line indicates a perfect agreement between the distributions.

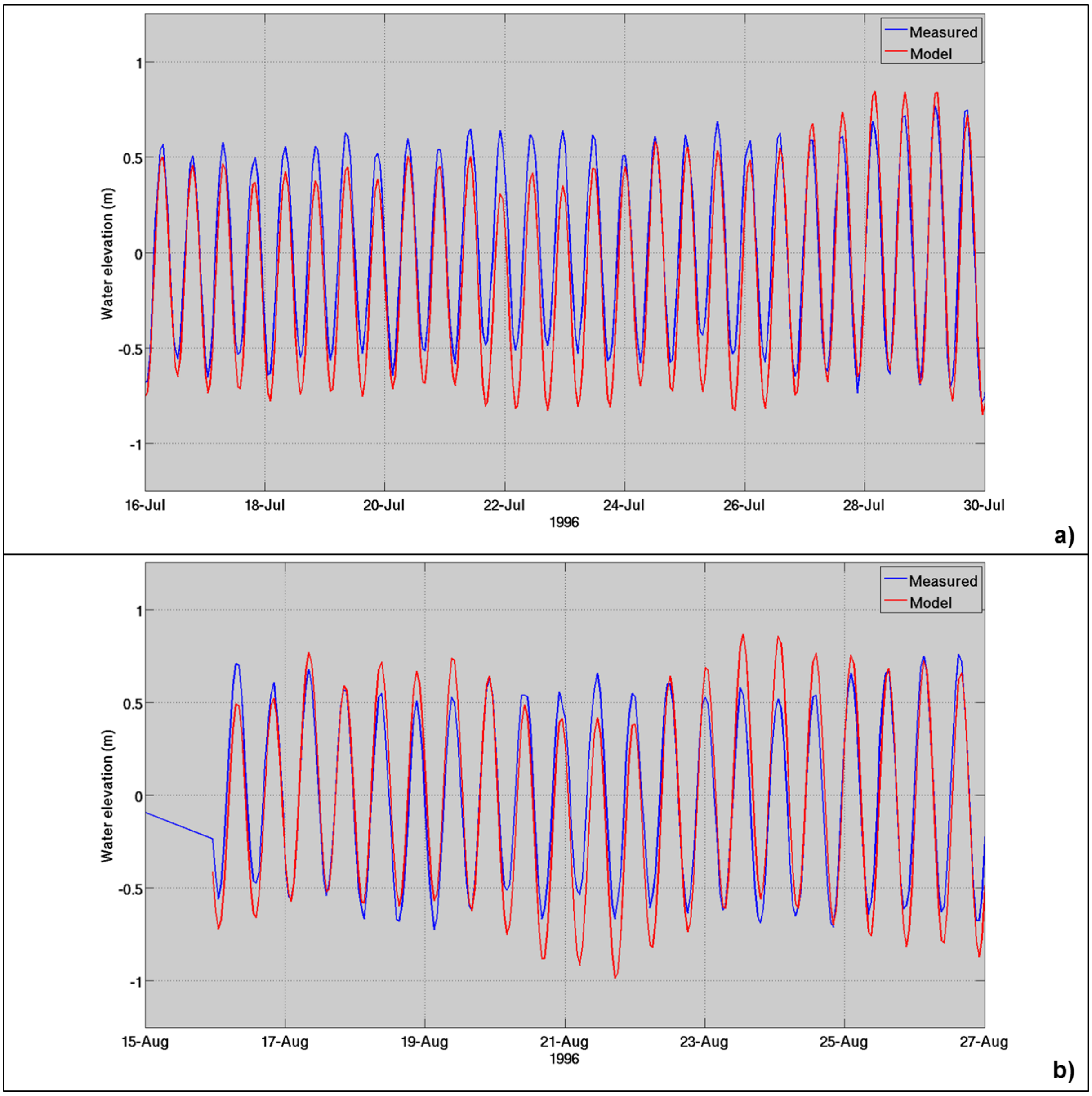

Figure 3.3 Comparison between measured and Delft3D model water elevation time series at site CM2 at 10 m (below sea level) for the first (a) and second deployment (b).

3.2. Verification of the hindcast sediment dynamics and morphology during 'La Niña' and 'El Niño' phases of ENSO

Two morphological accelerated simulations were carried out in order to predict the coastal dynamics over northern Poverty Bay during 'La Niña' (1998-1999)) and 'El Niño' (2002-2003) phases of ENSO In this section we examined the capability of the model to capture the main morphological patterns described in the scientific literature and observed in hydrographic surveys. A quantitative validation of the channel volumetric infilling rates was undertaken and is detailed in Section 3.3 and 3.4.

The predicted morphological changes associated with both 'La Niña' and 'El Niño' simulated periods are presented in Figure 3.4 and Figure 3.5 respectively, with differences between the two periods highlighting the importance of the incident wave dynamics and river discharges on the overall coastal dynamics.

The ‘La Niña’ simulation period was characterised by large river discharges due to increasing rainfalls and a predominance of easterly directed (coming from) incident waves as compared to the ‘El Niño’ simulated period. As such, the wave energy available to entrain and transport surficial sediment within the port environs was relatively reduced during the ‘La Niña’ simulation (due to sheltering), leading to comparatively greater accretion of the Waikanae and Midway beaches and a reduction in the offshore diabathic sediment transport, including into the shipping channel. This process is expected to be partially compensated by increasing fluvial suspended sediment discharges from the Turanganui River; however, the model results suggest that wave processes dominate the southward migration of sediment.

By contrast, increased accretion of sediment over western Poverty Bay is predicted to occur during ‘La Niña’ conditions due to a relative increase in wave energy and the input of fluvial derived sediment.

From a validation perspective, the very limited amount of measured data at the offshore disposal ground makes it difficult to either qualitatively or quantitatively validate the morphological model in this area.

As described by Black et al. (1997) and Beamsley (2003), the entrance to Eastland Port and the Swinging Basin act as a sediment trap, with sediment accretion expected under both ‘La Niña’ and ‘El Niño’ conditions (Figure 3.4 and Figure 3.5). The energy gradient within the port entrance and Swinging Basin (Figure 3.6 to Figure 3.9) results in a gradient in sediment grain sizes, with fine-grained sand particles preferentially settling in the port entrance while finer sediment (i.e. Very Fine Sand and Mud) are held in suspension and advected into the Swinging Basin where they undergo relatively increased flocculation processes under spatially-varying salinity gradients near the river mouth and settle out of suspension. This grain-size gradient and sedimentation pattern within the port entrance and Swinging Basin is consistent with the measured in-situ surficial sediment grain size (Beamsley, 2003) and measured depth changes obtained from bathymetry surveys (Figure 3.10 and Figure 3.11) respectively. Further, model calibration and validation highlighted the importance of the role consolidation of the in-situ surficial sediment plays in maintaining the stability of the mixed sand-mud layer in the channel bottom.

Near the main breakwater tip, surficial sediment is entrained and transported into the channel by wave action. While the accretion of material occurs consistently along the channel margin in the ‘La Niña’ simulation, the predominance of southerly wave events in the ‘El Niño’ simulation and relatively reduced river discharge rate results in relatively greater accretion in the immediate lee of the submerged breakwater and a limited area of mild erosion immediately offshore of the submerged breakwater (Figure 3.5).

A detailed examination of the morphological response of the extended port environs was difficult due to the hydrographic survey sampling period and ongoing maintenance dredging activities. Further, the spatial coverage of the hydrographic surveys were limited to along the thalweg of the channel, and did not capture the morphological evolution of the channel batters adequately.

While the eastern section of the channel is exposed to accretion due to near-bed sediment supplies, the sediment dynamics over the western section is mainly linked to the large deposition of silt occurring in the centre of Poverty Bay from the Waipaoa River. The formation of a mud blanket between the 12 m and 15 m isobath in the model is consistent with the sediment dynamics of the embayment described in Smith (1988). Enhanced accretion is expected in the outer parts of the channel under both ‘La Niña’ and ‘El Niño’ conditions (Figure 3.4 and Figure 3.5).

The beach areas, except Kaiti Beach, are characterised by nearshore coastal progradation in agreement with Smith (1988) and Foster and Carter (1997). Smith (1988) notes that, based on aerial photographs, approximately 2000 $m^3.yr^{-1}$ of sediment is supplied annually to Kaiti Beach , which is not accounted for in the model. The resultant volumetric changes are, however, negligible compared to the magnitude of the sediment fluxes near the Turanganui River mouth and adjacent beaches.

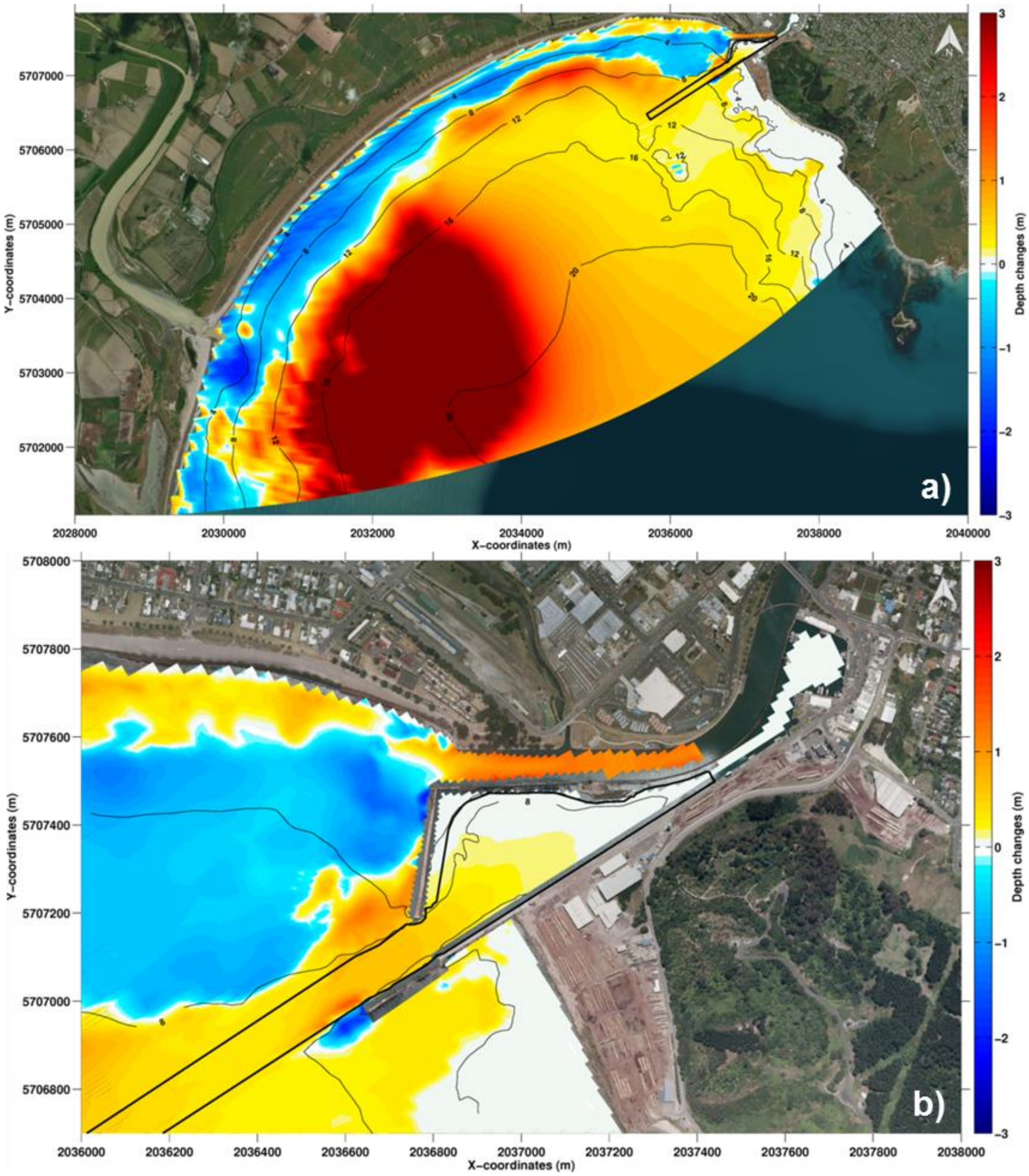

Figure 3.4 Depth changes predicted by the morphological model after one year based on the input reduction approach between June 1998 and May 1999 (La Niña). Red and blue colours indicate bed accretion and erosion patterns, respectively.

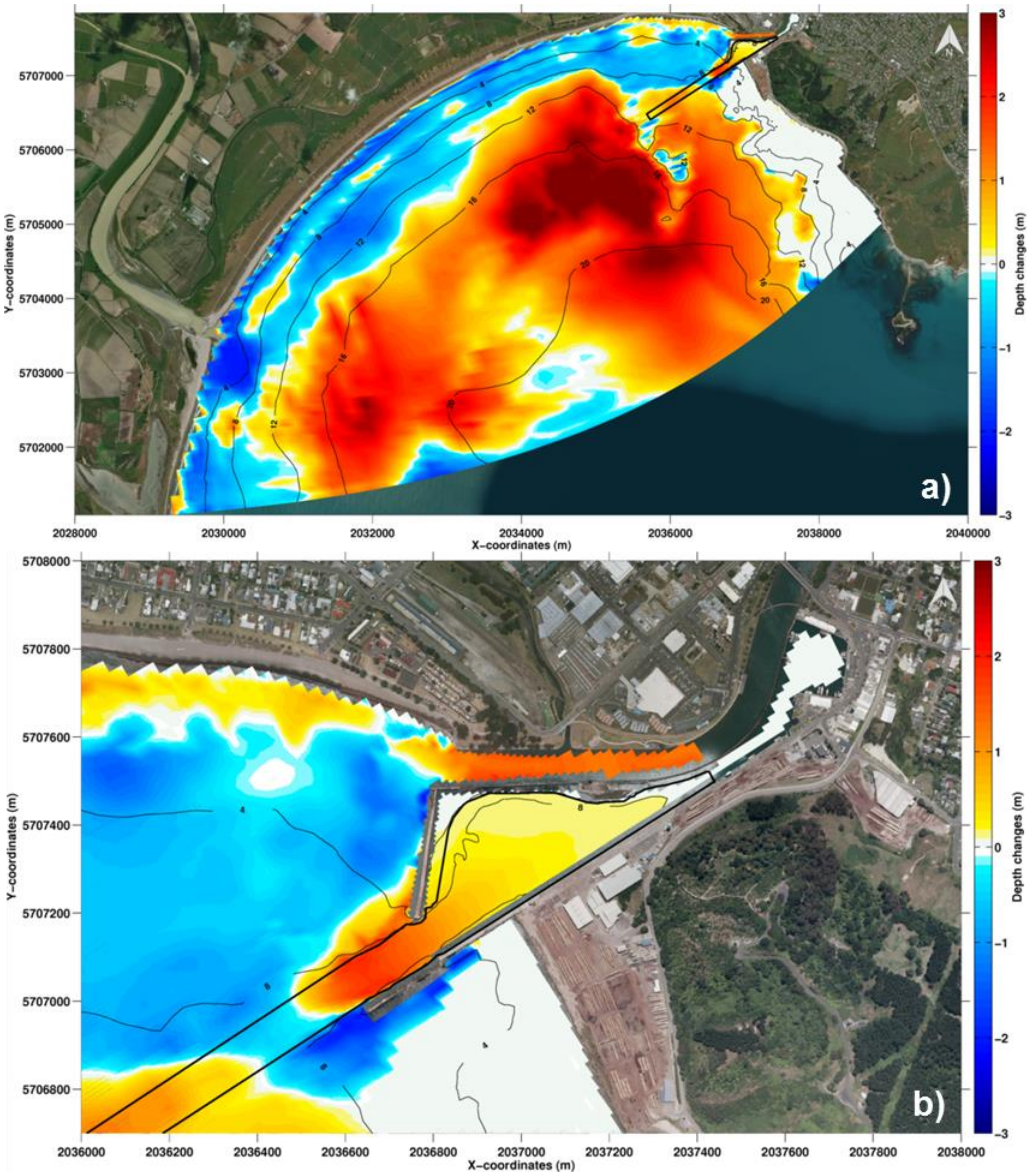

Figure 3.5 Depth changes predicted by the morphological model after one year based on the input reduction approach between June 2002 and May 2003 (El Niño). Red and blue colours indicate bed accretion and erosion patterns, respectively.

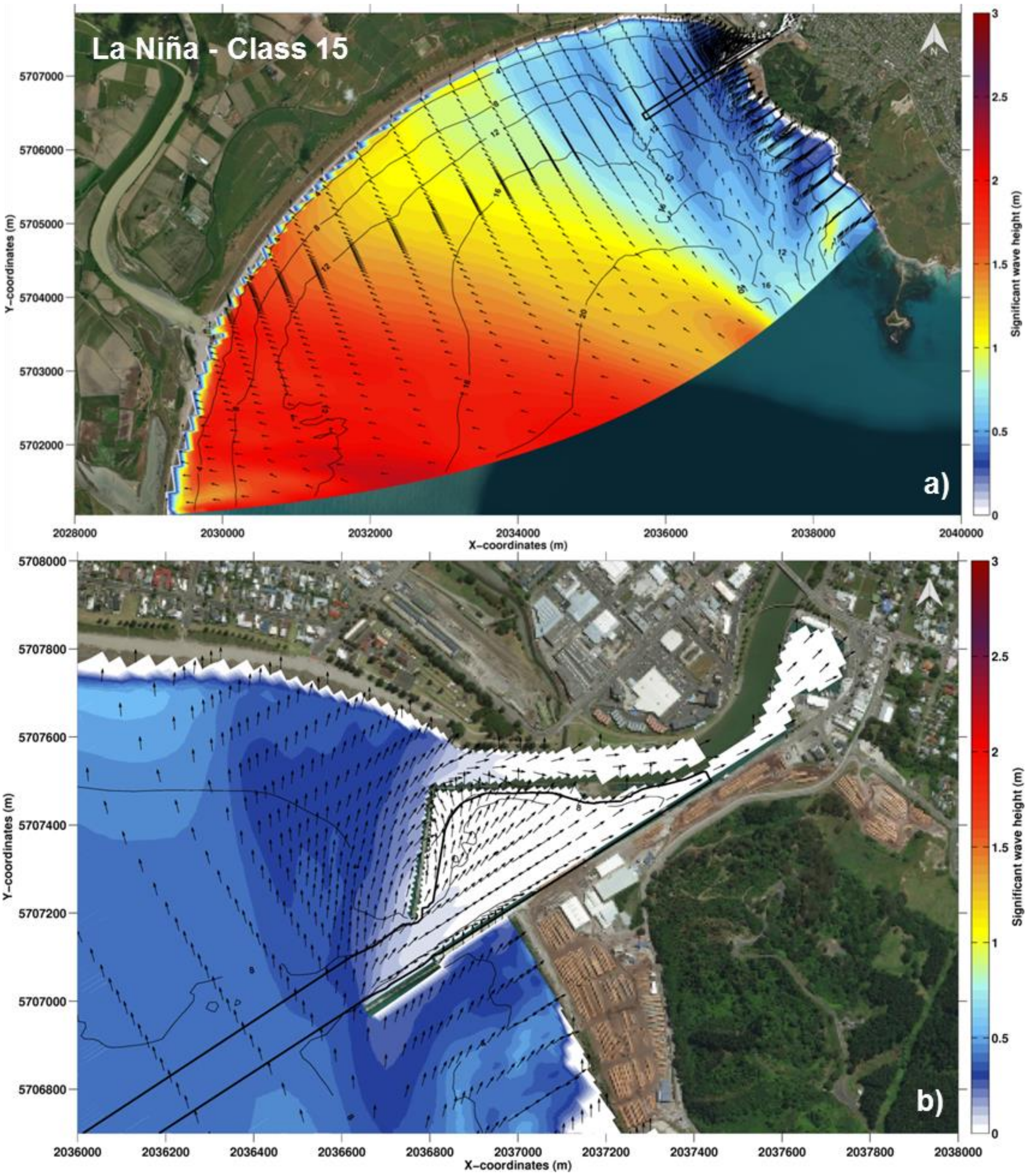

Figure 3.6 Significant wave height fields for Class 15 during 'La Niña' phase of ENSO over northern Poverty Bay (a) and Eastland Port (b). The black polygon indicates the dredged area used to estimate the channel volumetric infilling rates.

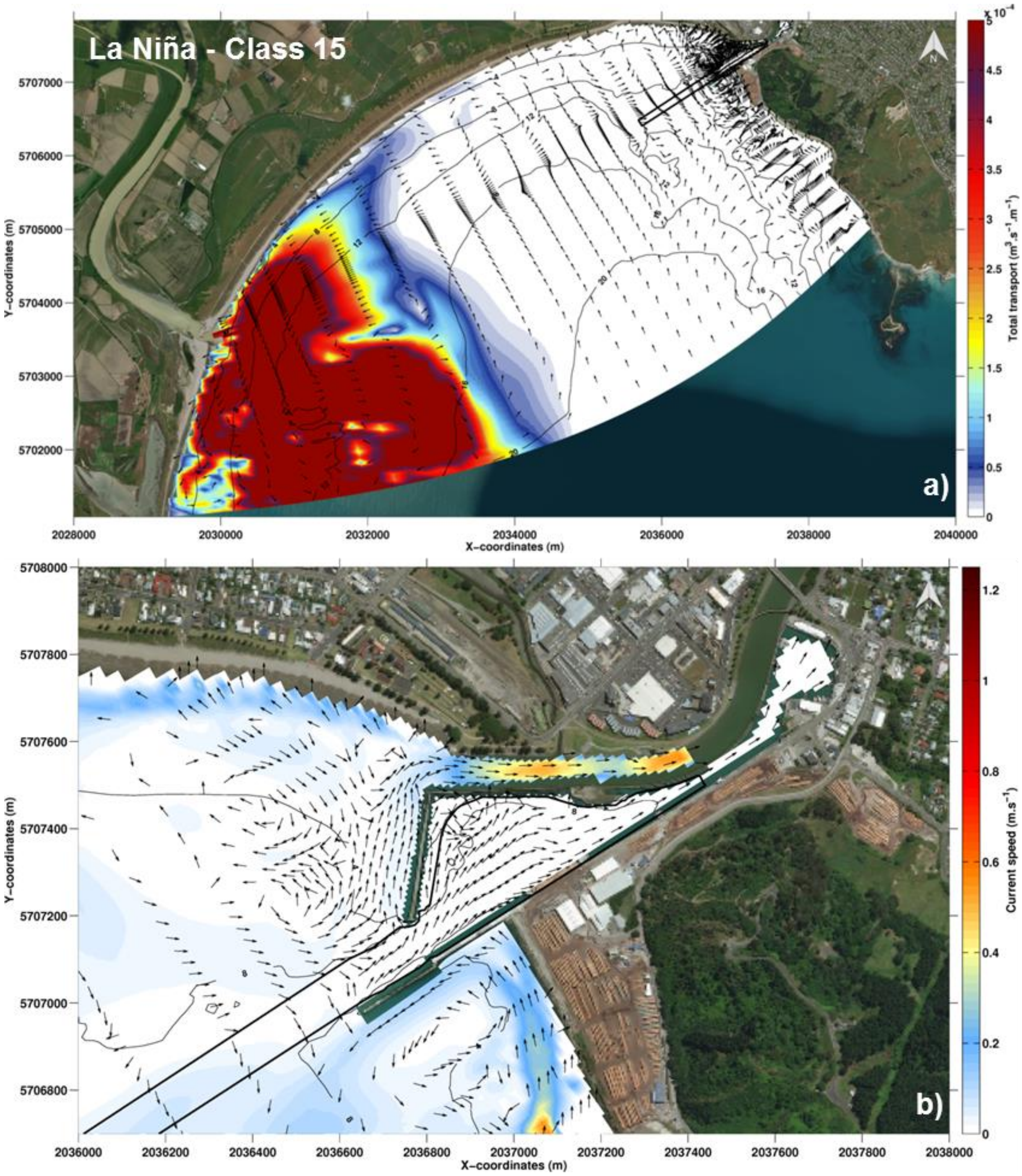

Figure 3.7 Total sediment mean transport for Class 15 during 'La Niña' phase of ENSO over northern Poverty Bay (a) and Eastland Port (b). The black polygon indicates the dredged area used to estimate the channel volumetric infilling rates.

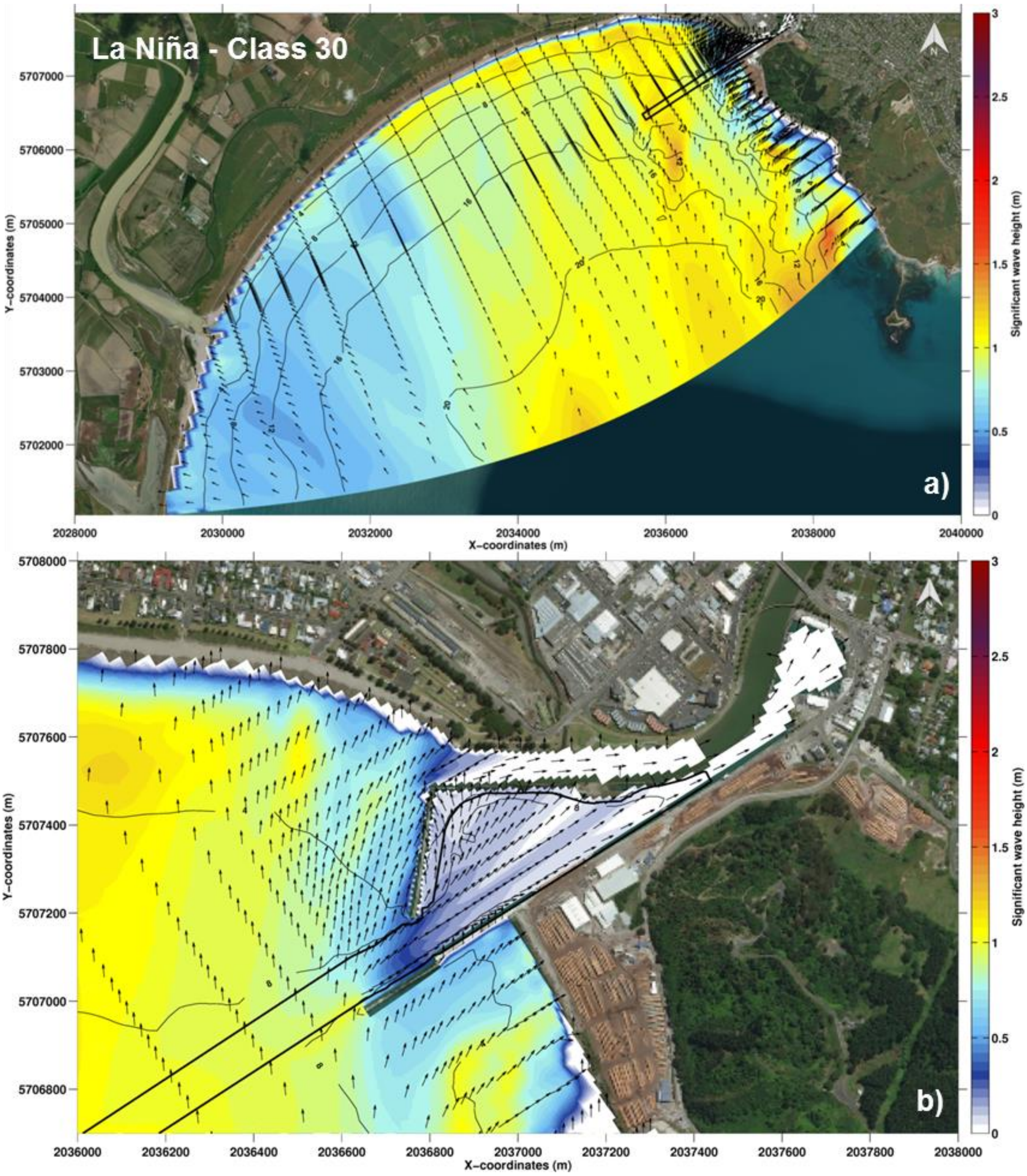

Figure 3.8 Significant wave height fields for Class 30 during 'La Niña' phase of ENSO over northern Poverty Bay (a) and Eastland Port (b). The black polygon indicates the dredged area used to estimate the channel volumetric infilling rates.

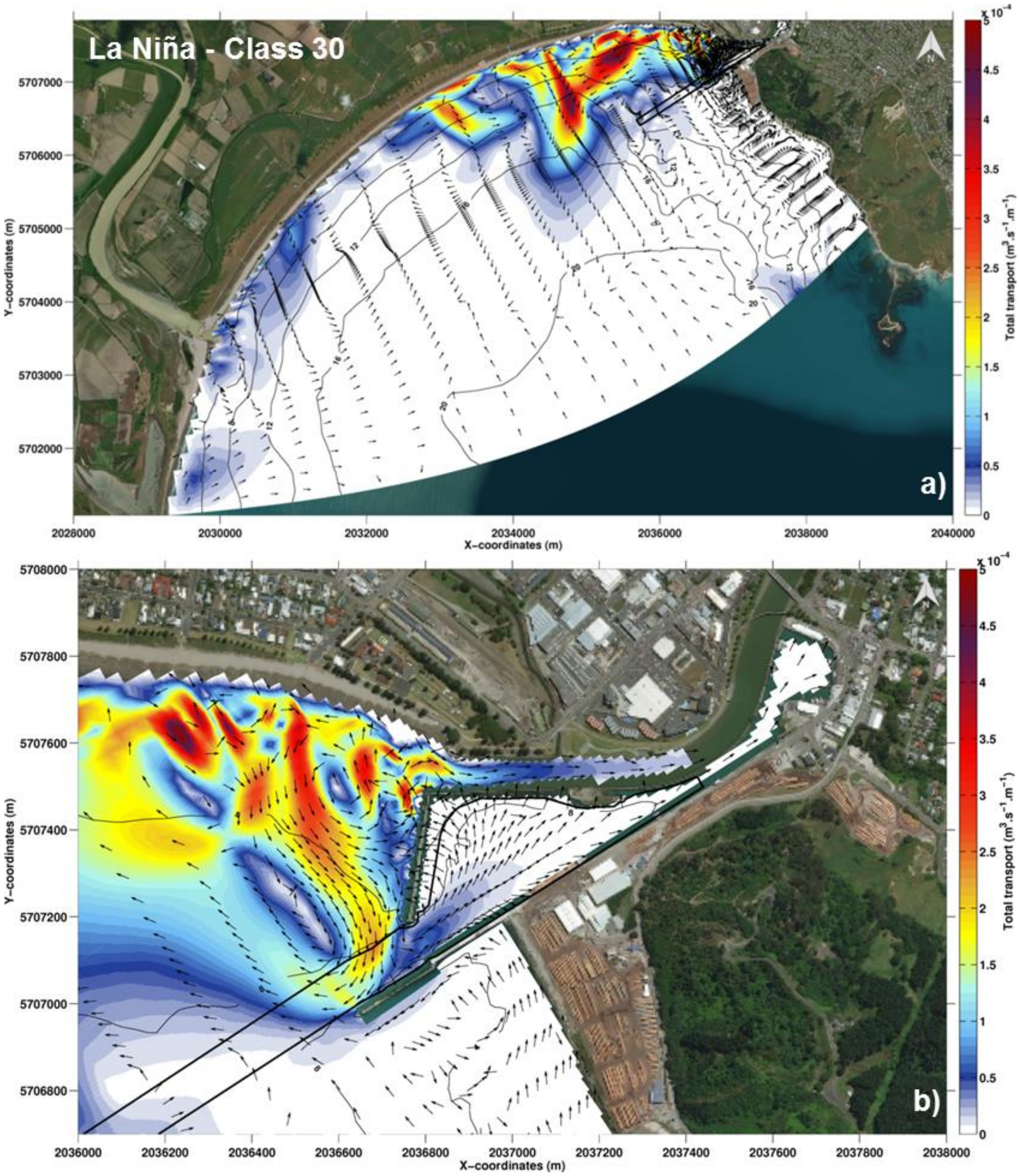

Figure 3.9 Total sediment mean transport for Class 30 during ‘La Niña’ phase of ENSO over northern Poverty Bay (a) and Eastland Port (b). The black polygon indicates the dredged area used to estimate the channel volumetric infilling rates.

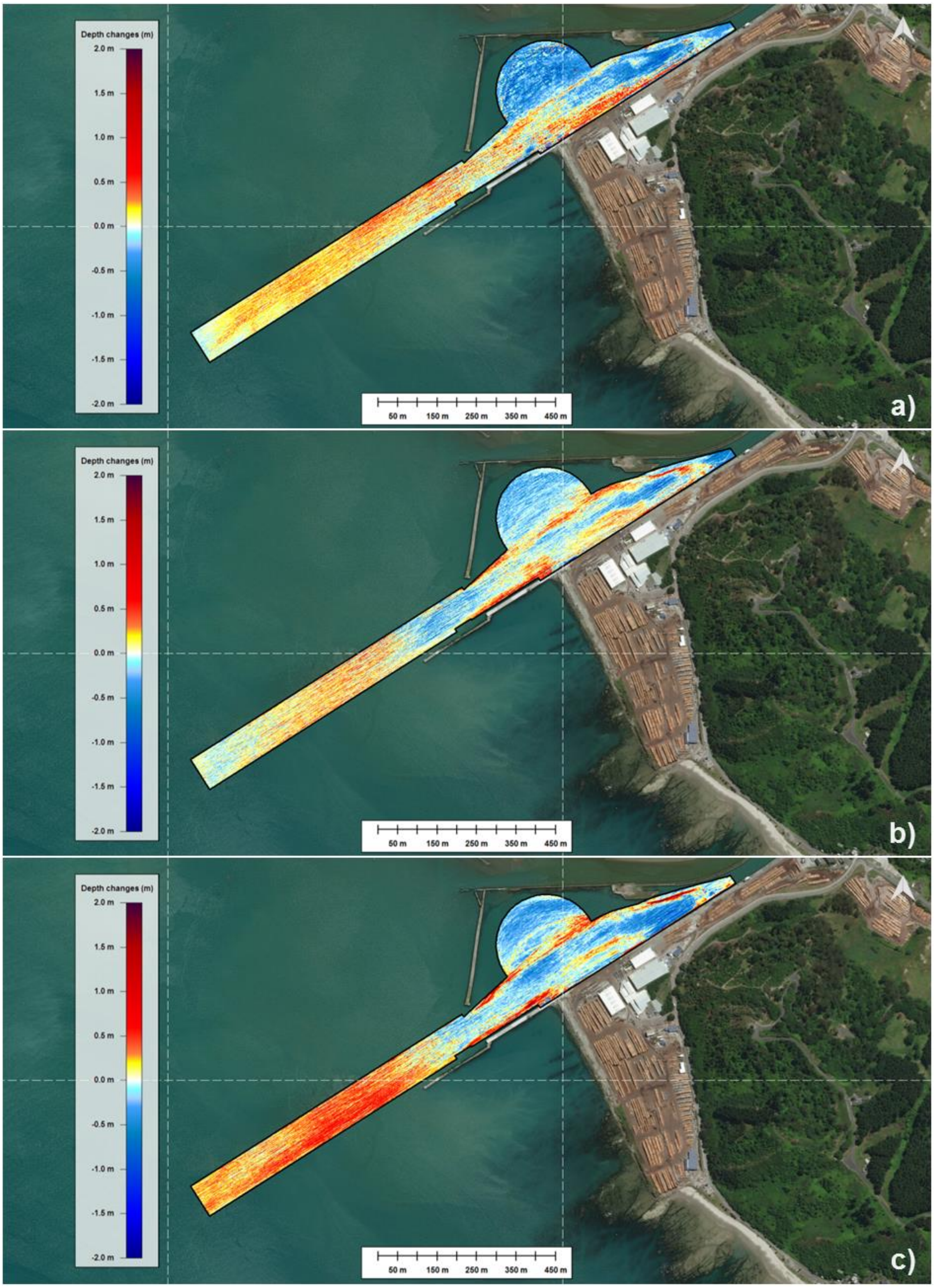

Figure 3.10 Depth changes observed between 2006 – 2009 (a), 2009 – 2012 (b) and 2012 – 2014 (c) within the navigation channel and the inner basin of Eastland Port. Note that dredging operations were performed over these periods. Yellow to red colours indicate infilling processes while blue colours highlight sediment removal related to the dredging.

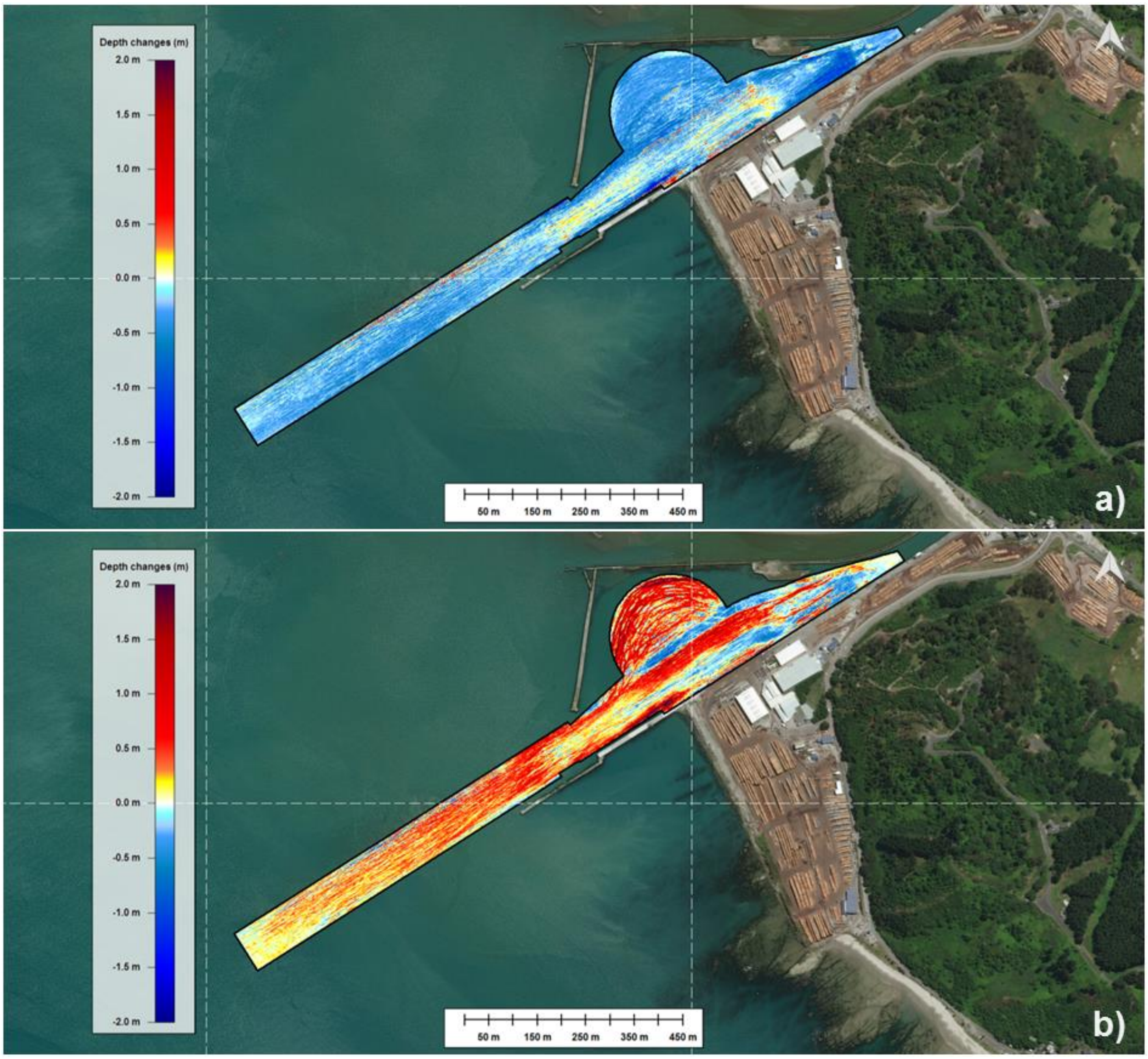

Figure 3.11 Depth changes observed between 2014 – 2015 (a) and 2016 – 2017 (b) within the navigation channel and the inner basin of Eastland Port. Note that dredging operations were performed over these periods. Yellow to red colours indicate infilling processes while blue colours highlight sediment removal related to the dredging.

3.3. Annual volumetric infilling rates

Infilling of the Eastland Port navigation channel and inner basin occurs over time, requiring a continuous maintenance dredging programme to maintain the navigable design depth. Eastland Port estimated that approximately 80,000 $m^3.yr^{-1}$ and 20,000 $m^3.yr^{-1}$ of sediments deposit into the navigation channel and inner basin at Eastland Port (Eastland Port, 2013). These estimates were obtained by considering both hydrographic survey and dredging records between 2009 and 2013. Previously, Black et al. (1997) provided a total infilling rate of 103,000 $m^3.yr^{-1}$ over a surface area of 137,300 m^2 covering both the outer channel and the inner basin based on sediment transport numerical modelling (Table 3.2).

Following calibration and validation of the morphological model, predicted infilling rates of 74,695 $m^3.yr^{-1}$ and 120,240 $m^3.yr^{-1}$ were estimated for the combined channel and inner harbour areas under ‘La Niña’ and ‘El Niño’ phases of ENSO respectively. During the ‘La Niña’ period, 80.4% (60,087 $m^3.yr^{-1}$) and 19.6%

(14,608 $m^3.yr^{-1}$) of the infilling volume is expected to occur in the shipping channel and inner basin respectively, while during the 'El Niño' phase, 77% (92,593 $m^3.yr^{-1}$) and 23% (27,647 $m^3.yr^{-1}$) respectively (Table 3.2).

Beamsley (2003) determined the margin of error of the estimated total infilling rate in the channel as the sum of the errors associated with both the hydrographic surveys and the volume estimated to have been removed during maintenance dredging. The author considered error-bounds of ±0.17 m for the hydrographic surveys taking into account the echo sounder, tidal gauge/reading and heave compensation accuracies. The estimation accuracy of the dredged volume during maintenance operations was approximately 10%. As such, the total error-bounds of the estimated channel infilling rate provided by EP were approximately ±33,000 $m^3.yr^{-1}$. The predicted volumetric infilling rates for both phases of ENSO were therefore within the limits of the error-bounds.

Table 3.2 Average annual infilling rates provided by Gisborne District Council (GDC) from dredging records and bathymetry surveys, and the medium-term numerical modelling. Estimates are provided for the outer channel, the inner basin and the sum of both areas.

Source	Conditions	Annual infilling rate [$m^3.yr^{-1}$]			Deviation
		Outer channel	Inner basin	Total	
GDC	Average (2009/2015)	80,000 ±26,400	20,000 ±6,600	100,000 ±33,000	-
Black et al. (1997)	Average	-	-	103,000	+3.0%
Medium-term modelling	La Niña (1998/1999)	60,087	14,608	74,695	-25.3%
Medium-term modelling	El Niño (2002/2003)	92,593	27,647	120,240	+20.2%

3.4. Predicted channel depth profiles after one year

As part of the port infilling assessment, we extracted eight depth profiles (Figure 3.12) from the initial and the one year predicted bathymetries at Eastland Port for both 'La Niña' and 'El Niño' phases of ENSO. Associated depth transects are given in Figure 3.13 to Figure 3.16. Variations in the derived depth profiles between the 'La Niña' and 'El Niño' phases of ENSO are a function of the different incident wave climate and river discharges.

During 'La Niña', sediment accretion after one year is expected to range from approximately 0.9 m in the channel to 0.08 m in the swinging basin (Figure 3.13 to Figure 3.16). The maximum accretion is expected along the southern margin of the channel at approximately 100 m from the main breakwater tip (segment S1, Figure 3.13). In contrast, this area is characterised by 0.15 m of seabed erosion relative to the existing bathymetry in the 'El Niño' simulation due to the predominance of southerly wave events during the 'El Niño' period and relatively reduced river discharge.

At the main breakwater tip (S2, Figure 3.14) the morphological model predicts erosion on the southern channel batter and slope, however this is expected to be somewhat over-predicted by the model. This area is certainly subjected to considerable sediment transport processes during high wave energy periods. However, it is likely that the characteristics of the seabed in the model do not fully replicate a realistic degree of consolidation within this dynamic area and insufficient data on the surficial sediment in the area is available to address this issue, and it is likely the surficial sediment here is coarser than represented in the model. The impact of such bias on the overall model outcome is expected to be relatively insignificant considering the volume of material.

Within the port entrance and Swinging Basin (profiles S4 to S7, Figure 3.15 and Figure 3.16) the morphological model predicts similar accretional trends for both the ‘La Niña’ and ‘El Niño’ periods, however approximately twice as much deposition is expected within the Swinging basin during ‘El Niño’ periods.

These results are globally in agreement with the depth changes observed from the bathymetry surveys, except along the steep margin of the berth pocket. There, the model seems to under-predict somewhat the accretion of material and this is attributed to a lack of precision in the model grid.

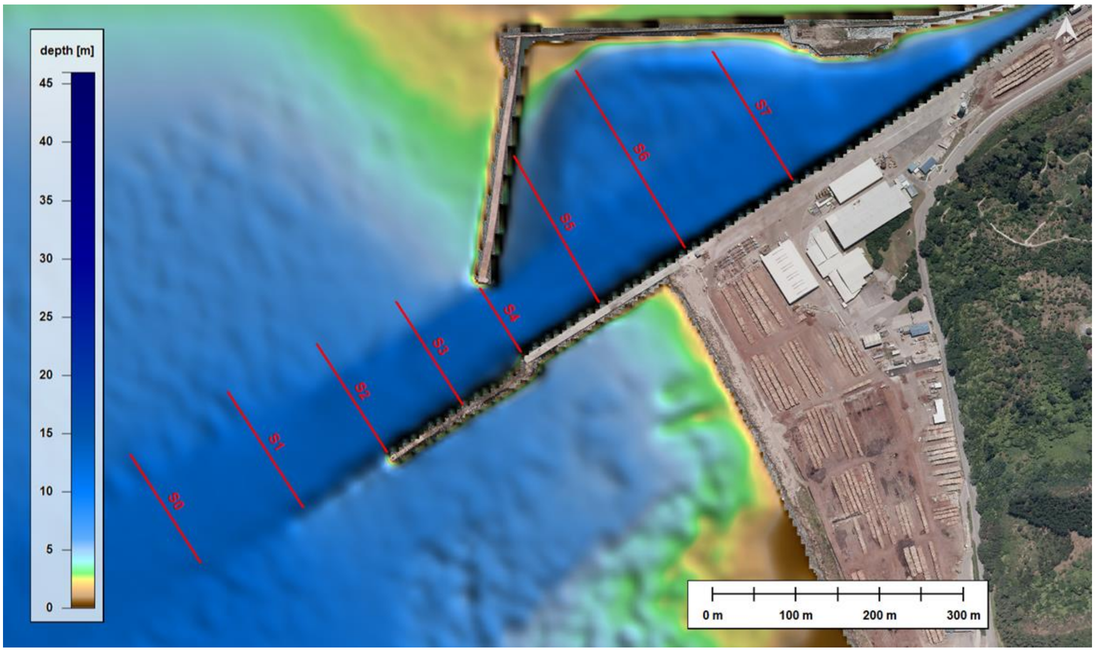

Figure 3.12 Sections (red lines) used to compare the initial and predicted depth profiles after one year of morphological simulation at Eastland Port. Also given the existing bathymetry (MSL datum) over the area.

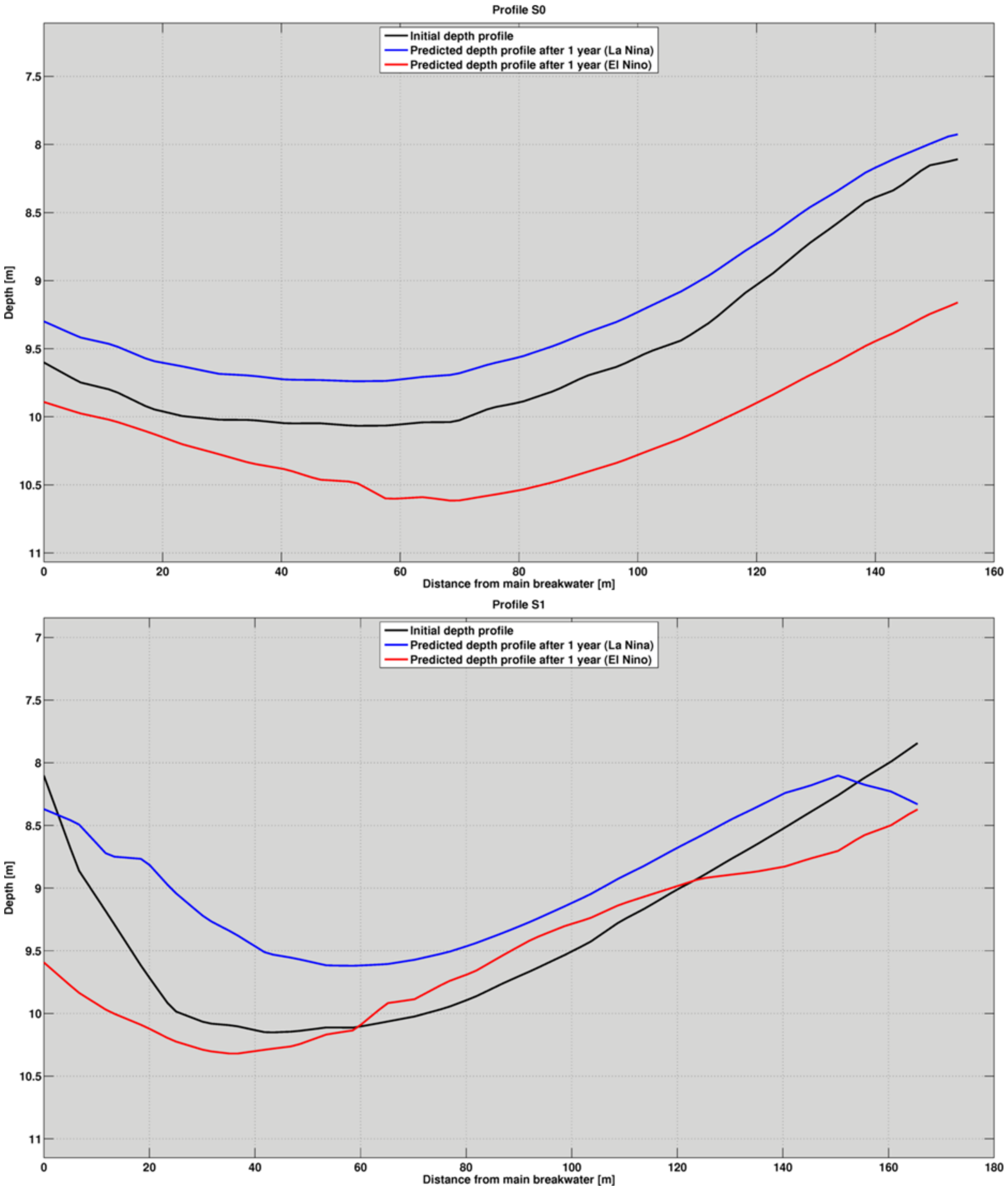

Figure 3.13 Depth profiles extracted from the existing (Black) and the predicted (Blue='La Niña', Red='El Niño') bathymetries along segments S0 (top) and S1 (bottom) shown in Figure 3.12.

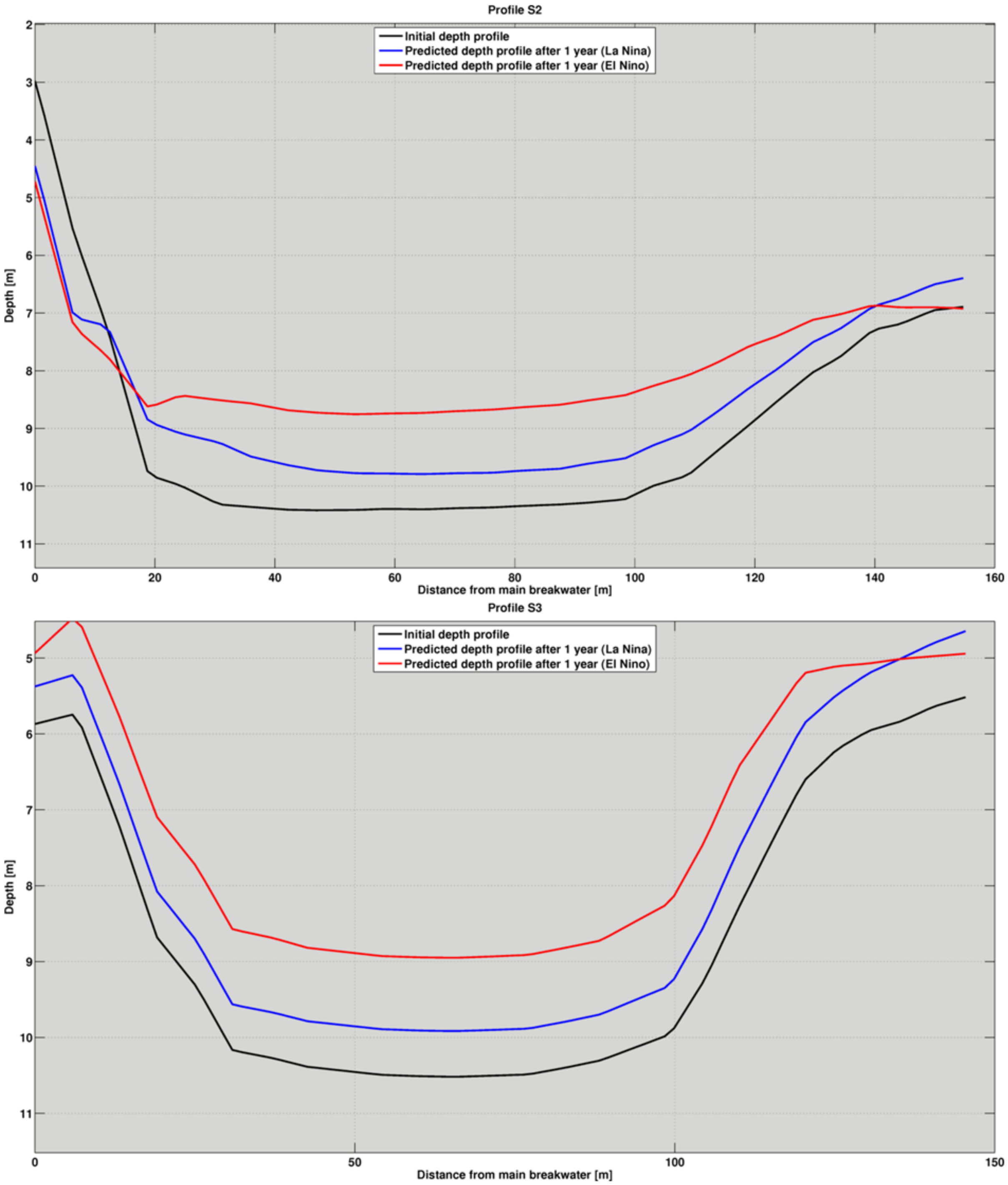

Figure 3.14 Depth profiles extracted from the existing (Black) and the predicted (Blue=‘La Niña’, Red=‘El Niño’) bathymetries along segments S2 (top) and S3 (bottom) shown in Figure 3.12.

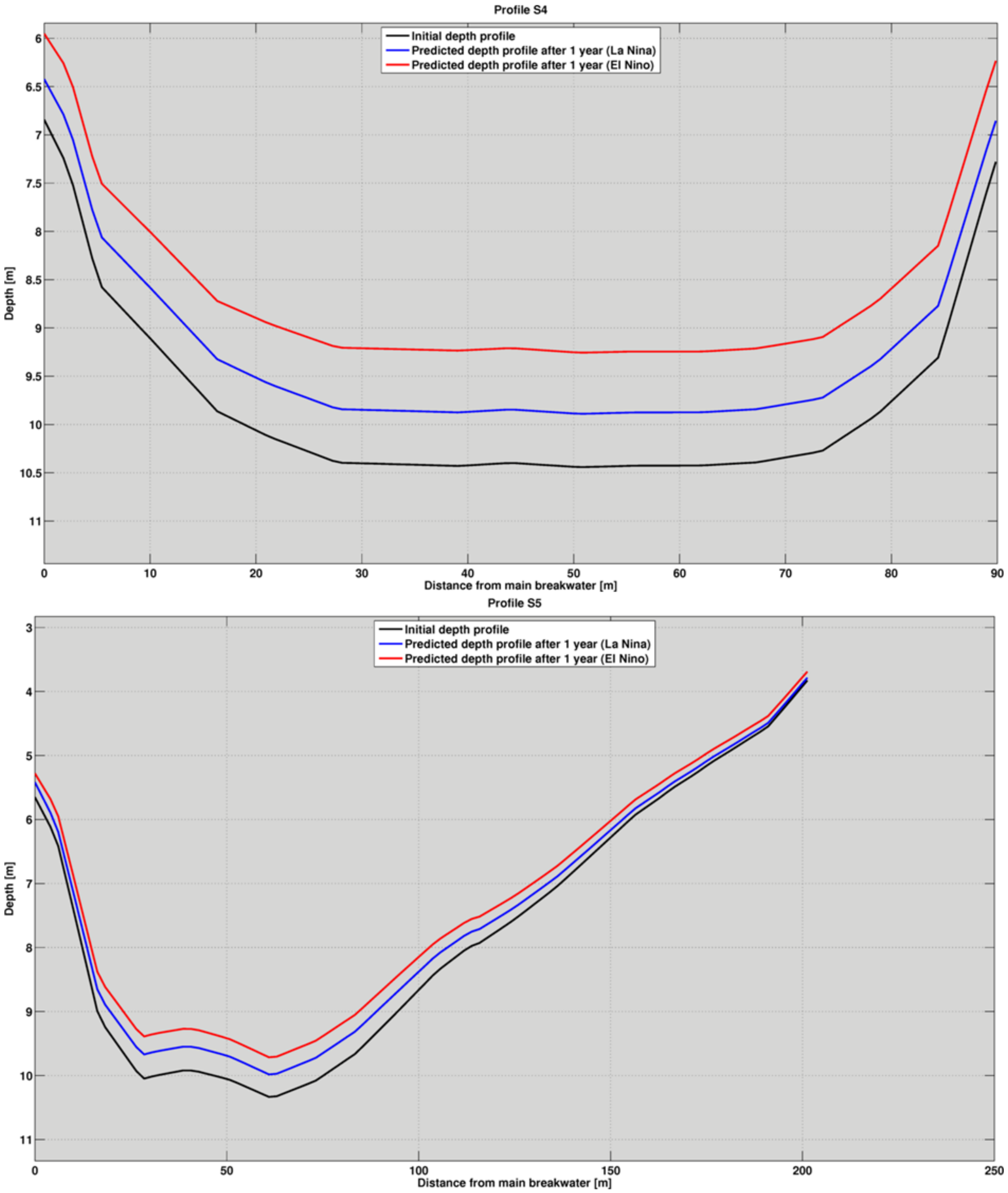

Figure 3.15 Depth profiles extracted from the existing (Black) and the predicted (Blue='La Niña', Red='El Niño') bathymetries along segments S4 (top) and S5 (bottom) shown in Figure 3.12.

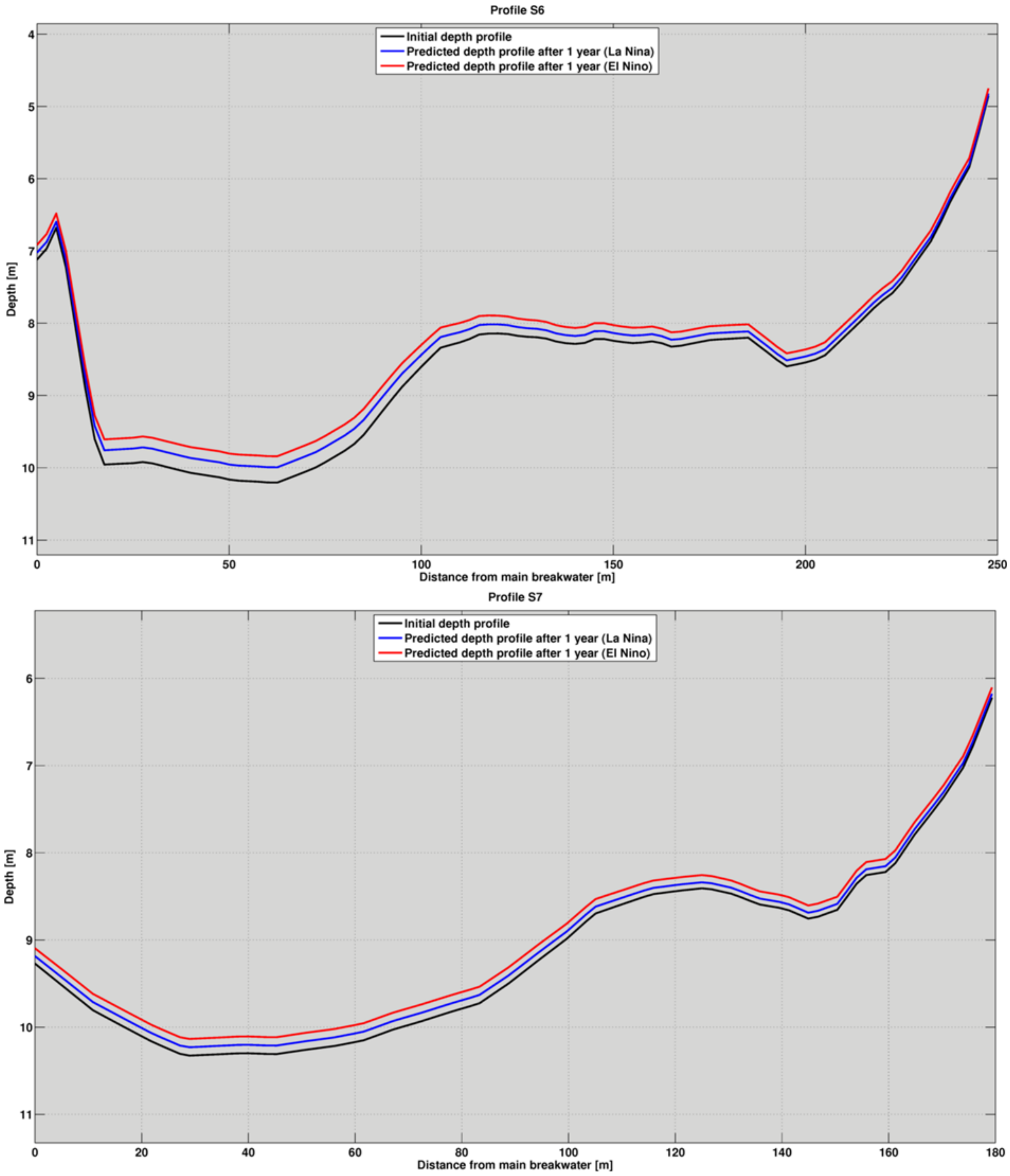

Figure 3.16 Depth profiles extracted from the existing (Black) and the predicted (Blue=‘La Niña’, Red=‘El Niño’) bathymetries along segments S6 (top) and S7 (bottom) shown in Figure 3.12.

3.5. Daily volumetric infilling rates

Additionally to the annual morphological accelerated simulations, a fifteen day historical simulation was performed from July 7th to July 23rd, 2002. This period was characterised by high incident wave energy conditions and river discharges into Poverty Bay (see Figure 2.14 and Figure 2.15 respectively). This simulation was used to investigate the daily variability of the infilling processes under a range of conditions at Eastland Port. Morphological results were saved every three hours (Figure 3.17) and averaged on a daily basis.

The average volumetric daily infilling rate over the simulated period was 830 $m^3.day^{-1}$ (Table 3.3). Based on the scale provided by Black et al. (1997), such rates are describes stormy to sever conditions. This is consistent with the fluvial sediment load and wave conditions during the simulated period as shown in Figure 2.14 and Figure 2.15, and Figure 3.18 and Figure 3.19.

While low to moderate waves favour the accretion of sand into the channel (particularly during significant fluvial discharges), energetic storm conditions with significant wave heights exceeding 2-m actively entrain the surficial sediment from the outer channel and can lead to periods of mild erosion (i.e. 13th and 15th July, 2002, Figure 3.17 and Figure 3.20). Enhanced infilling processes occur immediately after at the harbour entrance and within the basin due to decreasing bed shear stresses. In this configuration, the model predicted 3-hourly infilling rates up to 1500 $m^3.hr^{-1}$. A very quick and significant accretion of material may thus happen at the entrance to Eastland Port and within the inner basin during significant fluvial events combined with low incident wave heights.

Table 3.3 Average daily and annual infilling rates provided by previous studies and the present numerical modelling.

Source	**Conditions**	**Daily infilling rate**	**Annual infilling rate**	**Absolute mean bed level change**
		[$m^3.day^{-1}$]	**[$m^3.day^{-1}$]**	**[m]**
(Black et al., 1997)	Average	282	103,000	0.75
	Stormy	690	252,000	1.84
	Sever	2,000	730,000	5.32
(Beamsley, 2003)	Average to stormy	470	171,415	1.25
Input reduction 1	La Niña	205	74,695	0.54
Input reduction 2	El Niño	329	120,240	0.88
Event 1	Average to stormy	829	302,840	2.20

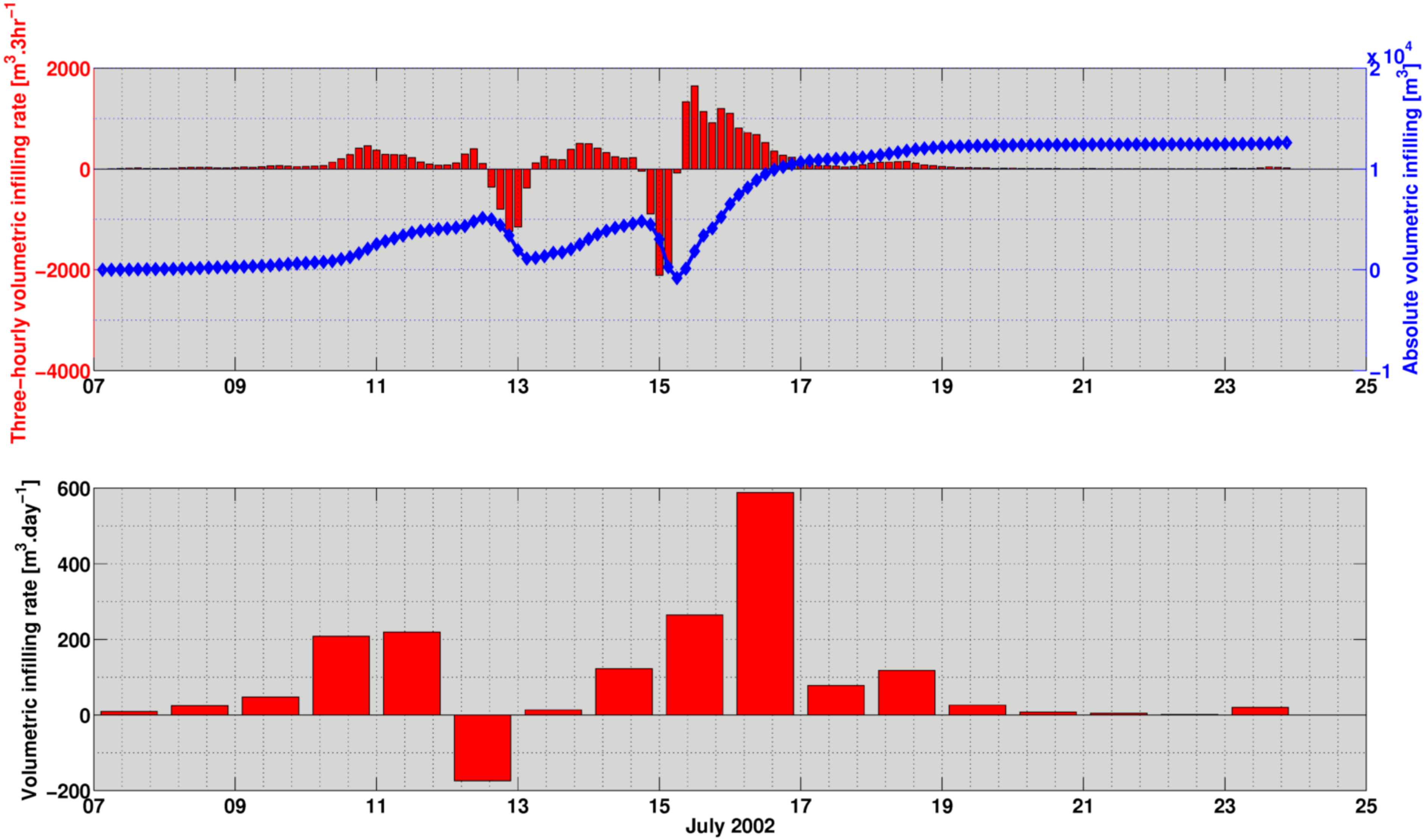

Figure 3.17 Predicted three-hourly volumetric infilling rates and absolute volumetric infilling within the channel and the inner basin (top). The bottom panel displays the volumetric infilling rates on a daily basis.

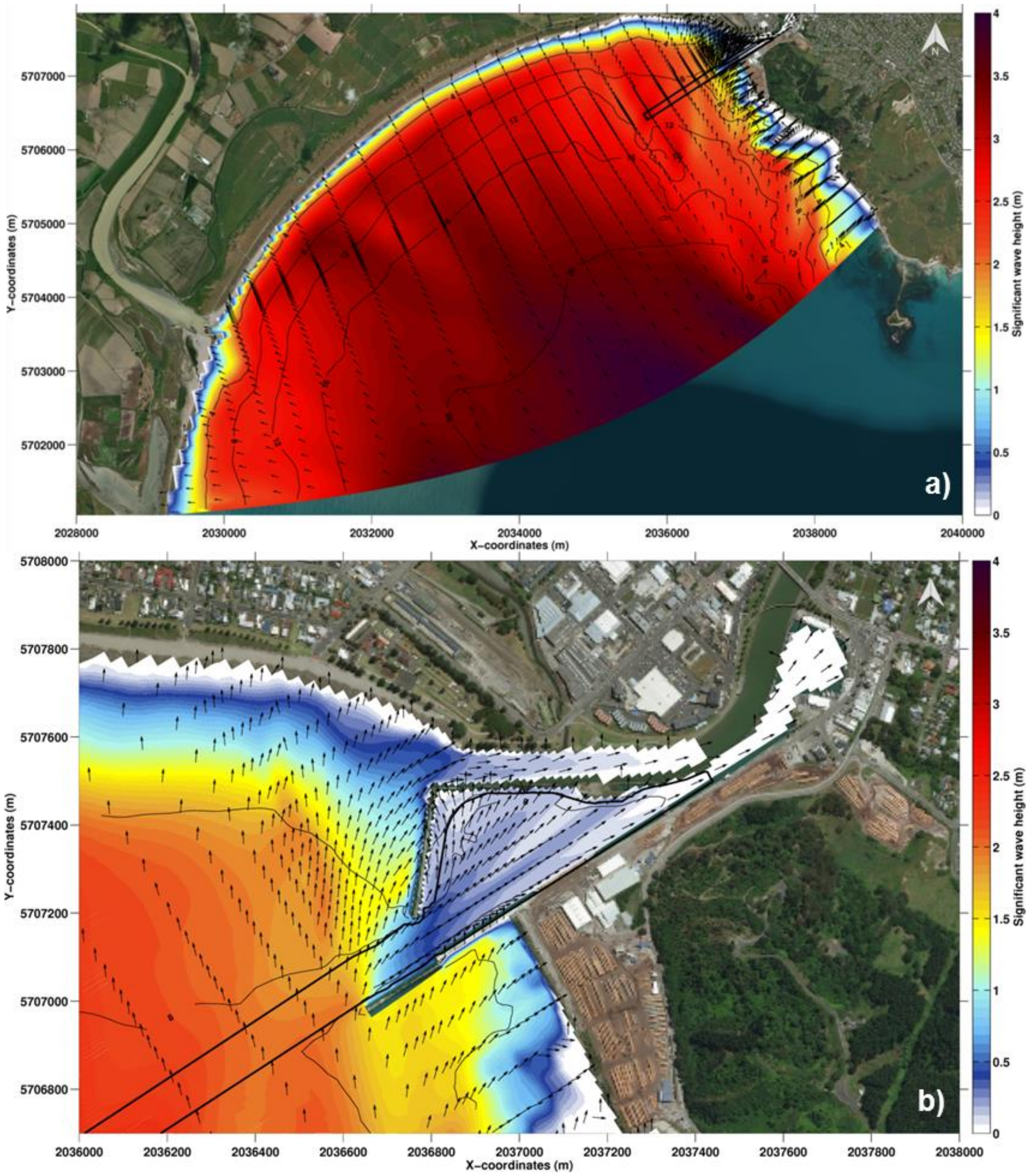

Figure 3.18 Significant wave height fields during peak storm conditions on July 15th 2002 over northern Poverty Bay (a) and Eastland Port (b). The black polygon indicates the dredged area used to estimate the channel volumetric infilling rates.

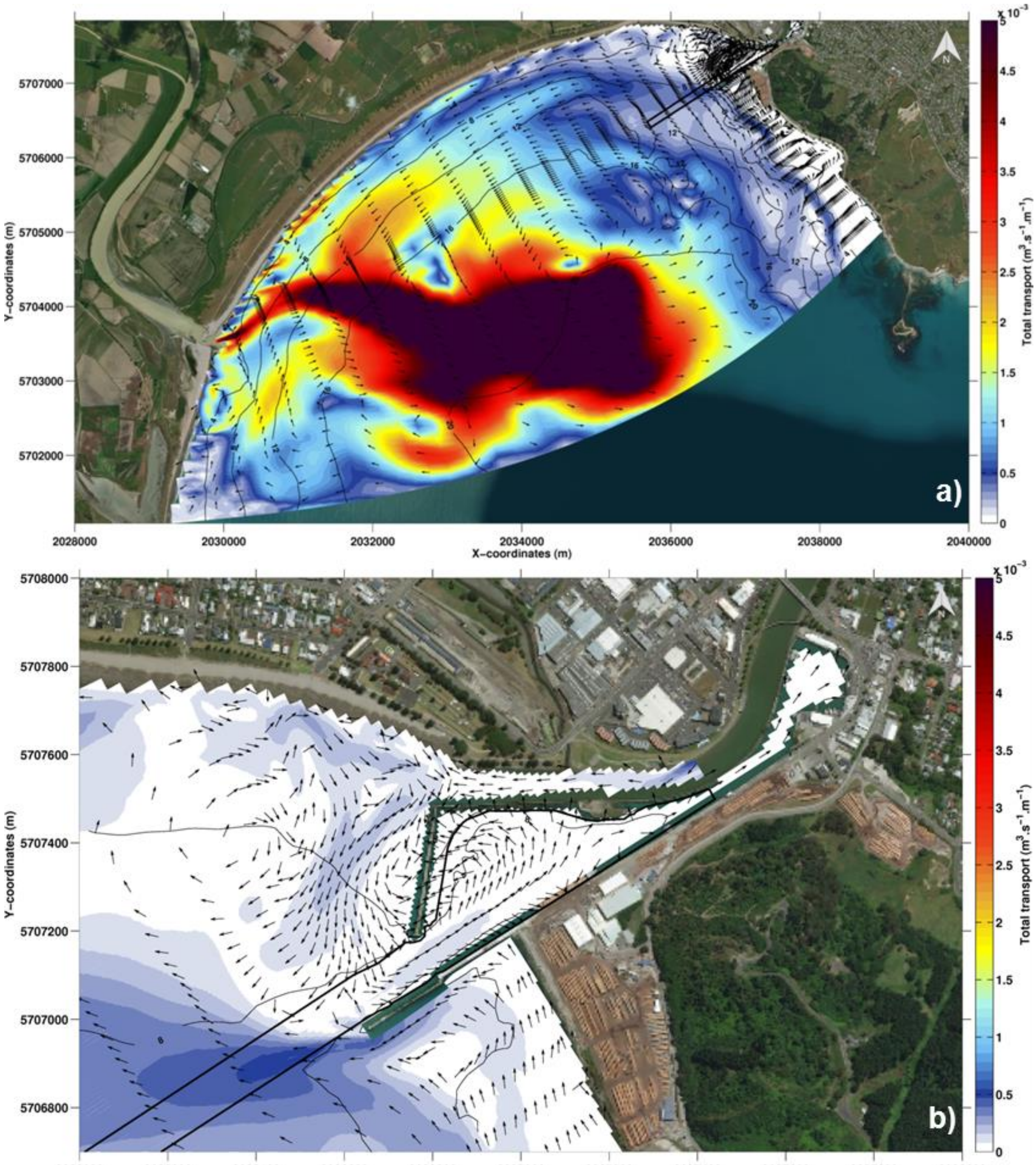

Figure 3.19 Total sediment transport during peak storm conditions on July 15th 2002 over northern Poverty Bay (a) and Eastland Port (b). The black polygon indicates the dredged area used to estimate the channel volumetric infilling rates.

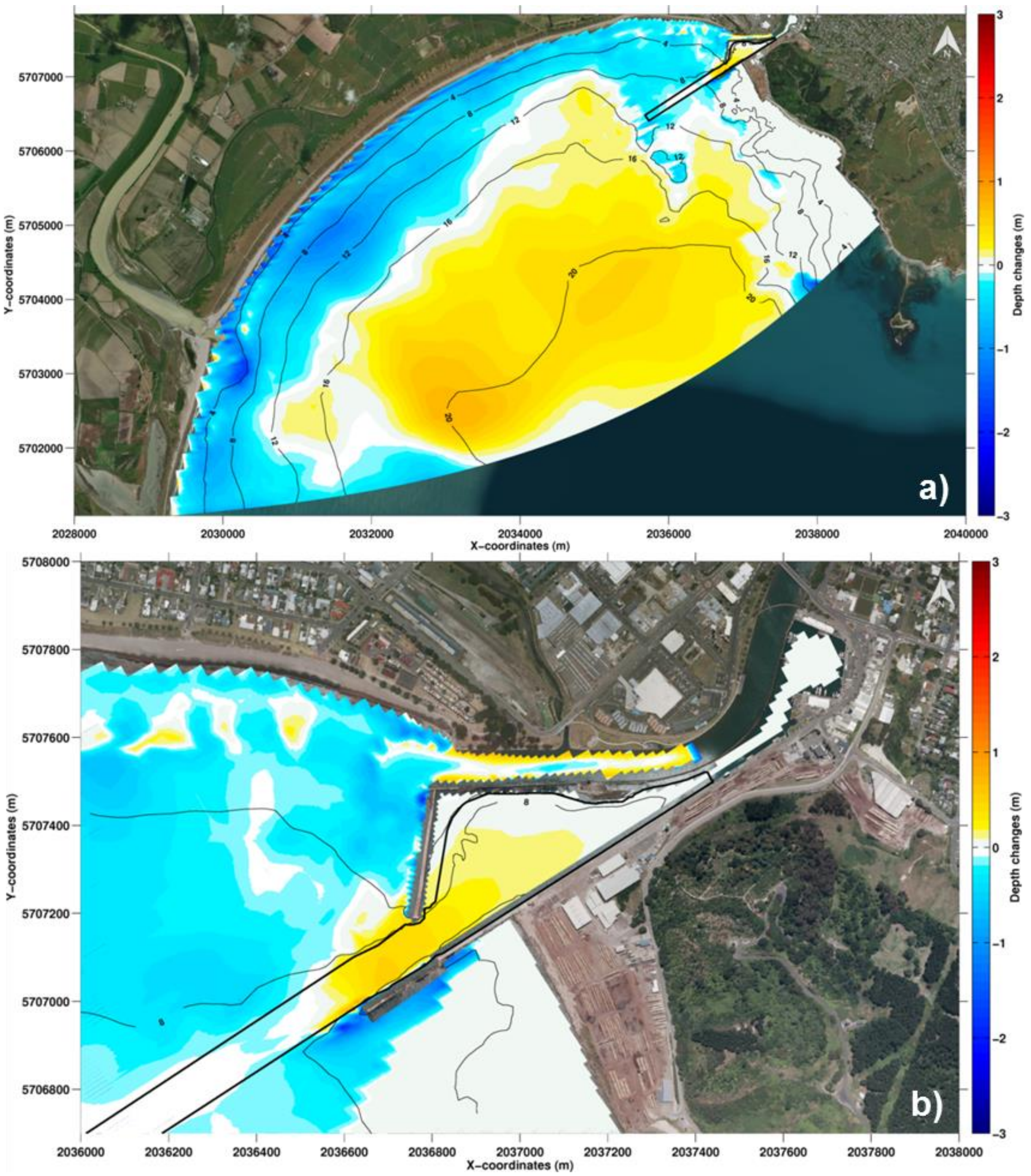

Figure 3.20 Depth changes predicted by the morphological model after 15 days under storm conditions from July 7th to July 23rd 2002 over northern Poverty Bay (a) and Eastland Port (b). Red and blue colours indicate bed accretion and erosion patterns, respectively.

4. SUMMARY

The open-source Delft3D system was used to run high-resolution process-based morphodynamic simulations over northern Poverty Bay and Eastland Port. The numerical modelling involved fully-coupled wave, current and seabed interactions.

The modelling approach consisted in replicating the sediment dynamics over two complete one year periods by applying an input reduction technique and morphological acceleration factors. In addition, a fifteen day historical simulation was performed to examine the capability of the model in simulating the sediment dynamics during storm conditions associated with large river discharges.

Both the hydrodynamic and the morphological models were validated against in situ measured data and estimates of the channel volumetric infilling rate. Additionally, the predicted morphological patterns were also qualitatively compared to the dominant patterns described in the scientific literature.

It has been demonstrated that the numerical model replicated successfully the dominant physical and morphological processes in the bay. At Eastland Port, the predicted daily and annual infilling rates were close to the estimates provided by the Eastland Port from historical bathymetry surveys and dredging records. The morphological changes simulated over northern Poverty Bay were also broadly consistent with the patterns described in the previous studies.

The present numerical modelling provides a well-founded method to assess the morphological evolution of proposed changes to the shipping channel and Swinging Basin and evaluate likely future Maintenance Dredging requirements, inclusive of associated channel infilling error-bounds.

5. REFERENCES

Andersen, T.J., Fredsoe, J., Pejrup, M., 2007. In situ estimation of erosion and deposition thresholds by Acoustic Doppler Velocimeter (ADV). Estuar. Coast. Shelf Sci. 75, 327–336.

Bagnold, R.A., 1966. An approach to the sediment transport problem from general physics. US government printing office.

Battjes, J.A., Janssen, J., 1978. Energy loss and set-up due to breaking of random waves, in: Coastal Engineering 1978. pp. 569–587.

Beamsley B.J., 2003. Hydro and Sediment Dynamics of Northern Poverty Bay, New Zealand. Centre of Excellence in Coastal Oceanography and Marine Geology, incorporating the Coastal Marine Group, Department of Earth Sciences, The University of Waikato, nad the National Institute of Water and Atmospheric Research, Hamilton.

Becker, J.J., Sandwell, D.T., Smith, W.H.F., Braud, J., Binder, B., Depner, J., Fabre, D., Factor, J., Ingalls, S., Kim, S.H., others, 2009. Global bathymetry and elevation data at 30 arc seconds resolution: SRTM30_PLUS. Mar. Geod. 32, 355–371.

Black, K.P., Gorman, R.G., Stephens, S.A., Beamsley, B.J., Healy, T.R., Bell, R.G., Oldman, J.W., 1997. Numerical Modelling for the Port Gisborne Expansion, A report on behalf of Port Gisborne Ltd., Centre of Excellence in Coastal Oceanography and Marine Geology, incorportating the Coastal Marine Group, Department of Earth Sciences, The university of Waikato, and the National Institute of Water and Atmospheric Research, Hamilton.

Booij, N., Ris, R.C., Holthuijsen, L.H., 1999. A third-generation wave model for coastal regions: 1. Model description and validation. J. Geophys. Res. Oceans 104, 7649–7666.

Brown, J.M., Davies, A.G., 2009. Methods for medium-term prediction of the net sediment transport by waves and currents in complex coastal regions. Cont. Shelf Res. 29, 1502–1514.

CERC, U.A., 1984. Shore protection manual. US Army Corps Eng. Wash.

Collins, J.I., 1972. Prediction of shallow-water spectra. J. Geophys. Res. 77, 2693–2707.

Dastgheib, A., 2012. Long-term process-based morphological modeling of large tidal basins. UNESCO-IHE, Institute for Water Education.

De Vriend, H.J., Capobianco, M., Chesher, T., De Swart, H. de, Latteux, B., Stive, M.J.F., 1993. Approaches to long-term modelling of coastal morphology: a review. Coast. Eng. 21, 225–269.

Deltares, 2017a. User Manual Delft3D-FLOW. draft version 3.15. Deltares.

Deltares, 2017b. User Manual Delft3D-WAVE. draft version 3.05. Deltares.

Deltares, 2014. User Manual Delft3D-Functional Specifications. draft version 2.20. Deltares.

Dissanayake, D., Ranasinghe, R., Roelvink, J.A., 2012. The morphological response of large tidal inlet/basin systems to relative sea level rise. Clim. Change 113, 253–276.

Eastland Port, 2013. Maintenance Dredging Liaison Group - Annual Report 2013 to the Gisborne District Council.

Enet, F., Nahon, A., Van Vledder, G., Hurdle, D., 2006. Evaluation of diffraction behind a semi-infinite breakwater in the SWAN Wave Model, in: Proceedings of Ninth International Symposium on Ocean Wave Measurement and Analysis-WAVES06.[Links].

Engelund, F., Hansen, E., 1967. A monograph on sediment transport in alluvial streams. Tech. Univ. Den. 0stervoldgade 10 Cph. K.

Engquist, B., Majda, A., 1979. Radiation boundary conditions for acoustic and elastic wave calculations. Commun. Pure Appl. Math. 32, 313–357.

Engquist, B., Majda, A., 1977. Absorbing boundary conditions for numerical simulation of waves. Proc. Natl. Acad. Sci. 74, 1765–1766.

Foster, G., Carter, L., 1997. Mud sedimentation on the continental shelf at an accretionary margin—Poverty Bay, New Zealand. N. Z. J. Geol. Geophys. 40, 157–173.

Fredsøe, J., 1984. Turbulent boundary layer in wave-current motion. J. Hydraul. Eng. 110, 1103–1120.

Giardino, A., Brière, C., van der Werf, J.J., 2011. Morphological modelling of bar dynamics with Delft3D. Deltares Neth.

Gisborne District Council, 1994. Unpublished Report - Waipaoa River at Kanakanaia monthly suspended sediment yields.

Griffiths, G.A., Glasby, G.P., 1985. Input of river-derived sediment to the New Zealand continental shelf: I. Mass. Estuar. Coast. Shelf Sci. 21, 773–787.

Grunnet, N.M., Walstra, D.-J.R., Ruessink, B.G., 2004. Process-based modelling of a shoreface nourishment. Coast. Eng. 51, 581–607.

Healy, T., Stephens, S., Black, K., Gorman, R., Cole, R., Beamsley, B., 2002. Port redesign and planned beach renourishment in a high wave energy sandy-muddy coastal environment, Port Gisborne, New Zealand. Geomorphology 48, 163–177.

Hicks, D.M., Gomez, B., Trustrum, N.A., 2004. Event suspended sediment characteristics and the generation of hyperpycnal plumes at river mouths: East Coast continental margin, North Island, New Zealand. J. Geol. 112, 471–485.

Hicks, D.M., Gomez, B., Trustrum, N.A., 2000. Erosion thresholds and suspended sediment yields, Waipaoa River basin, New Zealand. Water Resour. Res. 36, 1129–1142.

Ikeda, S., 1982. Lateral bed load transport on side slopes. J. Hydraul. Div. 108, 1369–1373.

Ikeda, S., Parker, G., Kimura, Y., 1988. Stable width and depth of straight gravel rivers with heterogeneous bed materials. Water Resour. Res. 24, 713–722.

Kensington, G.L., 1990. Port development and dredge spoil dispersion in northern Poverty Bay. University of Waikato.

Kniskern, T.A., 2007. Shelf sediment dispersal mechanisms and deposition of the Waiapu River Shelf, New Zealand.

Krone, R.B., 1993. Sedimentation revisited. Nearshore Estuar. Cohesive Sediment Transp. 108–125.

Latteux, B., 1995. Techniques for long-term morphological simulation under tidal action. Mar. Geol. 126, 129–141.

Lesser, G.R., 2009. An approach to medium-term coastal morphological modelling. UNESCO-IHE, Institute for Water Education.

Lesser, G.R., Roelvink, J. v, Van Kester, J., Stelling, G.S., 2004. Development and validation of a three-dimensional morphological model. Coast. Eng. 51, 883–915.

Luijendijk, A.P., Ranasinghe, R., de Schipper, M.A., Huisman, B.A., Swinkels, C.M., Walstra, D.J., Stive, M.J., 2017. The initial morphological response of the Sand Engine: A process-based modelling study. Coast. Eng. 119, 1–14.

MetOcean Solutions, 2017a. Eastland Port Maintenance Dredging and Disposal Project. Hydrodynamic hindcast validation (No. P0331- 01).

MetOcean Solutions, 2017b. Eastland Port Maintenance Dredging and Disposal Project. Wave hindcast validation (No. P0331- 05).

Miller, K.R., 1981. Surficial sediments and sediment transport in Poverty Bay. University of Waikato.

Moriarty, J.M., Harris, C.K., Hadfield, M.G., 2015. Event-to-seasonal sediment dispersal on the Waipaoa River Shelf, New Zealand: A numerical modeling study. Cont. Shelf Res. 110, 108–123.

Orpin, A.R., Alexander, C., Carter, L., Kuehl, S., Walsh, J.P., 2006. Temporal and spatial complexity in post-glacial sedimentation on the tectonically active, Poverty Bay continental margin of New Zealand. Cont. Shelf Res. 26, 2205–2224.

Partheniades, E., 1965. Erosion and deposition of cohesive soils. J. Hydraul. Div. 91, 105–139.

Portela, L.I., Ramos, S., Teixeira, A.T., 2013. Effect of salinity on the settling velocity of fine sediments of a harbour basin. J. Coast. Res. 65, 1188–1193.

Pullar, W.A., Penhale, H.R., 1970. Periods of recent infilling of Gisborne plains basin-associated marker beds and changes in shoreline. N. Z. J. Sci. 13, 410.

Ramli, A.Y., de Lange, W., Bryan, K., Mullarney, J., 2015. Coupled flow-wave numerical model in assessing the impact of dredging on the morphology of Matakana Banks, in: Australasian Coasts & Ports Conference 2015: 22nd Australasian Coastal and Ocean Engineering Conference and the 15th Australasian Port and Harbour Conference. Engineers Australia and IPENZ, p. 758.

Reniers, A.J., Roelvink, J.A., Thornton, E.B., 2004. Morphodynamic modeling of an embayed beach under wave group forcing. J. Geophys. Res. Oceans 109.

Ris, R.C., Holthuijsen, L.H., Booij, N., 1999. A third-generation wave model for coastal regions: 2. Verification. J. Geophys. Res. Oceans 104, 7667–7681.

Roelvink, J.A., 2006. Coastal morphodynamic evolution techniques. Coast. Eng. 53, 277–287.

Sander, R.M., 1993. Chemical investigation into the effects of dredge spoil dumping in Poverty Bay. University of Waikato.

Shi, B., Wang, Y.P., Yang, Y., Li, M., Li, P., Ni, W., Gao, J., 2015. Determination of critical shear stresses for erosion and deposition based on in situ measurements of currents and waves over an intertidal mudflat. J. Coast. Res. 31, 1344–1356.

Smith, R.K., 1988. Poverty Bay, New Zealand: a case of coastal accretion 1886–1975. N. Z. J. Mar. Freshw. Res. 22, 135–142.

Stephens, S.A., Bell, R.G., Black, K.P., 2001. Complex circulation in a coastal embayment: Shelf-current, wind and density-driven circulation in Poverty Bay, New Zealand. J. Coast. Res. 45–59.

Van der Wegen, M., Jaffe, B.E., Roelvink, J.A., 2011. Process-based, morphodynamic hindcast of decadal deposition patterns in San Pablo Bay, California, 1856–1887. J. Geophys. Res. Earth Surf. 116.

Van der Wegen, M., Roelvink, J.A., 2008. Long-term morphodynamic evolution of a tidal embayment using a two-dimensional, process-based model. J. Geophys. Res. Oceans 113.

van der Westhuysen, A.J., Zijlema, M., Battjes, J.A., 2007. Nonlinear saturation-based whitecapping dissipation in SWAN for deep and shallow water. Coast. Eng. 54, 151–170.

Van Rijn, 2016. Initiation of motion and suspension; Critical bed-shear stress for sand-mud mixtures. Technical Note.

Van Rijn, L.C., 1993. Principles of sediment transport in rivers, estuaries and coastal seas. Aqua publications Amsterdam.

Van Rijn, L.C., Walstra, D.J.R., Ormondt, M. van, 2004. Description of TRANSPOR2004 and Implementation in Delft3D-ONLINE. Z3748.

Verboom, G.K., Segal, A., 1987. Weakly-Reflective Boundary Conditions for Shallow Water Equations, in: Research in Numerical Fluid Mechanics. Springer, pp. 115–129.

Verboom, G.K., Slob, A., 1984. Weakly-reflective boundary conditions for two-dimensional shallow water flow problems, in: Finite Elements in Water Resources. Springer, pp. 621–633.

Walstra, D.J.R., Hoekstra, R., Tonnon, P.K., Ruessink, B.G., 2013. Input reduction for long-term morphodynamic simulations in wave-dominated coastal settings. Coast. Eng. 77, 57–70.

Walstra, D.J.R., Ormondt, M. van, Roelvink, J.A., 2004. Shoreface nourishment scenarios: detailed morphodynamic simulations with Delft3D for various shoreface nourishment designs. Z3748.

Weppe, S., McComb, P., Coe, L., 2015. Numerical Model Studies to Support the Sustainable Management of Dredge Spoil Deposition in a Complex Nearshore Environment, in: The Proceedings of the Coastal Sediments 2015.

Williams, R.D., Measures, R., Hicks, D.M., Brasington, J., 2016. Assessment of a numerical model to reproduce event-scale erosion and deposition distributions in a braided river. Water Resour. Res. 52, 6621–6642.